INVERSE PROBLEMS IN BIOLUMINESCENCE TOMOGRAPHY AND WAVE IMAGING: THEORY, ALGORITHM AND IMPLEMENTATION

By

Tianyu Yang

A DISSERTATION

Submitted to
Michigan State University
in partial fulfillment of the requirements
for the degree of

Computational Mathematics, Science and Engineering—Doctor of Philosophy

2024

ABSTRACT

Ultrasound modulated bioluminescence tomography (UMBLT) is a technique for imaging the 3D distribution of biological objects such as tumors by using a bioluminescent source as a biomedical indicator. It uses bioluminescence tomography (BLT) with a series of perturbations caused by acoustic vibrations. UMBLT outperforms BLT in terms of spatial resolution. The current UMBLT algorithm in the transport regime requires measurement at every boundary point in all directions, and reconstruction is computationally expensive. In Chapter 2, we will first introduce the UMBLT model in both the diffusive and transport regimes, and then formulate the image reconstruction problem as an inverse source problem using internal data. Second, we present an improved UMBLT algorithm for isotropic sources in the transport regime. Third, we generalize an existing UMBLT algorithm in the diffusive regime to the partial data case and quantify the error caused by uncertainties in the prescribed optical coefficients.

The inverse boundary value problem (IBVP) of wave equation aims to recover medium distribution via boundary measurement of wave propagation. Using an important identity that connects boundary data and internal wave states, one can recover the medium's interior structure by selecting suitable boundary sources. In Chapter 3, we will first introduce the IBVP and the key identity. Second, we present a direct wave speed reconstruction algorithm with vanished wave potential. Third, we apply linearization on IBVPs to derive algorithms with nonvanishing parameters for both wave speed and wave potential reconstruction.

ACKNOWLEDGEMENTS

First of all, I would like to express my deepest appreciation to my advisor and committee chair, Professor Yang Yang, for his guidance, support, and encouragement though my Ph.D. study. He led me into the area of inverse problems and helped me to establish a deep understanding of theoretical and numerical PDE theory. I would like to express my thanks to my dissertation committee members, Professor Jianliang Qian, Professor Zhen Qiu, and Professor Adam Alessio, for their guidance as well.

I would like to thank Dr. Albert Chua, Liantao Li and Henry Fessler for sharing their ideas and research during group meetings. I would like to thank Remy Liu, Jiaxin Yang, Shuyang Qin, Dr. He Lyu, Dr. Hao Wang, Dr. Qi Lyu, Kang Yu, Liantao Li, Dr. Danqi Qu, Dr. Ziyi Xi, Dr. Runze Su, Dr. Wenjie Qi, Dr. Binbin Huang for the hotpot, barbecue, movies, mahjong, poker, and other activities we enjoyed together.

Finally, I would like to thank my parents, Mr. Fashen Yang and Mrs. Lihua Chen, for their support in pursuing a Ph.D. far away from home.

TABLE OF CONTENTS

CHAPTER 1

INTRODUCTION

Inverse Problems are defined as the inverse of *Forward Problems*. Forward problems typically involve determining the status of a physical system or predicting an outcome based on model parameters, such as calculating a rocket's trajectory or simulating the spread of water pollution. The forward map of the physical system (model) is formulated as

$$\mathfrak{F} : X \to Y, \qquad \mathfrak{F}(p) = d, \tag{1.1}$$

where the operator $\mathfrak{F}$ describes the relation between model parameter space X with the observed data space Y, p denote the parameters and d denote the data.

Inverse problems focus on determining model parameters p from measurement data d, i.e. inverting the operator $\mathfrak{F}$. Inverse problems are considered when the model parameters p of interest cannot be measured directly or practically, such as generating 3D images of internal organs or reconstructing the seismic velocity structure of the Earth.

In mathematics, a *well-posed* problem, which is introduced by Jacques Hadamard (1865-1963), satisfies the following three properties:

(1) Existence: The problem has a solution,

(2) Uniqueness: The solution is unique,

(3) Stability: The solution's behavior changes continuously with the initial conditions.

Unlike well-posed problems, *ill-posed* problems violate at least one of the three properties. Forward problems are usually well-posed, while inverse problems are usually ill-posed, which means that either $\mathfrak{F}$ is not invertible or $\mathfrak{F}^{-1}$ is not continuous. Assuming that $\mathfrak{F}^{-1}$ exists, the model parameter p is theoretically given by

$$p = \mathfrak{F}^{-1} m.$$

If the observation carry measurement error $\varepsilon \in Y$, the reconstructed parameter becomes

$$\tilde{p} = \mathfrak{F}^{-1}\tilde{m} = \mathfrak{F}^{-1}[m + \varepsilon] = p + \mathfrak{F}^{-1}\varepsilon.$$

The difference between $\tilde{p}$ and p could be relatively large depending on the behavior of $\mathfrak{F}^{-1}$, even if the measurement error ε is relatively small. In these cases, the theory of regularization of ill-posed problems have been considered by A. N. Tikhonov and his followers [48, 63, 77, 93].

When the physical model describes the propagation of lights, the 3D structure of an object is reconstructed using light that has been transmitted and scattered. During light propagation, two main effects occur: absorption and scattering. For example, in photoelectric absorption, the photon is completely absorbed by the atom electron; in Rayleigh scattering, the photon is scattered, with the effect proportional to the fourth power of its frequency. In this case, it is common to assume that the model is time and frequency independent. For *Optical Tomography*, a series of near-infrared sources are attached on the surface of the object. The scattered field are measured on the same surface in order to generate images of soft tissues [34, 50, 100]. For *Bioluminescence Tomography*, biologists use transfection technology to generate an internal light source. The distribution of different optical coefficients can be recovered by measuring the output flux through the boundary [29, 69, 101]. However, both Optical Tomography and Bioluminescence Tomography have poor resolution due to the ill-posedness [35]. The diffusive nature of the photons is cause for the ill-posedness, which means the obtained images have low resolution and are very sensitive to noise.

In order to improve the resolution, a high resolution modality is combined; these combinations are known as *Hybrid inverse problems*, also called coupled-physics inverse problems, which combine a high resolution modality with a high contrast modality for better reconstruction. For example, in *Ultrasound Modulated Optical Tomography* [64, 80, 99] and *Ultrasound Modulated Bioluminescence Tomography* [6, 8, 28], a series of ultrasound perturbations are performed to the medium in order to generate more measurements, thereby overcoming the ill-posedness of the original inverse problems.

In Chapter 2, we introduce one of the hybrid inverse problems, *Ultrasound Modulated Bioluminescence Tomography*(UMBL). Depending on the scattering effects of medium, we introduce UMBLT under transport regime in Section 2.2 and diffusive regime in Section 2.3. The algorithms

in both full and partial data cases, as well as the uncertainty quantifications are given.

When the physical model describes the propagation of waves, the corresponding inverse problem are concerned with extracting information about structural features from scattered wave measurements. For example, in *Ultrasound Computerized Tomography*, a series of transducers are placed around the object. Each transducer will send acoustic waves into the object and other transducers will collect the waves. It can image soft tissue with high resolution [53,73,79]. If the wave are generated from external sources, the forward problems are formulated as *boundary value problems* of wave equation, and the inverse problems are called *inverse boundary value problems* of wave equation. Under this framework, the Neumann boundary condition represent the external sources, and the measurement is the Dirichlet value of the solution, or equivalently, the Neumann-to-Dirichlet map Λ. *Boundary Control Method* is an effective approach to solve the inverse boundary value problems [13, 47, 51, 88]. This method allow us generate a special input (Neumann boundary condition) such that the solution will reach a desired state at a fixed time, and the existance of such input is guaranteed by Tataru's theorem in [90]. With Blagoveščenskiĭ's identity [21], one can connect the boundary data with internal waves, which help recover the structure features, such as wave speed.

In Chapter 3, we introduce nonlinear *Inverse Boundary Value Problems* of wave equation with potential. In Section 3.2, we introduce a direct wave speed reconstruction algorithm with vanished wave potential. In Section 3.3, we consider wave equation with non-vanished potential. We apply linearization method to the inverse boundary value problems to derive algorithms for recovering wave speed and wave potential, respectively.

CHAPTER 2

ULTRASOUND MODULATED BIOLUMINESCENCE TOMOGRAPHY

2.1 Introduction

Bioluminescence is the production and emission of light by a living organism; It is widely occured in vertebrates and invertebrates, such as in firefly, anglerfish. This phenomenon can be utilized in a medical imaging method called *Bioluminescence tomography (BLT)*. BLT aims to reconstruct images of biological objects, like tumors, by using the bioluminescent source as a biomedical indicator. Specifically, scientists tag biological entities or process components (e.g. bacteria, tumor cells, immune cells, or genes) with reporter genes that encode one of a number of light-generating enzymes (luciferases) [29]. By measuring the light generated by the luciferin-luciferase reaction, one can image the 3D distribution of the internal source, which can be used for diagnosing diseases.

However, BLT have one main weakness, the spatial resolution of BLT is poor. This is because changes of light source will only cause relatively small changes on the measured data, the measurement error might have a large effect on the reconstruction. Even worse, sometimes different sources can lead to same measurement [35]. In order to prevent the worst case, which means we need to uniquely determine the source from the boundary measurement, BLT need additional information about the source, like its geometric aspect. One effective approach to enhance the spatial resolution of BLT is to use the *ultrasound modulation*, and the new method is called *Ultrasound Modulated Bioluminescence tomography (UMBLT)*. This method performs BLT under series of acoustic modulations to perturb the medium's optical properties. With different type of ultrasound, the measured data are different, which means the measured data are increased and different sources can not give same measurement with all types of ultrasound modulations, which can help overcome the weakness of BLT.

The first BLT scanner was developed by *G. Wang et al.* in 2003 [94] and the first small animal study using BLT was conducted by Chaudhari et al. in 2005 [27]. In 2004, *G. Wang et al.* gave uniqueness theorems of BLT under diffusion approximation [95], which is a simplified model for

strongly scattering medium based on diffusion equation. They proved the source can be uniquely determined from the boundary measurement if the source is a linear combination of impulses or ball sources. They also gave a summary of uniqueness theorems under different assumptions proposed by other people. In 2007, the uniqueness theorem of BLT under transport regime was given [9], they proved the source can be uniquely determined when the scattering kernel k is invariant of rotation and is relatively small under certain norm. One year later, *Stefanov and Uhlmann* gave a generic result of BLT that when attenuation coefficient σ and scattering kernel k are continuous, the source can be uniquely determined from boundary measurement when (σ, k) is in a open dense subset which contains a neighbor of $(0, 0)$ [85].

The inverse problem of UMBLT was first considered under diffusion approximation by *Bal and Schotland* [8]. They showed the well-posedness of the problem and developed an inversion formula by assuming the diffusion and absorption coefficients are given. Two years later, the inverse problem of UMBLT under transport regime was considered by *Bal, Chung and Schotland* [6]. They assumed the scattering kernel is invariant under rotation, all optical coefficients are continuous and σ, k are known. They showed the well-posedness of the problem and give an algorithm to reconstruct the source. They first derive an internal functional from the boundary measurements. Theoretically the directional derivative of photon intensity $\theta \cdot \nabla u$ can be extract from the internal functional, and then the interior value of the photon intensity u can be calculated using $\theta \cdot \nabla u$ and the corresponding boundary value, which can be used to calculate the source term. However, in this proposed algorithm, the reconstruction of photon intensity needs measurement on every boundary points with all directions and needs lots of computation. To this end we designed a more efficient algorithm for UMBLT under transport regime when the source is isotropic [28], where the source can be directly reconstruct by inverting a linear operator.

2.2 UMBLT under Transport Regime

The UMBLT method aims to image the distribution of light source. In order to model the UMBLT, we need to model the light propagation first. The propagation of light through a medium X is affected by absorption, emission, and scattering processes, which can be modeled using

standard *Radiative Transfer Equation (RTE)*. Such problem is called the UMBLT under transport regime [6, 28]. In this section, we consider following RTE model:

$$\theta \cdot \nabla u + \sigma(x)u - \int_{\mathbb{S}^{n-1}} k(x, \theta, \theta')u(x, \theta') \, \mathrm{d}\theta' = S(x, \theta), \tag{2.1}$$

$$u|_{\Gamma_-} = 0, \tag{2.2}$$

where u denote the intensity of light at spatial location x traveling in direction θ, σ is attenuation coefficient, k is the scattering kernel, S is an isotropic source, X is a bounded subset of $\mathbb{R}^n$ with smooth boundary, $\Gamma_\pm$ are the outgoing/incoming boundary, which are defined as

$$\Gamma_\pm = \left\{(x, \theta) \in \partial X \times \mathbb{S}^{n-1} \mid \pm\theta \cdot \nu \geq 0\right\}.$$

The vibration of the medium under acoustic modulation can be modeled using the time-harmonic plane wave with frequency ω as

$$p = A \cos(\omega t) \cos(q \cdot x + \varphi), \tag{2.3}$$

where p is the pressure, q is the wave vector and φ is the phase. Since the pressure is related to the changes of local density of the medium, the effect of the acoustic modulation on the optical properties [7] can be modeled as

$$\sigma_\varepsilon(x) \coloneqq (1 + \varepsilon \cos(q \cdot x + \varphi))\sigma(x), \tag{2.4}$$

$$k_\varepsilon(x, \theta, \theta') \coloneqq (1 + \varepsilon \cos(q \cdot x + \varphi))k(x, \theta, \theta'), \tag{2.5}$$

$$S_\varepsilon(x, \theta) \coloneqq (1 + \varepsilon \cos(q \cdot x + \varphi))S(x, \theta), \tag{2.6}$$

where $0 \leq \varepsilon \ll 1$ is a small parameter related to the amplitude, frequency, time, density and acoustic wave speed.

With the acoustic modulation, the model of UMBLT is the following modulated RTE with modulated optical properties and the same boundary condition

$$\theta \cdot \nabla u_\varepsilon + \sigma_\varepsilon(x)u_\varepsilon - \int_{\mathbb{S}^{n-1}} k_\varepsilon(x, \theta, \theta')u_\varepsilon(x, \theta') \, \mathrm{d}\theta' = S_\varepsilon(x), \tag{2.7}$$

$$u_\varepsilon|_{\Gamma_-} = 0. \tag{2.8}$$

The solution of the modulated RTE is denote as u_ε, notice that when $\varepsilon = 0$, it is exactly the solution of the standard RTE. Under different modulations, our measurement is the operator

$$\Lambda_S^\varepsilon : \mathbb{R}^n \times \{0, \frac{\pi}{2}\} \to C(\Gamma_+), \qquad (q, \varphi) \mapsto u_\varepsilon|_{\Gamma_+}, \qquad \varepsilon \geq 0, \tag{2.9}$$

which is the light flows out through the boundary under different modulations. The goal is to reconstruct source S from the measurement assuming σ_ε, k_ε, X are given.

Throughout this section, we make the following assumptions to ensure well-posedness of some forward boundary value problems.

(A1): σ, k and S are continuous on $\overline{X}$; moreover, $\sigma \geq c > 0$ and $k \geq c > 0$ for some constant c everywhere in X.

(A2): Set $\rho \coloneqq \left\| \int_{\mathbb{S}^{n-1}} k(x, \theta, \theta') \, \mathrm{d}\theta' \right\|_{L^\infty(X \times \mathbb{S}^{n-1})}$, one of the following inequalities holds:

$$\left(\inf_{x \in \overline{X}} \sigma \right) - \rho \geq \alpha \tag{2.10}$$

where $\alpha > 0$ is a positive constant, or

$$\operatorname{diam}(X)\rho < 1 \tag{2.11}$$

where $\operatorname{diam}(X) \coloneqq \sup\{|x - y| : \ x, y \in X\}$ is the diameter of X.

To ensure the integral in (2.1) is self-adjoint over $X \times S^{n-1}$, we assume the scattering kernel k is invariant under rotation, which means

$$k(x, \theta, \theta') = k(x, \theta \cdot \theta'),$$

then we can derive an internal functional for reconstruction.

Under these assumptions, the following well-posedness theorem holds in the function space $L^p(\mathbb{S}^{n-1}, C(\overline{X}))$, where the norm is defined as

$$\|u\|_{L^p(\mathbb{S}^{n-1}, C(\overline{X}))} \coloneqq \left(\int_{\mathbb{S}^{n-1}} \|u(x, \theta)\|_{C(\overline{X})}^p \, \mathrm{d}\theta \right)^{\frac{1}{p}}.$$

Proposition 2.1 ([6, Theorem 2.1]). *Suppose the assumptions (A1)(A2) hold. Then for any* $f_- \in C(\Gamma_-)$*, the RTE* (2.1) *has a unique solution* $u \in L^p(\mathbb{S}^{n-1}, C(\overline{X}))$ *(*$1 \le p \le \infty$*) with the boundary condition* $u|_{\Gamma_-} = f_-$*. Moreover, if* (2.10) *holds, we have the estimate*

$$\|u\|_{L^p(\mathbb{S}^{n-1},C(\overline{X}))} \le \frac{1}{\alpha}\left((\rho+\alpha)\|f_-\|_{L^p(\mathbb{S}^{n-1},C(\partial X))} + \|S\|_{L^p(\mathbb{S}^{n-1},C(\overline{X}))}\right).$$

If instead (2.11) *holds, we have the estimate*

$$\|u\|_{L^p(\mathbb{S}^{n-1},C(\overline{X}))} \le \frac{1}{1-\operatorname{diam}(X)\rho}\left(\|f_-\|_{L^p(\mathbb{S}^{n-1},C(\partial X))} + \operatorname{diam}(X)\|S\|_{L^p(\mathbb{S}^{n-1},C(\overline{X}))}\right).$$

This well-posedness theorem can ensure the operators we defined later is well-defined, and can be used in the estimation of the operator norm.

We consider the adjoint RTE for derivation. Let $v = v(x,\theta)$ be the solution of the adjoint RTE with prescribed outgoing boundary condition g:

$$-\theta\cdot\nabla v + \sigma v - \int_{\mathbb{S}^{n-1}} k(x,\theta,\theta')v(x,\theta')\,\mathrm{d}\theta' = 0 \tag{2.12}$$

$$v|_{\Gamma_+} = g. \tag{2.13}$$

Theoretically, we know v in the entire space $X\times\mathbb{S}^{n-1}$. Multiply v on both sides of (2.7), multiply u_ε on both sides of (2.12), subtract two equations and integrate over $X\times\mathbb{S}^{n-1}$, integration by parts gives

$$\begin{aligned}\int_{\mathbb{S}^{n-1}}\int_{\partial X} u_\varepsilon v n\cdot\theta\,\mathrm{d}x\,\mathrm{d}\theta = &\int_X\int_{\mathbb{S}^{n-1}}\int_{\mathbb{S}^{n-1}}(k_\varepsilon - k)v(x,\theta)u_\varepsilon(x,\theta')\,\mathrm{d}\theta\,\mathrm{d}\theta'\,\mathrm{d}x\\ &+\int_X\int_{\mathbb{S}^{n-1}} vS_\varepsilon\,\mathrm{d}\theta\,\mathrm{d}x - \int_X\int_{\mathbb{S}^{n-1}}(\sigma_\varepsilon-\sigma)u_\varepsilon v\,\mathrm{d}\theta\,\mathrm{d}x.\end{aligned} \tag{2.14}$$

By the asymptotic expansion on ε, write $u_\varepsilon = u_0 + \varepsilon\delta u$, the first order term gives

$$\begin{aligned}&\int_{\mathbb{S}^{n-1}}\int_{\partial X}\delta u v n\cdot\theta\,\mathrm{d}x\,\mathrm{d}\theta\\ &\quad= -\int_X\int_{\mathbb{S}^{n-1}}\cos(q\cdot x+\varphi)\sigma u v\,\mathrm{d}\theta\,\mathrm{d}x + \int_X\int_{\mathbb{S}^{n-1}}\cos(q\cdot x+\varphi)vS\,\mathrm{d}\theta\,\mathrm{d}x\\ &\qquad+\int_X\int_{\mathbb{S}^{n-1}}\int_{\mathbb{S}^{n-1}}\cos(q\cdot x+\varphi)k(x,\theta,\theta')v(x,\theta)u(x,\theta')\,\mathrm{d}\theta\,\mathrm{d}\theta'\,\mathrm{d}x.\end{aligned} \tag{2.15}$$

Notice that the LHS is known from the adjoint solution v and the boundary measurement u_ε, RHS is an inner product of a cosine function and another function over X. By varying q and φ, the RHS

is exactly the Fourier coefficient of a function's Fourier transform, and we denote the function as H_v:

$$\begin{aligned} H_v(x) \coloneqq & -\int_{\mathbb{S}^{n-1}} \sigma u v \, \mathrm{d}\theta + \int_{\mathbb{S}^{n-1}} v S \, \mathrm{d}\theta \\ & + \int_{\mathbb{S}^{n-1}} \int_{\mathbb{S}^{n-1}} k(x,\theta,\theta') v(x,\theta) u(x,\theta') \, \mathrm{d}\theta' \, \mathrm{d}\theta \\ = & \int_{\mathbb{S}^{n-1}} v(x,\theta) \theta \cdot \nabla u(x,\theta) \, \mathrm{d}\theta, \end{aligned} \tag{2.16}$$

Then we construct the internal functional H_v from the boundary measurement Λ_S^ε.

2.2.1 Anisotropic Source

The optical coefficients in biological objects could depend on both location and direction. For example, since each muscle is made up of muscle fiber groups, the ability of light to propagate along fiber direction and perpendicular to fiber direction differs significantly. In this section, we consider the reconstruction of anisotropic source $S(x,\theta)$, which depend both on spatial location and direction [6].

Let

$$\tau_+(x,\theta) = \min\{t > 0 | x + t\theta \in \partial X\}. \tag{2.17}$$

Since

$$u(x,\theta) = u(x + \tau_+\theta, \theta) - \int_0^{\tau_+(x,\theta)} \theta \cdot \nabla u(x + t\theta, \theta) \, \mathrm{d}t, \tag{2.18}$$

Once $\theta \cdot \nabla u(x,\theta)$ can be reconstructed from the internal functional H_v, the forward RTE solution $u(x,\theta)$ can be calculated by (2.18), then the source $S(x,\theta)$ can be calculated by substituting $u(x,\theta)$ into (2.1).

In order to reconstruct $\theta \cdot \nabla u(x,\theta)$, the controllability of RTE is required:

Proposition 2.2 ([6, Theorem 1.3])**.** *Suppose X, k and σ are given. Then for any point $x_0 \in X$ and any continuous function h on $L^p(\mathbb{S}^{n-1})$, there is a function $g \in L^p(\mathbb{S}^{n-1}, L^\infty(\partial X))$ such that the boundary value problem* (2.12)(2.13) *has a unique solution $v \in L^p(\mathbb{S}^{n-1}, L^\infty(X))$ which is continuous in a neighbourhood of x_0, and satisfies the property that $v(x_0,\theta) = h(\theta)$, for all $\theta \in \mathbb{S}^{n-1}$. Moreover, for any $1 \le p \le \infty$,*

$$\|v\|_{L^p(\mathbb{S}^{n-1}, L^\infty(X))} + \|g\|_{L^p(\mathbb{S}^{n-1}, L^\infty(\partial X))} \le C \|h\|_{L^p(\mathbb{S}^{n-1})}, \tag{2.19}$$

where C depends only on X, k and σ.

With the controllability theorem, for any $x_0 \in X$, we can arrange $v(x_0, \theta)$ to be any continuous function in θ, then knowing $H_v(x_0, \theta)$ for any v is equivalent to knowing $\theta \cdot \nabla u(x_0, \theta)$, thus we can recover $\theta \cdot \nabla u(x, \theta)$ from the internal functional H_v.

2.2.2 Isotropic Source

The inversion formula in Section 2.2.1 requires measurement on each boundary points $(x, \theta) \in \Gamma_+$, which is hard in practice. Besides, the reconstruction needs a lot of computations, since the inversion formula is point-to-point. To this end, we focus on the inverse problem of UMBLT in full RTE model with an isotropic source [28], i.e. the source $S = S(x)$ is independent of the angle θ. We built a more efficient inversion formula to reduce the requirement of measurement and computation.

Since S is independent of θ, the internal functional can be written as

$$\begin{aligned} H_v(x) &= \int_{\mathbb{S}^{n-1}} v(x,\theta)\theta \cdot \nabla u(x,\theta)\,\mathrm{d}\theta \\ &= \int_{\mathbb{S}^{n-1}} v(x,\theta)\left[\mathcal{A}u(x,\theta) + S(x)\right]\mathrm{d}\theta, \\ &= \int_{\mathbb{S}^{n-1}} v(x,\theta)\mathcal{A}u(x,\theta)\,\mathrm{d}\theta + S(x)\int_{\mathbb{S}^{n-1}} v(x,\theta)\,\mathrm{d}\theta, \end{aligned} \tag{2.20}$$

where

$$\mathcal{A}u(x,\theta) \coloneqq -\sigma(x)u(x,\theta) + \int_{\mathbb{S}^{n-1}} k(x,\theta,\theta')u(x,\theta')\,\mathrm{d}\theta'. \tag{2.21}$$

and the norm of S in Proposition 2.1 becomes

$$\|S\|_{L^p(\mathbb{S}^{n-1},C(\overline{X}))} = \mathrm{Vol}(\mathbb{S}^{n-1})^{\frac{1}{p}}\|S\|_{C(\overline{X})},$$

where $\mathrm{Vol}(\mathbb{S}^{n-1})$ denote the volume of $(n-1)$-dimensional unit ball.

With (A1)(A2), we can choose a suitable adjoint solution satisfies $v_0 \geq c > 0$ [28, Lemma 2]. Dividing (2.20) by $\int_{\mathbb{S}^{n-1}} v_0(x,\theta)\,\mathrm{d}\theta$ on both sides gives

$$\frac{H_{v_0}(x)}{\int_{\mathbb{S}^{n-1}} v_0(x,\theta)\,\mathrm{d}\theta} \coloneqq S(x) + \frac{\int_{\mathbb{S}^{n-1}} \mathcal{A}u(x,\theta)v_0(x,\theta)\,\mathrm{d}\theta}{\int_{\mathbb{S}^{n-1}} v_0(x,\theta)\,\mathrm{d}\theta}, \tag{2.22}$$

notice that the LHS is known, the first term on RHS is exactly the source S we want to reconstruct and the second term is linear in u, which is linearly depend on S, the RHS can be written as an identity operator plus a linear operator act on S. To represent the linear operator, we define the following three operators.

The first one is the source-to-solution operator $\mathcal{S}$:

$$\mathcal{S} : C(\overline{X}) \to L^p(\mathbb{S}^{n-1}, C(\overline{X})), \qquad S \mapsto u \tag{2.23}$$

with the norm estimation from the well-posedness Theorem 2.1

$$\|\mathcal{S}\|_{C(\overline{X})\to L^p(\mathbb{S}^{n-1},C(\overline{X}))} \leq \begin{cases} \frac{\mathrm{Vol}(\mathbb{S}^{n-1})^{\frac{1}{p}}}{\alpha} & \left(\inf_{x\in\overline{X}} \sigma\right) - \rho \geq \alpha \\ \frac{\mathrm{diam}(X)\mathrm{Vol}(\mathbb{S}^{n-1})^{\frac{1}{p}}}{1-\mathrm{diam}(X)\rho} & \mathrm{diam}(X)\rho < 1 \end{cases} \tag{2.24}$$

The second operator is

$$\mathcal{K}_{v_0} : L^p(\mathbb{S}^{n-1}, C(\overline{X})) \to C(\overline{X}), \qquad u(x,\theta) \mapsto \int_{\mathbb{S}^{n-1}} \mathcal{A}u(x,\theta) v_0(x,\theta)\, \mathrm{d}\theta \tag{2.25}$$

where the operator $\mathcal{A}$ is introduced in (2.21). $\mathcal{K}_{v_0}$ is a bounded operator and

$$\|\mathcal{K}_{v_0}\|_{L^p(\mathbb{S}^{n-1},C(\overline{X}))\to C(\overline{X})} \leq \|v_0\|_{C(\overline{X})}(\|\sigma\|_{C(\overline{X})} + \rho)\mathrm{Vol}(\mathbb{S}^{n-1})^{1-\frac{1}{p}} \tag{2.26}$$

The third operator is the multiplication operator

$$\mathcal{M}_{v_0} : C(\overline{X}) \to C(\overline{X}), \qquad f(x) \mapsto \frac{1}{\int_{\mathbb{S}^{n-1}} v_0(x,\theta)\, \mathrm{d}\theta} f(x). \tag{2.27}$$

It is bounded since v_0 is chosen in such a way that $\int_{\mathbb{S}^{n-1}} v_0(x,\theta)\, \mathrm{d}\theta$ is bounded away from zero. We have

$$\|\mathcal{M}_{v_0}\|_{C(\overline{X})\to C(\overline{X})} \leq \frac{1}{\inf_{x\in\overline{X}} \left(\int_{\mathbb{S}^{n-1}} v_0(x,\theta)\, \mathrm{d}\theta\right)}. \tag{2.28}$$

Then (2.22) can be represented as

$$\mathcal{M}_{v_0}[H_{v_0}] = (Id + \mathcal{M}_{v_0} \circ \mathcal{K}_{v_0} \circ \mathcal{S})[S].$$

To invert linear operator $Id + \mathcal{M}_{v_0} \circ \mathcal{K}_{v_0} \circ \mathcal{S}$, there are two approaches. The first one is to prove $\mathcal{M}_{v_0} \circ \mathcal{K}_{v_0} \circ \mathcal{S}$ is a contraction under certain norm, then we can use Neumann series to invert this

operator. The second approach is to prove $\mathcal{M}_{v_0} \circ \mathcal{K}_{v_0} \circ \mathcal{S}$ is compact over certain function space, then $Id + \mathcal{M}_{v_0} \circ \mathcal{K}_{v_0} \circ \mathcal{S}$ is a Fredholm operator, we can use Fredolm inversion to solve S.

For the first approach, the inversion formula is given in the following theorem

Theorem 2.3 ([28, Theorem 3]). *Suppose the assumptions (A1)(A2) hold. If the following inequality holds*

$$\frac{\|v_0\|_{C(\overline{X})}(\|\sigma\|_{C(\overline{X})} + \rho)\mathrm{diam}(X)\mathrm{Vol}(\mathbb{S}^{n-1})}{(1 - \mathrm{diam}(X)\rho)\inf_{x\in\overline{X}}\left(\int_{\mathbb{S}^{n-1}} v_0(x,\theta)\,\mathrm{d}\theta\right)} < 1 \text{ when } \mathrm{diam}(X)\rho < 1, \tag{2.29}$$

then the operator $\mathcal{M}_{v_0} \circ \mathcal{K}_{v_0} \circ \mathcal{S}$ is a contraction, and the source S can be computed from the following Neumann series:

$$S = \sum_{j=0}^{\infty} (-\mathcal{M}_{v_0} \circ \mathcal{K}_{v_0} \circ \mathcal{S})^j (\mathcal{M}_{v_0}[H_{v_0}]).$$

For the second approach, we need additional assumptions on optical coefficients. For $s \in \mathbb{R}$, let $W^{s,2}$ be the usual L^2-based Sobolev space, for $1 \le p \le \infty$, let $\mathcal{H}_p^1$ be the following function space

$$\mathcal{H}_p^1 := \left\{u \in L^p(X \times \mathbb{S}^{n-1}) \mid \theta \cdot \nabla u \in L^p(X \times \mathbb{S}^{n-1})\right\}$$

with norm

$$\|u\|_{\mathcal{H}_p^1} = \left(\int_{X\times\mathbb{S}^{n-1}} |u|^p + |\theta \cdot \nabla u|^p \,\mathrm{d}x\,\mathrm{d}\theta\right)^{\frac{1}{p}}.$$

we make following assumptions

(A3): $\sigma(x) \ge \sigma_0 > 0$ everywhere in X for some constant σ_0.

(A4): $\|\frac{1}{\sigma(x)}\int_{\mathbb{S}^{n-1}} k(x,\theta,\theta')\,\mathrm{d}\theta'\|_{L^\infty(X\times S^{n-1})} \le k_0 < 1$ for some constant k_0.

(A5): $\sigma(x) \in W^{1,2}(X)$, $k(x,\theta,\theta') \in W^{1,2}(X)$ for any $\theta, \theta' \in \mathbb{S}^{n-1}$.

Here (A3) and (A4) are to ensure the well-posedness of forward RTE in $\mathcal{H}_2^1$, see Proposition 2.4. (A5) is used in the averaging lemma [32].

Proposition 2.4 ([1, Theorem 3.2]). *For any $S(x) \in L^2(X)$, the boundary value problem* (2.1) (2.2) *admits a unique solution $u \in \mathcal{H}_2^1$. Moreover, the following estimate holds for some constants $C,\ \tilde{C} > 0$ independent of S and u :*

$$C\|S\|_{L^2(X)} \le \|u\|_{\mathcal{H}_2^1} \le \tilde{C}\|S\|_{L^2(X)}.$$

Proposition 2.5. *The operator $\mathcal{M}_{v_0} \circ \mathcal{K}_{v_0} \circ \mathcal{S} : L^2(X) \to L^2(X)$ is compact.*

Proof. Since X is bounded and $S(x) \in C(\overline{X})$, we have $S(x) \in L^2(X)$, hence $u \in \mathcal{H}_2^1$ by Proposition 2.4. Similarly, we have $v_0, \sigma v_0 \in L^2(X \times \mathbb{S}^{n-1})$. Moreover,

$$\begin{aligned}
&\left(\int_X \int_{\mathbb{S}^{n-1}} \left| \int_{\mathbb{S}^{n-1}} k(x,\theta,\theta') v_0(x,\theta') \, \mathrm{d}\theta' \right|^2 \mathrm{d}\theta \, \mathrm{d}x \right)^{\frac{1}{2}} \\
\leq & \mathrm{Vol}(\mathbb{S}^{n-1})^{\frac{1}{2}} \left(\int_X \int_{\mathbb{S}^{n-1}} \int_{\mathbb{S}^{n-1}} (\sup |k|)^2 \, |v_0(x,\theta')|^2 \, \mathrm{d}\theta' \, \mathrm{d}\theta \, \mathrm{d}x \right)^{\frac{1}{2}} \\
= & \sup |k| \mathrm{Vol}(\mathbb{S}^{n-1}) \|v_0\|_{L^2(X \times \mathbb{S}^{n-1})} < \infty,
\end{aligned}$$

then from (2.12), we have $\theta \cdot \nabla v_0(x,\theta) \in L^2(X \times \mathbb{S}^{n-1})$, thus $v_0 \in \mathcal{H}_2^1$.

The assumption (A5) ensures $\sigma u v_0 \in \mathcal{H}_2^1$ and $\int_{\mathbb{S}^{n-1}} k(x,\theta,\theta') u(x,\theta) v_0(x,\theta) \, \mathrm{d}\theta' \in \mathcal{H}_2^1$, then the Averaging Lemma (see [32, Theorem 1.1]) implies $\mathcal{K}_{v_0} \circ \mathcal{S}[S] \in W^{\frac{1}{2},2}(X)$.

As the embedding $W^{\frac{1}{2},2}(X) \hookrightarrow L^2(X)$ is compact, the operator $\mathcal{K}_{v_0} \circ \mathcal{S}$ is a compact operator from $(C(\overline{X}), \|\cdot\|_2)$ to $L^2(X)$, which can be extend to be a compact operator defined on the entire space $L^2(X)$. We slightly abuse the notation and denote such extension again by $\mathcal{K}_{v_0} \circ \mathcal{S}$.

On the other hand, the multiplication operator $\mathcal{M}_{v_0}$ can be extended to be a bounded operator on $L^2(X)$. Thus, the operator $\mathcal{M}_{v_0} \circ \mathcal{K}_{v_0} \circ \mathcal{S} : L^2(X) \to L^2(X)$, as the composition of a bounded operator with a compact operator, is compact as well. □

We therefore have the following result due to the Fredholm alternative.

Theorem 2.6 ([28, Theorem 5])**.** *Suppose the assumptions (A1)~(A5) hold. If 0 is not an eigenvalue of the Fredholm operator $Id + \mathcal{M}_{v_0} \circ \mathcal{K}_{v_0} \circ \mathcal{S}$, then $(Id + \mathcal{M}_{v_0} \circ \mathcal{K}_{v_0} \circ \mathcal{S})^{-1}$ is a bounded linear operator on $L^2(X)$, and the source S can be computed as*

$$S = (Id + \mathcal{M}_{v_0} \circ \mathcal{K}_{v_0} \circ \mathcal{S})^{-1} (\mathcal{M}_{v_0}[H_{v_0}]).$$

Then the stability estimation is immediately obtained from the inversion formulae

Corollary 2.7. *Suppose the assumptions (A1)~(A5) hold. Let S and $\tilde{S}$ be two different sources with corresponding internal functional H_{v_0} and $\tilde{H}_{v_0}$, respectively. If 0 is not an eigenvalue of the*

operator $Id + \mathcal{M}_{v_0} \circ \mathcal{K}_{v_0} \circ \mathcal{S}$*, then the following stability estimate holds*

$$\|S - \tilde{S}\|_{L^2(X)} \leq C\|H_{v_0} - \tilde{H}_{v_0}\|_{L^2(X)}$$

for some constant $C > 0$ *depending on* σ*,* k*,* v_0*,* X *yet independent of* S *and* $\tilde{S}$*.*

2.2.3 Numerical Experiment

In this section, we test our algorithm in Section 2.2.2. For the numerical experiment, we consider the two dimension cases, X is a square in $\mathbb{R}^2$, the coordinate is denoted as (x_1, x_2), and we choose the scattering kernel to be the Henyey-Greenstein function

$$k(x, \theta, \theta') = \frac{1}{2\pi} \frac{1 - g^2}{1 + g^2 - 2g\cos\phi},$$

where ϕ is the angle between θ and θ', and $-1 \leq g \leq 1$ is the anisotropy parameter of the medium.

In this section, we present a number of numerical experiments. We discretize the spatial domain into a 121×121 uniform grid and the angular space into $M = 8$ directions for the forward issue. In order to prevent the inverse crime, we interpolate the measurement using a spatial 61×61 uniform grid for the reconstruction. Employing a 121×121 spatial grid with a coarser angular mesh $M = 8$ and a finer mesh $M = 16$, we compared the forward solutions. Next, a projection of the $M = 16$ solution onto the coarser mesh is made, and the results are compared with the previous solution. Relative L^2-error as a result is 0.0447%. All the numerical experiments are performed on a Windows 10 laptop with Intel Core i7-9750H 2.6GHz CPU and 16GB RAM.

2.2.3.1 RTE Solver

In order to develop a RTE solver, since u depend on the spatial domain X and angular domain $\mathbb{S}^1$, we uniformly discrete the angular space and use upwind scheme for spatial discretization.

The angular space $[0, 2\pi)$ is uniformly discretized into M angles, denote as $\omega_i = (i-1)\Delta\omega$ with $\Delta\omega = \frac{2\pi}{M}$. Then the integral over $\mathbb{S}^1$ can be discretized using the trapezoidal rule

$$\int_{\mathbb{S}^1} k(x, \theta', \theta)u(x, \theta)\,\mathrm{d}\theta \approx \sum_{i=1}^{M} k(x, \theta', \theta_i)u(x, \theta_i)\Delta\omega.$$

The spatial discretization uses the upwind scheme, which is

$$\frac{\partial u}{\partial x_1}(x_1, x_2, \theta_i) \approx \operatorname{sgn}(\cos\omega_i)\frac{u(x_1 + \operatorname{sgn}(\cos\omega_i)\Delta x_1, x_2, \theta_i) - u(x_1, x_2, \theta_i)}{\Delta x_1},$$
$$\frac{\partial u}{\partial x_2}(x_1, x_2, \theta_i) \approx \operatorname{sgn}(\sin\omega_i)\frac{u(x_1, x_2 + \operatorname{sgn}(\sin\omega_i)\Delta x_2, \theta_i) - u(x_1, x_2, \theta_i)}{\Delta x_2}.$$

where Δx_1 and Δx_2 are the spacings along the x_1-direction and x_2-direction, respectively. Although the fraction in the scheme above is not an approximation of the derivative when $\sin\omega_i$ or $\cos\omega_i$ is 0, but in these cases, the product with the sign function is still 0 as expected.

With the discretization in spatial domain and angular spaces, we use the Jacobi iteration method to solve the RTE and the adjoint RTE.

Given a known source S, we generate the measurement $H_v(x)$ in the following steps. First, we find the solution $u(x, \theta)$ by solving the forward problem (2.1) (2.2) using the RTE solver. This, together with the known attenuation coefficient and scattering kernel, is employed to compute $\mathcal{A}u(x, \theta)$ in (2.21). Finally, we solve the adjoint RTE (2.12) (2.13) to get v, and compute $H_v(x)$ in (2.20) with the trapezoidal rule. Since $\theta \in \mathbb{S}^1$ is periodic, the discrete integration is simply

$$\int_{\mathbb{S}^1} f(\theta)\,\mathrm{d}\theta \approx \sum_{i=1}^{M} f(\theta_i)\Delta\theta.$$

We test our algorithms in continuous and discontinuous cases based on the assumptions of inversion formulae.

2.2.3.2 Neumann Series Inversion

The algorithm for Theorem 2.3 is simple. The operator $\mathcal{S}$ can be implemented using the forward RTE solver, the operator $\mathcal{K}_{v_0}$ and $\mathcal{M}_{v_0}$ can be discretized using the trapezoidal rule, then the reconstruction can be done by an iteration, see Algorithm 2.1

2.2.3.3 Fredholm Inversion

The Fredholm inversion in Theorem 2.6 boils down to solving the linear system (2.31). For this purpose, we discretize the source S with respect to some basis functions. Two types of basis functions are used, one is polynomial functions of the form $\{x_1^i x_2^j\}_{i,j\geq 0,\, i+j\leq 10}$, which is used to

Data: adjoint RTE solution v_0, measurement H_{v_0}, scattering kernel $k(x, \theta, \theta')$, attenuation coefficient $\sigma(x)$, domain X.

$S \leftarrow 0$;
$\Delta S \leftarrow \mathcal{M}_{v_0}[H_{v_0}]$;
$\varepsilon \leftarrow 10^{-6}$;
while $\|\Delta S\|_{L^2} > \varepsilon$ **do**
  $S \leftarrow S + \Delta S$;
  $\Delta S \leftarrow \mathcal{M}_{v_0} \circ \mathcal{K}_{v_0} \circ \mathcal{S}[\Delta S]$;
end
return S;

Algorithm 2.1 Neumann Series Reconstruction.

represent the smooth feature of the source; the other is the following functions

$$f_{ij} = \max\left\{1 - \max\left\{20\left|x_1 - \frac{i}{20}\right|, 20\left|x_2 - \frac{j}{20}\right|\right\}, 0\right\}, \quad i, j \in \{0, 1, \ldots, 20\}.$$

which is inspired from the finite element basis functions. Note f_{ij} a pyramid-shaped function with the tip at $(\frac{i}{20}, \frac{j}{20})$, it captures some information of singularities. We write the expansion of a source S with respect to these basis functions as

$$S(x_1, x_2) \approx \sum_{i,j\geq 0, i+j\leq 10} c_{ij} x_1^i x_2^j + \sum_{0\leq i,j\leq 20} c'_{ij} f_{ij} =: \sum_i \tilde{c}_i b_i, \tag{2.30}$$

where c_{ij}, c'_{ij} are the coefficients of the expansion. We use $\{b_i(x_1, x_2)\}$ to denote these basis functions and $\{\tilde{c}_i\}$ the correponding coefficients.

Denote $\mathcal{T} := Id + \mathcal{M}_{v_0} \circ \mathcal{K}_{v_0} \circ \mathcal{S}$, then the internal measurement (2.22) can be represented as

$$\mathcal{M}_{v_0}[H_{v_0}] = \mathcal{T}[S] \approx \sum_i \tilde{c}_i \mathcal{T}[b_i].$$

We can compute the inner product with $\mathcal{T}[b_j]$ as follows:

$$\langle \mathcal{M}_{v_0}[H_{v_0}], \mathcal{T}[b_j] \rangle \approx \sum_i \tilde{c}_i \langle \mathcal{T}[b_i], \mathcal{T}[b_j] \rangle. \tag{2.31}$$

Solving the linear equation (2.31) gives the coefficient $\tilde{c}_i$, and then we can numerically reconstruct the projection of the source S on the chosen basis.

2.2.3.4 Experiment 1: Continuous Source

In this experiment, we choose the spatial domain $X = [0, 0.2]^2$ with attenuation coefficient $\sigma_1(x_1, x_2) = 0.1 + 0.1x_1$ and anisotropy parameter $g = 0.5$ in the scattering kernel. v_0 is chosen as

the adjoint solution with boundary condition $v_0|_{\Gamma_+} = 1$. The source is chosen as

$$S_1(x_1, x_2) = e^{-100[(x_1-0.08)^2+(x_2-0.12)^2]},$$

see Figure 2.1.

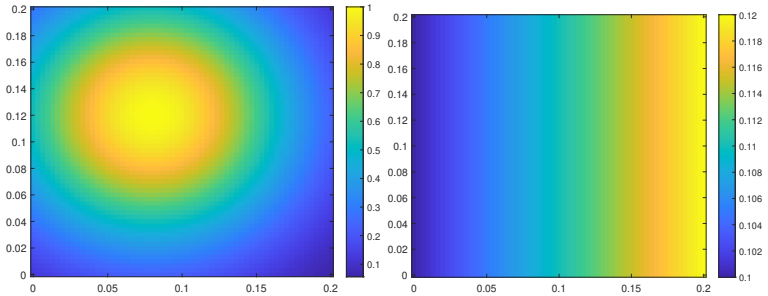

Figure 2.1 Left: source S_1. Right: attenuation coefficient σ_1.

Such choice of optical coefficients gives the following numerical values:

$$\|v_0\|_{C(\overline{X})} \approx 1.2603, \qquad \inf_{x\in\overline{X}} \left(\int_{\mathbb{S}^1} v_0(x,\theta)\, \mathrm{d}\theta \right) \approx 6.4870.$$

On the other hand, $\rho \equiv 1$ for any anisotropy parameter between -1 and 1, thus

$$\frac{\|v_0\|_{C(\overline{X})}(\|\sigma_1\|_{C(\overline{X})} + \rho)\mathrm{diam}(X)\mathrm{Vol}(\mathbb{S}^1)}{(1 - \mathrm{diam}(X)\rho)\inf_{x\in\overline{X}} \left(\int_{\mathbb{S}^1} v_0(x,\theta)\, \mathrm{d}\theta \right)} \approx 0.5392 < 1,$$

thus the optical coefficients satisfy the condition of Theorem 2.3. Applying Neumann series inversion with different levels of Gaussian noise added to H_{v_0} gives the following result, see Figure 2.2.

2.2.3.5 Experiment 2: Discontinuous Source

We choose the spatial domain $X = [0, 1]^2$ with attenuation coefficient $\sigma_1(x_1, x_2) = 0.1 + 0.1x_1$. The anisotropy parameter is still $g = 0.5$ and v_0 is chosen as the adjoint solution with boundary condition $v_0|_{\Gamma_+} = 1$. The source S_2 is chosen as the Shepp-Logan Phantom, see left and right panels of Figure 2.3.

Apply Neumann series inversion with different levels of Gaussian noise added to H_{v_0} gives the following result, see Figure 2.4.

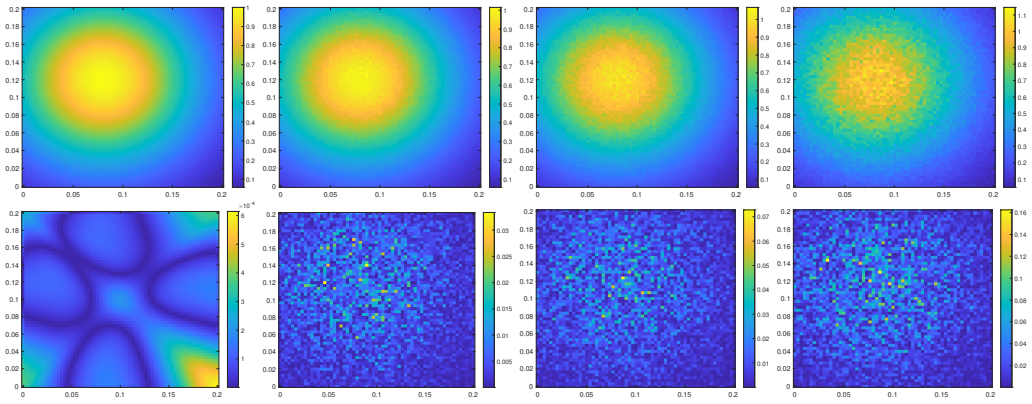

Figure 2.2 Reconstructed S_1 using Neumann series. For the first row, 0%, 1%, 2%, 5% random noises are added to H_{v_0}. The relative L^2 errors of the reconstructions are 0.0268%, 1.0682%, 2.1759%, 5.4680%, respectively. The second row displays the corresponding differences between the ground truth and the reconstructions.

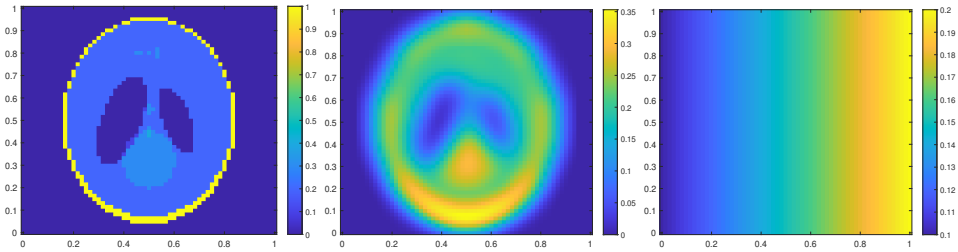

Figure 2.3 Left: Shepp-Logan Phantom S_2. Center: Smoothed Shepp-Logan Phantom S_3. Right: attenuation coefficient σ_1.

The errors of reconstruction is very large since we choose finitely many continuous basis to approximate a discontinuous source. If we change the source to the Gaussian filtered Shepp-Logan Phantom, see the middle panel of Figure 2.3, the reconstruction becomes better, see Figure 2.5.

2.2.3.6 More experiments:

We also test the performance of the inversion formulae in different cases, such as Neumann inversion beyond the assumption of Theorem 2.3, and the Fredholm inversion in continuous case, see [28, section 4.2] for more details.

2.3 UMBLT under Diffusive Regime

Biological objects are usually strongly scattering medium. The light propagation in strongly scattering medium is diffusive. It can be simplified as diffusive regime, which is called the diffusion approximation [5], see also Appendix A. The diffusive regime models the light propagation using

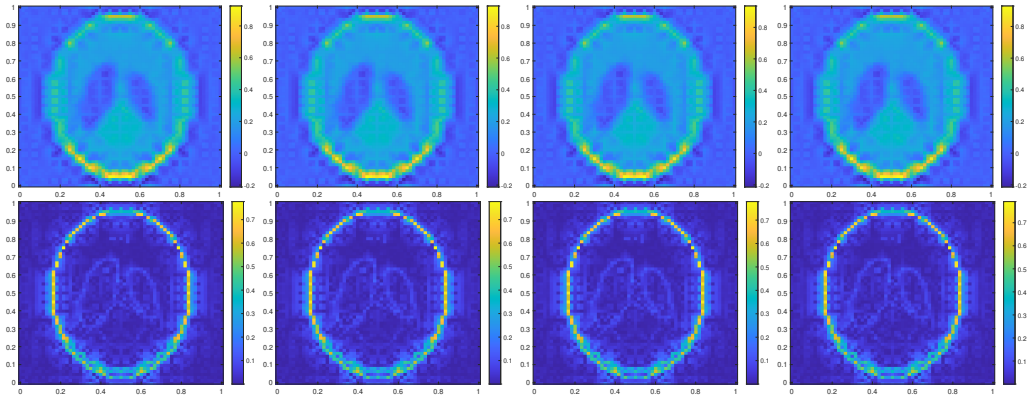

Figure 2.4 Reconstructed S_2 using Fredholm inversion. For the first row, 0%, 1%, 2%, 5% random noises are added to H_{v_0}. The relative L^2 errors of the reconstructions are 57.5806%, 57.5818%, 57.5880%, 57.6199%, respectively. The second row displays the corresponding differences between the ground truth and the reconstructions.

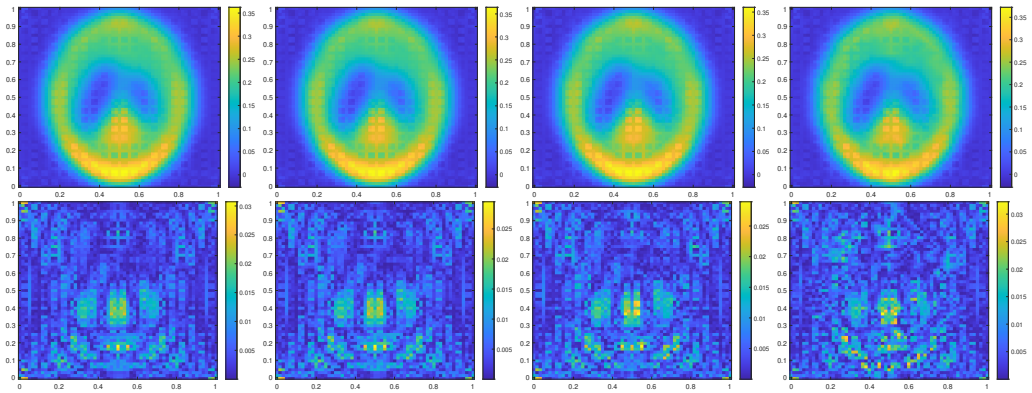

Figure 2.5 Reconstructed S_3 using Fredholm inversion. For the first row, 0%, 1%, 2%, 5% random noises are added to H_{v_0}. The relative L^2 errors of the reconstructions are 4.3211%, 4.3405%, 4.4136%, 5.0152%, respectively. The second row displays the corresponding differences between the ground truth and the reconstructions.

the following diffusion equation [8]

$$-\nabla \cdot D(x)\nabla\phi(x) + \sigma_a(x)\phi(x) = S(x) \qquad \text{in } X. \tag{2.32}$$

$$\phi + \ell\nu \cdot D\nabla\phi = 0 \qquad \text{on } \partial X. \tag{2.33}$$

where the positive definite matrix function D is the diffusion coefficient, σ_a is the absorption coefficient, ℓ is the extrapolation length, ν is the outer normal vector and ϕ is the angularly averaged intensity of light.

The ultrasound modulation is modeled as [8]

$$D_\varepsilon(x) \coloneqq (1+\varepsilon(2\gamma-1)\cos(q\cdot x+\varphi))D(x), \tag{2.34}$$

$$\sigma_{a,\varepsilon}(x) \coloneqq (1+\varepsilon(2\gamma+1)\cos(q\cdot x+\varphi))\sigma_a(x), \tag{2.35}$$

$$S_\varepsilon(x) \coloneqq (1+\varepsilon\cos(q\cdot x+\varphi))S(x), \tag{2.36}$$

where γ is the elasto-optical constant, q is the wave vector, φ is the phase and $0 \le \varepsilon \ll 1$ is a small parameter related to the amplitude, frequency, time, density and acoustic wave speed.

Then the UMBLT under diffusion approximation is modeled as

$$-\nabla\cdot D_\varepsilon(x)\nabla\phi_\varepsilon(x)+\sigma_{a,\varepsilon}(x)\phi_\varepsilon(x) = S_\varepsilon(x) \quad \text{in } X. \tag{2.37}$$

$$\phi_\varepsilon + \ell\nu\cdot D_\varepsilon\nabla\phi_\varepsilon = 0 \quad \text{on } \partial X. \tag{2.38}$$

Under different modulations, our measurement is the Neumann boundary value

$$-\nu\cdot D_\varepsilon\nabla\phi_\varepsilon|_{\mathcal{G}}, \qquad \varepsilon \ge 0,$$

which is considered as the output flux on boundary. Here $\mathcal{G}\subset\partial X$ is a relatively open subset which denotes the region of measurement. The goal is to reconstruct the distribution of S assuming D, σ_a, Γ and X are given.

2.3.1 Full Data Case

In this section, we start with a simple case $\mathcal{G}=\partial X$, which means we can make measurement on the entire boundary. Such case is called UMBLT under diffusive regime with full data [8]. Similar to the UMBLT under transport regime, we consider the adjoint diffusion equation with prescribed Robin boundary condition g

$$-\nabla\cdot D(x)\nabla\psi(x)+\sigma_a(x)\psi(x) = 0 \quad \text{in } X. \tag{2.39}$$

$$\psi + l\nu\cdot D\nabla\psi = g \quad \text{on } \partial X. \tag{2.40}$$

Since D and σ_a are known, we know ψ in the entire space X. Multiply ψ on both sides of (2.37), multiply ϕ_ε on both sides of (2.39), subtract two equations and integrate over X. Integration by

parts gives

$$\int_{\partial X} g\nu \cdot D_\varepsilon \nabla \phi_\varepsilon \, \mathrm{d}x = \int_X (D_\varepsilon - D_0)\nabla\phi_\varepsilon \cdot \nabla\psi + (\sigma_{a,\varepsilon} - \sigma_{a,0})\phi_\varepsilon\psi - \psi S_\varepsilon \, \mathrm{d}x, \tag{2.41}$$

By the asymptotic expansion on ε, write $\nu \cdot D_\varepsilon \nabla \phi_\varepsilon = \nu \cdot D\nabla\phi_0 + \varepsilon\delta\Phi$, the first order term gives

$$\int_{\partial X} g\delta\Phi \, \mathrm{d}x = \int_X ((2\gamma - 1)D\nabla\phi_0 \cdot \nabla\psi + (2\gamma + 1)\sigma_a\phi_0\psi - \psi S)\cos(q \cdot x + \varphi) \, \mathrm{d}x. \tag{2.42}$$

Notice that the LHS is theoretically known from the Neumann boundary measurement and the adjoint boundary condition, RHS is an inner product of a cosine function and another function over X. By varying q and φ, the RHS is exactly the Fourier coefficient of a function's Fourier transform, and we denote the function as H_ψ:

$$H_\psi \coloneqq (2\gamma - 1)D\nabla\phi_0 \cdot \nabla\psi + (2\gamma + 1)\sigma_a\phi_0\psi - \psi S. \tag{2.43}$$

For a specific $\psi_0 > 0$, dividing ψ_0 on both sides and substitute (2.32) to replace the S term, we have the following PDE

$$F_{\psi_0} \coloneqq \frac{H_{\psi_0}}{\psi_0} = (2\gamma - 1)D\nabla\phi_0 \cdot \nabla \log\psi_0 + 2\gamma\sigma_a\phi_0 + \nabla \cdot D(x)\nabla\phi_0 \tag{2.44}$$

with boundary condition (2.33). Once 0 is not an eigenvalue of the PDE, the solution ϕ_0 can be uniquely determined, substitute ϕ_0 to (2.32) will give us S.

2.3.2 Partial Data Case

In the proposed full data algorithms, see Section 2.3.1, the measurement is required on the entire boundary ∂X. But in practice, it is hard to obtain all data on the boundary. For example, for the brain imaging, the sensors could only be placed on the top half of head, the data in the neck-direction will lost. A natural question is: Can we determine the source from measurements only on a subset on the boundary? Such question is considered as inverse problem with partial data. If the sources can be determined from partial data, then the full data measurement is redundant, the partial data algorithm would be an improved algorithm for those sources.

Suppose we can only measure on a relatively open subset $\mathcal{G} \subset \partial X$, i.e. $\delta\Phi$ in (2.42) is known only on a subset $\mathcal{G}$. A natural idea is to choose a special prescribed boundary condition g such that

g is supported on $\mathcal{G}$, then the left hand side of (2.42) is still known from the boundary measurement and boundary condition g. In this case, we need to show that there exist such boundary condition g support on $\mathcal{G}$ and gives positive adjoint solution ψ.

Instead of consider adjoint equation (2.39) with Robin boundary condition (2.40), we consider the following diffusion equation with mixed boundary condition

$$-\nabla \cdot D(x)\nabla\psi(x) + \sigma_a(x)\psi(x) = 0 \quad \text{in } X. \tag{2.45}$$

$$\psi + \ell\nu \cdot D\nabla\psi = 0 \quad \text{on } \partial X \setminus \mathcal{G}. \tag{2.46}$$

$$\psi = f \quad \text{on } \mathcal{G}. \tag{2.47}$$

Once we find a positive solution ψ to this mixed boundary value problem, we can simply take $g = (\psi + \ell\nu \cdot D\nabla\psi)|_{\partial X}$ to be the prescribed boundary condition in the adjoint problem (2.39)-(2.40).

Throughout this section, the following hypotheses are made upon the anisotropic diffusion coefficient $D(x)$ and the scattering coefficient $\sigma_a(x)$:

H1 $D(x) = I$ near ∂X, where I is the identity matrix.

H2 $\sigma_a \in C^\alpha(X), D_{ij} \in C^{1,\alpha}(X)$

H3 $D(x)$ is uniformly elliptic for all $x \in X$, that is, there exists a constant $\lambda > 0$ such that

$$\frac{1}{\lambda}|\xi|^2 \geq \xi^\top D(x)\xi \geq \lambda|\xi|^2 \quad \text{a.e. on } \overline{X}$$

holds for any $\xi \in \mathbb{R}^n$.

H4 $\sigma_a \geq 0$ a.e. on $\overline{X}$.

Theorem 2.8 ([65, Theorem 1]). *Assume that*

$$\sigma_a \in C^\alpha(X), \qquad D_{ij} \in C^{1,\alpha}(X), \qquad f \in C(\mathcal{G}) \cap L^\infty(\mathcal{G}),$$

then (2.45)-(2.47) *has a unique solution* $\psi \in C^2(\overline{X} \setminus \overline{\mathcal{G}}) \cap C^0(\overline{X})$

Theorem 2.9 ([97]). *Under the hypotheses **H1**-**H4**. If the Dirichlet boundary condition $f \in C(\mathcal{G}) \cap L^\infty(\mathcal{G})$ is positive, then the mixed boundary value problem* (2.45)-(2.47) *admits a unique solution $\psi \in C^2(\overline{X} \setminus \overline{\mathcal{G}}) \cap C^0(\overline{X})$ which is positive on $\overline{X}$.*

Proof. Theorem 2.8 ensure that (2.45)-(2.47) have a unique solution $\psi \in C^2(\overline{X} \setminus \overline{\mathcal{G}}) \cap C^0(\overline{X})$.

Assuming that ψ has a negative value on $\overline{X}$, the minimum is reached on the boundary ∂X, according to the weak maximum principle [41, Section 6.4 Theorem 2]. The minimum is attained on $\partial X \setminus \mathcal{G}$ since $\psi|_{\mathcal{G}} > 0$. Assume that $\psi(x_0) = \inf_{x \in \overline{X}} \psi < 0$ and that $x_0 \in \partial X \setminus \mathcal{G}$. The Robin boundary condition (2.46) states that $\nu \cdot D\nabla\psi > 0$, meaning that $\partial_\nu \psi(x_0) > 0$ because $D(x) = I$ is close to ∂X. This contradicts the assumption $\psi(x_0) = \inf_{x \in \overline{X}} \psi$, implying that $\psi \geq 0$.

The strong maximum principle [41, Section 6.4 Theorem 4] indicate that $\psi|_X > 0$, otherwise $\psi \equiv 0$, which contradict to $\psi|_{\mathcal{G}} = f > 0$. It remains to prove $\psi|_{\partial X} > 0$.

Assume on $x_0 \in \partial X \setminus \mathcal{G}$, $\psi(x_0) = \inf_{x \in \overline{X}} \psi = 0$. Apply the Hopf Lemma [41, Section 6.4 Lemma] on $-\psi$ shows that $\partial_\nu \psi(x_0) < 0$, which contradict to the boundary condition $\psi(x_0) + \ell \nu \cdot D\nabla\psi = 0$, thus $\psi|_{\partial X} > 0$.

Thus ψ is a positive solution in $C^2(\overline{X} \setminus \overline{\mathcal{G}}) \cap C^0(\overline{X})$. Since $\overline{X}$ is compact, ψ have positive lower bound. □

The theorem above ensures that one can construct a suitable positive adjoint solution ψ, then the source S can be recovered under the same process as the full data case.

2.3.3 Uncertainty Quantification

The reconstruction methods described in Section 2.3.1 and Section 2.3.2 depend primarily on precise prior knowledge of the optical coefficients (D, σ) to solve the elliptic equation (2.44) (along with boundary conditions) for ϕ_0. The rationale is that these optical coefficients can be measured beforehand using other imaging modalities, such as optical tomography [5]. In practice, the imaging process in these additional modalities inevitably introduces inaccuracies in the optical coefficients, which have an impact on UMBLT reconstruction. In the following two sections, we will use the continuous and discretized models to quantify the impact on the reconstruction of the

bio-luminescence source S caused by optical coefficient inaccuracies.

Let (D, σ_a) be the underlying true optical coefficients, and $(\tilde{D}, \tilde{\sigma}_a)$ be the optical coefficients that are reconstructed through additional imaging modalities before performing UMBLT. Observe that $(\tilde{D}, \tilde{\sigma}_a)$ do not play a role in the derivation of the internal data: This is because the boundary integral on the left hand side of (2.42) remains the same, thus we can derive H_ψ as before. Hereafter, we will assume that the internal data H_ψ has been accurately extracted, and focus on quantifying the uncertainty of the reconstructed source S. The full data and partial data cases will be handled in one shot, since the reconstruction process are identical once a suitable positive adjoint solution $\psi_0 > 0$ is chosen.

2.3.3.1 Uncertainty Quantification with Continuous Diffusive Model

We record a regularity result for the diffusion equation with Robin boundary conditions.

Proposition 2.10 ([33, Theorem 2.4]). *Suppose D is uniformly elliptic, $D_{ij} \in L^\infty(X)$, $\sigma_a \geq 0$ a.e. For $S \in L^2(X)$ and $g \in H^{\frac{1}{2}}(\partial X)$, the following boundary value problem*

$$-\nabla \cdot D(x)\nabla\phi(x) + \sigma_a(x)\phi(x) = S(x) \quad \text{in } X. \tag{2.48}$$

$$\phi + \ell\nu \cdot D\nabla\phi = g \quad \text{on } \partial X. \tag{2.49}$$

admits a unique solution $\phi \in H^2(X)$ with the estimation

$$\|\phi\|_{H^2(X)} \leq C(\|S\|_{L^2(X)} + \|g\|_{H^{\frac{1}{2}}(\partial X)}) \tag{2.50}$$

where C is a constant independent of ϕ.

Then we have the following global uncertainty quantification (UQ) estimate for the aforementioned UMBLT reconstruction in the diffusive regime.

Theorem 2.11 ([97]). *Suppose all optical coefficients and solutions satisfy*

$$\|D_{ij}\|_{W^{1,\infty}(X)}, \|\tilde{D}_{ij}\|_{W^{1,\infty}(X)} \leq C_D, \qquad \|\phi\|_{W^{2,\infty}(X)}, \|\tilde{\phi}\|_{W^{2,\infty}(X)} \leq C_\phi,$$

$$\|\psi\|_{W^{2,\infty}(X)}, \|\tilde{\psi}\|_{W^{2,\infty}(X)} \leq C_\psi, \qquad \|\sigma_a\|_{L^\infty(X)} \leq C_\sigma,$$

$$\psi, \tilde{\psi} \geq c_\psi > 0,$$

where $C_D, C_\phi, C_\psi, C_\sigma, c_\psi$ are constants, and 0 is not eigenvalue of the following operators equipped with the zero Robin boundary condition:

$$\nabla \cdot D\nabla + (2\gamma - 1)D\nabla \log \psi_0 \cdot \nabla + 2\gamma\sigma_a, \quad \nabla \cdot \tilde{D}\nabla + (2\gamma - 1)\tilde{D}\nabla \log \tilde{\psi}_0 \cdot \nabla + 2\gamma\tilde{\sigma}_a,$$

then we can find constants $C_{1ij}, C_2 > 0$ such that

$$\|S - \tilde{S}\|_{L^2(X)} \leq \sum_{i \leq j} C_{1ij} \|(D - \tilde{D})_{ij}\|_{H^1(X)} + C_2 \|\sigma_a - \tilde{\sigma}_a\|_{L^2(X)} \tag{2.51}$$

Proof. Let ϕ and $\tilde{\phi}$ solve the diffusion equations

$$S = -\nabla \cdot [D\nabla\phi] + \sigma_a\phi, \qquad \tilde{S} = -\nabla \cdot [\tilde{D}\nabla\tilde{\phi}] + \tilde{\sigma}_a\tilde{\phi},$$

respectively. Subtract these equations to get

$$S - \tilde{S} = -\nabla \cdot [(D - \tilde{D})\nabla\phi] - \nabla \cdot [\tilde{D}\nabla(\phi - \tilde{\phi})] + (\sigma_a - \tilde{\sigma}_a)\phi + \tilde{\sigma}_a(\phi - \tilde{\phi}).$$

Taking the L^2-norms on both sides, we have

$$\begin{aligned}
&\|S - \tilde{S}\|_{L^2(X)} \\
&\leq \|\nabla \cdot [(D - \tilde{D})\nabla\phi]\|_{L^2(X)} + \|\nabla \cdot [\tilde{D}\nabla(\phi - \tilde{\phi})]\|_{L^2(X)} + \|(\sigma_a - \tilde{\sigma}_a)\phi\|_{L^2(X)} + \|\tilde{\sigma}_a(\phi - \tilde{\phi})\|_{L^2(X)} \\
&\leq \sum_{ij} \|\partial_j\phi\|_{L^\infty(X)} \|\partial_i(D - \tilde{D})_{ij}\|_{L^2(X)} + \sum_{ij} \|\partial_{ij}\phi\|_{L^\infty(X)} \|(D - \tilde{D})_{ij}\|_{L^2(X)} \\
&\quad + \sum_{ij} \|\partial_i\tilde{D}_{ij}\|_{L^\infty(X)} \|\partial_j(\phi - \tilde{\phi})\|_{L^2(X)} + \sum_{ij} \|\tilde{D}_{ij}\|_{L^\infty(X)} \|\partial_{ij}(\phi - \tilde{\phi})\|_{L^2(X)} \\
&\quad + \|\phi\|_{L^\infty(X)} \|\sigma_a - \tilde{\sigma}_a\|_{L^2(X)} + \|\tilde{\sigma}_a\|_{L^\infty(X)} \|\phi - \tilde{\phi}\|_{L^2(X)} \\
&\leq c_1 \|\phi - \tilde{\phi}\|_{H^2(X)} + \sum_{i \leq j} c_{2ij} \|(D - \tilde{D})_{ij}\|_{H^1(X)} + c_3 \|\sigma_a - \tilde{\sigma}_a\|_{L^2(X)}
\end{aligned} \tag{2.52}$$

where the constants $c_1, c_{2ij}, c_3 > 0$ can be made explicit as follows:

$$\begin{aligned}
c_1 &= \sqrt{\|\tilde{\sigma}_a\|^2_{L^\infty(X)} + \sum_j \left[\sum_i \|\partial_i\tilde{D}_{ij}\|_{L^\infty(X)}\right]^2 + 4\sum_{i<j} \|\tilde{D}_{ij}\|^2_{L^\infty(X)} + \sum_i \|\tilde{D}_{ii}\|^2_{L^\infty(X)}} \\
c_{2ij} &= \sqrt{4\|\partial_{ij}\phi\|^2_{L^\infty(X)} + \left(\|\partial_i\phi\|_{L^\infty(X)} + \|\partial_j\phi\|_{L^\infty(X)}\right)^2} \qquad (i < j) \\
c_{2ii} &= \sqrt{\|\partial_{ii}\phi\|^2_{L^\infty(X)} + \|\partial_i\phi\|^2_{L^\infty(X)}} \\
c_3 &= \|\phi\|_{L^\infty(X)}
\end{aligned}$$

In order to estimate the term $\|\phi - \tilde{\phi}\|_{H^2(X)}$, we turn to the second order elliptic equations generated from the internal data $H_\psi = H_{\tilde{\psi}}$:

$$F_\psi = \frac{H_\psi}{\psi} = (2\gamma - 1)D\nabla\phi \cdot \nabla \log\psi + 2\gamma\sigma_a\phi + \nabla \cdot D\nabla\phi$$
$$F_{\tilde{\psi}} = \frac{H_\psi}{\tilde{\psi}} = (2\gamma - 1)\tilde{D}\nabla\tilde{\phi} \cdot \nabla \log\tilde{\psi} + 2\gamma\tilde{\sigma}_a\tilde{\phi} + \nabla \cdot \tilde{D}\nabla\tilde{\phi}.$$

Subtracting these equations gives

$$\begin{aligned}
&- \nabla \cdot \tilde{D}\nabla[\phi - \tilde{\phi}] - 2\gamma\tilde{\sigma}_a(\phi - \tilde{\phi}) - (2\gamma - 1)\tilde{D}\nabla(\phi - \tilde{\phi}) \cdot \nabla \log\psi \\
&= \frac{H_\psi}{\psi\tilde{\psi}}(\psi - \tilde{\psi}) + (2\gamma - 1)(D - \tilde{D})\nabla\phi \cdot \nabla \log\psi \\
&+ (2\gamma - 1)\tilde{D}\nabla\tilde{\phi} \cdot (\nabla \log\psi - \nabla \log\tilde{\psi}) + 2\gamma(\sigma_a - \tilde{\sigma}_a)\phi + \nabla \cdot [D - \tilde{D}]\nabla\phi,
\end{aligned}$$

This is a second order elliptic equation for $\phi - \tilde{\phi}$ with zero Robin boundary condition, we have the following regularity estimate by Proposition 2.10:

$$\begin{aligned}
&\|\phi - \tilde{\phi}\|_{H^2(X)} \\
\leq& C\bigg(\left\|\frac{H_\psi}{\psi\tilde{\psi}}(\psi - \tilde{\psi})\right\|_{L^2(X)} + |2\gamma - 1|\|(D - \tilde{D})\nabla\phi \cdot \nabla \log\psi\|_{L^2(X)} \\
&+ |2\gamma - 1|\|\tilde{D}\nabla\tilde{\phi} \cdot (\nabla \log\psi - \nabla \log\tilde{\psi})\|_{L^2(X)} + \|\nabla \cdot [D - \tilde{D}]\nabla\phi\|_{L^2(X)} + |2\gamma|\|(\sigma_a - \tilde{\sigma}_a)\phi\|_{L^2(X)}\bigg) \\
\leq& C\bigg(\frac{\|H_\psi\|_{L^\infty(X)}}{c_\psi^2}\|\psi - \tilde{\psi}\|_{L^2(X)} + |2\gamma - 1|\sum_{ij}\|\partial_i \log\psi\|_{L^\infty(X)}\|\partial_j\phi\|_{L^\infty(X)}\|(D - \tilde{D})_{ij}\|_{L^2(X)} \\
&+ |2\gamma - 1|\sum_{ij}\|\tilde{D}_{ij}\|_{L^\infty(X)}\|\partial_j\tilde{\phi}\|_{L^\infty(X)}\|\partial_i(\log\psi - \log\tilde{\psi})\|_{L^2(X)} + \sum_{ij}\|\partial_j\phi\|_{L^\infty(X)}\|\partial_i(D - \tilde{D})_{ij}\|_{L^2(X)} \\
&+ \sum_{ij}\|\partial_{ij}\phi\|_{L^\infty(X)}\|(D - \tilde{D})_{ij}\|_{L^2(X)} + |2\gamma|\|\phi\|_{L^\infty(X)}\|\sigma_a - \tilde{\sigma}_a\|_{L^2(X)}\bigg) \\
\leq& c_4\|\psi - \tilde{\psi}\|_{H^1(X)} + \sum_{i\leq j} c_{5ij}\|(D - \tilde{D})_{ij}\|_{H^1(X)} + c_6\|\sigma_a - \tilde{\sigma}_a\|_{L^2(X)}
\end{aligned} \tag{2.53}$$

where in the last inequality, we used the upper bound $\|\partial_i \log\psi\|_{L^\infty(X)} \leq \frac{1}{c_\psi}\|\partial_i\psi\|_{L^\infty(X)}$ and

$$\begin{aligned}
\|\partial_i(\log\psi - \log\tilde{\psi})\|_{L^2(X)} \leq& \frac{1}{c_\psi^2}\|\psi\partial_i\tilde{\psi} - \tilde{\psi}\partial_i\psi\|_{L^2(X)} = \frac{1}{c_\psi^2}\|(\psi - \tilde{\psi})\partial_i\tilde{\psi} - \tilde{\psi}\partial_i(\psi - \tilde{\psi})\|_{L^2(X)} \\
\leq& \frac{1}{c_\psi^2}\|\partial_i\tilde{\psi}\|_{L^\infty(X)}\|\psi - \tilde{\psi}\|_{L^2(X)} + \frac{1}{c_\psi^2}\|\tilde{\psi}\|_{L^\infty(X)}\|\partial_i(\psi - \tilde{\psi})\|_{L^2(X)}
\end{aligned}$$

The constants $c_4, c_{5ij}, c_6 > 0$ are defeind as

$$
\begin{aligned}
c_4 =& \frac{C|2\gamma-1|}{c_\psi^2}\left[\sum_i\left(\sum_j \|\tilde{D}_{ij}\|_{L^2(\overline{X})}\|\partial_j\phi\|_{L^\infty(\overline{X})}\|\tilde{\psi}\|_{L^\infty(\overline{X})}\right)^2\right. \\
&\left.+\left(\frac{\|H_\psi\|_{L^\infty(\overline{X})}}{|2\gamma-1|}+\sum_{ij}\|\tilde{D}_{ij}\|_{L^2(\overline{X})}\|\partial_j\phi\|_{L^\infty(\overline{X})}\|\partial_i\tilde{\psi}\|_{L^\infty(\overline{X})}\right)^2\right]^{\frac{1}{2}} \\
c_{5ij} =& C\cdot\left(\left(2\|\partial_{ij}\phi\|_{L^\infty(\overline{X})}+\frac{|2\gamma-1|}{c_\psi}\|\partial_i\psi\|_{L^\infty(\overline{X})}\|\partial_j\phi\|_{L^\infty(\overline{X})}+\frac{|2\gamma-1|}{c_\psi}\|\partial_j\psi\|_{L^\infty(\overline{X})}\|\partial_i\phi\|_{L^\infty(\overline{X})}\right)^2\right. \\
&\left.+\left(\|\partial_i\phi\|_{L^\infty(\overline{X})}+\|\partial_j\phi\|_{L^\infty(\overline{X})}\right)^2\right)^{\frac{1}{2}} \qquad (i<j) \\
c_{5ii} =& C\cdot\sqrt{\left(\|\partial_{ii}\phi\|_{L^\infty(\overline{X})}+\frac{|2\gamma-1|}{c_\psi}\|\partial_i\psi\|_{L^\infty(\overline{X})}\|\partial_i\phi\|_{L^\infty(\overline{X})}\right)^2+\|\partial_i\phi\|^2_{L^\infty(\overline{X})}} \\
c_6 =& |2\gamma|C\cdot\|\phi\|_{L^\infty(\overline{X})}
\end{aligned}
$$

It remains to estimate the term $\|\psi-\tilde{\psi}\|_{H^1(X)}$. Let us consider the adjoint equations

$$
\begin{aligned}
-\nabla\cdot D\nabla\psi+\sigma_a\psi &= 0, \\
-\nabla\cdot\tilde{D}\nabla\tilde{\psi}+\tilde{\sigma}_a\tilde{\psi} &= 0.
\end{aligned}
\tag{2.54}
$$

Subtract these two equations to get

$$
-\nabla\cdot\tilde{D}\nabla(\psi-\tilde{\psi})+\tilde{\sigma}_a(\psi-\tilde{\psi})=\nabla\cdot(D-\tilde{D})\nabla\psi-(\sigma_a-\tilde{\sigma}_a)\psi \tag{2.55}
$$

This is a second order elliptic equation for $\psi-\tilde{\psi}$ with the zero Robin boundary condition. Again, by the elliptic regularity result, we have

$$
\begin{aligned}
&\|\psi-\tilde{\psi}\|_{H^1(X)} \\
\leq& C(\|\nabla\cdot[(D-\tilde{D})\nabla\psi]\|_{L^2(X)}+\|(\sigma_a-\tilde{\sigma}_a)\psi\|_{L^2(X)}) \\
\leq& C\left(\sum_{ij}\|\partial_j\psi\|_{L^\infty(X)}\|\partial_i(D-\tilde{D})_{ij}\|_{L^2(X)}\right. \\
&\left.+\sum_{ij}\|\partial_{ij}\psi\|_{L^\infty(X)}\|(D-\tilde{D})_{ij}\|_{L^2(X)}+\|\psi\|_{L^\infty(X)}\|(\sigma_a-\tilde{\sigma}_a)\|_{L^2(X)}\right) \\
\leq& \sum_{i\leq j}c_{7ij}\|(D-\tilde{D})_{ij}\|_{H^1(X)}+c_8\|\sigma_a-\tilde{\sigma}_a\|_{L^2(X)}
\end{aligned}
\tag{2.56}
$$

with constants $c_{7ij}, c_8 > 0$, where

$$c_{7ij} = C \cdot \sqrt{\left(\|\partial_i\psi\|_{L^\infty(X)} + \|\partial_j\psi\|_{L^\infty(X)}\right)^2 + 4\|\partial_{ij}\psi\|^2_{L^\infty(X)}} \qquad (i < j)$$
$$c_{7ii} = C \cdot \sqrt{\|\partial_i\psi\|^2_{L^\infty(X)} + \|\partial_{ii}\psi\|^2_{L^\infty(X)}}$$
$$c_8 = C \cdot \|\psi\|_{L^\infty(X)}$$

Combining (2.52) (2.53) (2.56), we conclude that

$$\|S - \tilde{S}\|_{L^2(X)} \leq \sum_{i\leq j} C_{1ij}\|(D - \tilde{D})_{ij}\|_{H^1(X)} + C_2\|\sigma - \tilde{\sigma}\|_{L^2(X)}, \tag{2.57}$$

with $C_{1ij} = c_1c_4c_{7ij} + c_1c_{5ij} + c_{2ij}$ and $C_2 = c_1c_4c_8 + c_1c_6 + c_3$. Note that all the constants in this proof are explicit, except for the constant C that comes from the estimate of elliptic regularity. □

Remark 2.12. *Theorem 2.11 can be interpreted as follows. Squaring the estimate* (2.51) *gives*

$$\|S - \tilde{S}\|^2_{L^2(X)} \leq \mathfrak{C}\left(\|D - \tilde{D}\|^2_{H^1(X)} + \|\sigma_a - \tilde{\sigma}_a\|^2_{L^2(X)}\right)$$

where the constant $\mathfrak{C}$ is in terms of C_{1ij} and C_2. If we take S, D, σ_a to be the underlying ground-truth parameters and $\tilde{S}, \tilde{D}, \tilde{\sigma}_a$ the corresponding parameters with random uncertainty of mean zero, then $\mathbb{E}[\tilde{S}] = S$, $\mathbb{E}[\tilde{D}] = D$, $\mathbb{E}[\tilde{\sigma}_a] = \sigma_a$. Therefore, the estimate provides a quantitative error bound on the variance of the bioluminescent source.

2.3.3.2 Uncertainty Quantification with Discretized Diffusive Model

In the previous section, we considered the impact of inaccurate (D, σ_a) using continuous PDE models. However, for the subsequent numerical simulation, the PDEs have to be discretized into finite dimensional discrete models. This motivates us to study a similar UQ problem based on the finite difference discretization of the PDE model. The analysis in this section provides a finite dimensional counterpart of the infinite dimensional UQ estimate (2.51), bridging the gap between the infinite dimensional analysis and the finite dimensional numerical experiments.

We will consider the discretization of three diffusion-type equations: the forward problem (2.37) (2.38), the adjoint problem (2.39) (2.40), and the internal data problem (2.43) equipped with the

zero Robin boundary condition. These problems need to be discretized in order to implement the reconstruction procedure outlined in Section 2.3.1. The discretization procedure requires numerical evaluation of the terms $\nabla \cdot D\nabla\phi_0$, $D\nabla\phi_0 \cdot \nabla \log \psi_0$, and $\sigma_a\phi_0$. The last term can be readily evaluated on a grid. In the following, we explain how to discretize the first two differential operators using the staggered grid scheme.

We take X to be a 2D domain to agree with the setup of the subsequent numerical experiments. The 2D coordinates are written as (x, y). The problem in 3D can be considered likewise with an additional spatial variable. Let Δx, Δy denote the grid size on the x-direction and y-direction, respectively. We will discretize the divergence-form diffusion operator using the staggered grid scheme, see Figure 2.6. The black dots are indexed by (i, j), where $i = 1, 2, \ldots, N_x$, $j = 1, 2, \ldots, N_y$, white dots are indexed by $(i + \frac{1}{2}, j)$, where $i = 1, 2, \ldots, N_x - 1$, $j = 1, 2, \ldots, N_y$ and $(i, j + \frac{1}{2})$, where $i = 1, 2, \ldots, N_x$, $j = 1, 2, \ldots, N_y - 1$. For a function u, we use $u_{i,j}$ to represent an approximate value of $u(x_i, y_j)$, where $x_i = x_1 + (i - 1)\Delta x$ and $y_j = y_1 + (j - 1)\Delta y$ are the coordinates of the grid points.

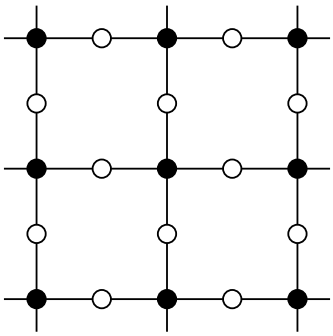

Figure 2.6 The illustration of staggered grid scheme. The zero and second order terms are defined on the grid points (black dots), the first order terms and D are defined on the edges (while dots).

Discretization with Isotropic D. We begin the discretization with an isotropic diffusion coefficient, that is, $D = D(x)$ is a scalar function.

Discretization of the Forward Problem. First, we consider discretization of the forward problem (2.37) (2.38). Using the staggered grid scheme, the operator $\nabla \cdot D\nabla$ is discretized as

$$\begin{aligned}
[\nabla \cdot D\nabla u]_{i,j} =& [\partial_x D\partial_x u + \partial_y D\partial_y u]_{i,j} \\
\approx& \frac{[D\partial_x u]_{i+\frac{1}{2},j} - [D\partial_x u]_{i-\frac{1}{2},j}}{\Delta x} + \frac{[D\partial_y u]_{i,j+\frac{1}{2}} - [D\partial_y u]_{i,j-\frac{1}{2}}}{\Delta y} \\
\approx& \frac{D_{i+\frac{1}{2},j}[u_{i+1,j} - u_{i,j}] - D_{i-\frac{1}{2},j}[u_{i,j} - u_{i-1,j}]}{\Delta x^2} \\
&+ \frac{D_{i,j+\frac{1}{2}}[u_{i,j+1} - u_{i,j}] - D_{i,j-\frac{1}{2}}[u_{i,j} - u_{i,j-1}]}{\Delta y^2} \\
=& \left[\frac{D_{i+\frac{1}{2},j}}{\Delta x^2}\right] u_{i+1,j} + \left[\frac{D_{i-\frac{1}{2},j}}{\Delta x^2}\right] u_{i-1,j} + \left[\frac{D_{i,j+\frac{1}{2}}}{\Delta y^2}\right] u_{i,j+1} + \left[\frac{D_{i,j-\frac{1}{2}}}{\Delta y^2}\right] u_{i,j-1} \\
&- \left[\frac{D_{i+\frac{1}{2},j}}{\Delta x^2} + \frac{D_{i-\frac{1}{2},j}}{\Delta x^2} + \frac{D_{i,j+\frac{1}{2}}}{\Delta y^2} + \frac{D_{i,j-\frac{1}{2}}}{\Delta y^2}\right] u_{i,j},
\end{aligned} \tag{2.58}$$

where $\approx$ denotes the staggered grid scheme approximation.

For the Robin boundary condition on the four boundaries (excluding the four corners), it is simply $u \pm 2D\partial_x u$ on the right/left boundary, $u \pm 2D\partial_y u$ on the top/bottom boundary. For the four corner points, e.g. the bottom left corner (Figure 2.7), the outgoing vector ν is chosen as $(-\frac{\sqrt{2}}{2}, -\frac{\sqrt{2}}{2})$. For example,

$$\begin{aligned}
[u + \ell\nu \cdot D\nabla u]_{1,1} =& u_{1,1} - \frac{\sqrt{2}\ell}{2}[D\partial_x u]_{1+\frac{1}{2},1} - \frac{\sqrt{2}\ell}{2}[D\partial_y u]_{1,1+\frac{1}{2}} \\
=& u_{1,1} + \frac{\sqrt{2}\ell}{2}\frac{D_{1+\frac{1}{2},1}}{\Delta x}[u_{1,1} - u_{1,2}] + \frac{\sqrt{2}\ell}{2}\frac{D_{1,1+\frac{1}{2}}}{\Delta y}[u_{1,1} - u_{2,1}] \\
=& \left[1 + \frac{\sqrt{2}\ell D_{1+\frac{1}{2},1}}{2\Delta x} + \frac{\sqrt{2}\ell D_{1,1+\frac{1}{2}}}{2\Delta y}\right] u_{1,1} - \frac{\sqrt{2}\ell D_{1+\frac{1}{2},1}}{2\Delta x} u_{1,2} - \frac{\sqrt{2}\ell D_{1,1+\frac{1}{2}}}{2\Delta y} u_{2,1}.
\end{aligned} \tag{2.59}$$

This discretization gives rise to a linear system with the unknowns $u_{i,j}$. In order to make this linear system explicit, we introduce the index function $\mathcal{I}(i,j) := (i-1)N_y + j$ and use $(i,j) \sim (i',j')$ to mean that the (i',j')-point is a neighbor of (i,j)-point. Denote by I the set of interior points, by B the set of non-corner boundary points, and by B_c the set of four corner points. According to the scheme (2.58), (2.59), the forward problem (2.37) (2.38) is discretized to yield the linear system

$$\mathbf{L}\boldsymbol{\phi}_0 = \mathbf{s}$$

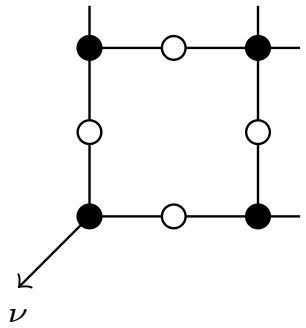

Figure 2.7 The outgoing vector at the corner.

where $\boldsymbol{\phi}_0$ consists of the vectorized values of the forward solution ϕ_0 at black dots such that $\boldsymbol{\phi}_{0\mathcal{I}(i,j)} = \phi_0(x_i, y_j)$.

$$\mathbf{L}_{\mathcal{I}(i,j),\mathcal{I}(i',j')} = \begin{cases} \sum_{(\tilde{i},\tilde{j})\sim(i,j)} \frac{D_{\frac{i+\tilde{i}}{2},\frac{j+\tilde{j}}{2}}}{|i-\tilde{i}|\Delta x^2+|j-\tilde{j}|\Delta y^2} + \sigma_{i,j}, & (i',j') = (i,j),\ (i,j) \in I \\ -\frac{D_{\frac{i+i'}{2},\frac{j+j'}{2}}}{|i-i'|\Delta x^2+|j-j'|\Delta y^2}, & (i',j') \sim (i,j),\ (i,j) \in I \\ 1 + \ell \sum_{I\ni(\tilde{i},\tilde{j})\sim(i,j)} \frac{D_{\frac{i+\tilde{i}}{2},\frac{j+\tilde{j}}{2}}}{|i-\tilde{i}|\Delta x+|j-\tilde{j}|\Delta y}, & (i',j') = (i,j),\ (i,j) \in B \\ -\ell \frac{D_{\frac{i+i'}{2},\frac{j+j'}{2}}}{|i-i'|\Delta x+|j-j'|\Delta y}, & I \ni (i',j') \sim (i,j) \in B, \\ 1 + \frac{\sqrt{2}\ell}{2} \sum_{(\tilde{i},\tilde{j})\sim(i,j)} \frac{D_{\frac{i+\tilde{i}}{2},\frac{j+\tilde{j}}{2}}}{|i-\tilde{i}|\Delta x+|j-\tilde{j}|\Delta y}, & (i',j') = (i,j),\ (i,j) \in B_c, \\ -\frac{\sqrt{2}\ell}{2} \frac{D_{\frac{i+i'}{2},\frac{j+j'}{2}}}{|i-i'|\Delta x+|j-j'|\Delta y}, & (i',j') \sim (i,j),\ (i,j) \in B_c, \\ 0 & \text{others} \end{cases} \tag{2.60}$$

$$\mathbf{s}_{\mathcal{I}(i,j)} = \begin{cases} S_{i,j}, & (i,j) \in I, \\ 0, & (i,j) \in B \cup B_c. \end{cases} \tag{2.61}$$

Before discussing further properties of the matrix $\mathbf{L}$, we recall the definition of some special matrices. Given a square matrix $A = (A_{kl})$, its k-th row is said to be *weakly diagonally dominant (WDD)* if $|A_{kk}| \geq \sum_{l\neq k} |A_{kl}|$, and the matrix A is said to be WDD if all the rows are WDD. Likewise, its k-th row is said to be *strictly diagonally dominant (SDD)* if $\geq$ is replaced by a strict inequality $>$, and the matrix A is said to be SDD if all the rows are WDD.

Definition 2.13. *A square matrix $A = (A_{kl})$ is said to be weakly chained diagonally dominant (WCDD) if*

- *A is WDD.*
- *For each row k that is not SDD, there exists $k_1, k_2, \ldots, k_p$ such that A_{kk_1}, $A_{k_1k_2}$, $\ldots$, $A_{k_{p-1}k_p}$, A_{k_pl} are nonzero and the row $A_{l,:}$ is SDD.*

Proposition 2.14. $\mathbf{L}$ *is a WCDD matrix.*

Proof. First, we show $\mathbf{L}$ is WDD. As $D > 0$, $\sigma_a \geq 0$ everywhere, all the off-diagonal terms (see Row 2, 4, 6, 7 in (2.60)) are non-positive and all the diagonal terms (see Row 1, 3, 5 in (2.60)) are non-negative. It suffices to show that

$$\mathbf{L}_{\mathcal{I}(i,j),\mathcal{I}(i,j)} \geq \sum_{(i',j')\neq(i,j)} -\mathbf{L}_{\mathcal{I}(i,j),\mathcal{I}(i',j')}.$$

Move all the terms in this inequality to the left side. It suffices to show that any row sum of $\mathbf{L}$ is non-negative. This is obvious from the definition of $\mathbf{L}$ in (2.60), where the row sum of the $\mathcal{I}(i,j)$-th row is $\sigma_{i,j}$ when $(i,j) \in I$, and the row sum of the $\mathcal{I}(i,j)$-th row is 1 when $(i,j) \in B \cup B_c$. This proves that $\mathbf{L}$ is WDD. Moreover, the analysis shows that the $\mathcal{I}(i,j)$-th row is SDD when $(i,j) \in B \cup B_c$.

Next, we show the chain condition. If the $\mathcal{I}(i,j)$-th row is not SDD, then $(i,j) \in I$. As the finite difference grid is connected, there exist $(i_1,j_1),\ldots,(i_p,j_p)$ such that $(i_p,j_p) \in B \cup B_c$ and $(i,j) \sim (i_1,j_1) \sim \cdots \sim (i_p,j_p)$. Notice that the definition of $\mathbf{L}$ has the property that $\mathbf{L}_{\mathcal{I}(i,j),\mathcal{I}(i',j')} < 0$ for $(i,j) \sim (i',j')$ (see Row 2,4,6 in (2.60)), we conclude the entries $\mathbf{L}_{\mathcal{I}(i,j),\mathcal{I}(i_1,j_1)}$, $\ldots$, $\mathbf{L}_{\mathcal{I}(i_{p-1},j_{p-1}),\mathcal{I}(i_p,j_p)}$ are all negative, and the row $\mathbf{L}_{\mathcal{I}(i_p,j_p),:}$ is SDD since $(i_p,j_p) \in B \cup B_c$. □

Proposition 2.15 ([82])**.** *WCDD matrices are invertible.*

As a result, the discretized forward problem admits a unique solution $\boldsymbol{\phi}_0 = \mathbf{L}^{-1}\mathbf{s}$.

Discretization of the Adjoint Problem. The adjoint problem(2.39), (2.40) takes a similar form as the forward problem, except that the source g is imposed on the boundary. Therefore, the adjoint problem can be discretized likewise to yield a linear system

$$\mathbf{L}\boldsymbol{\psi} = \mathbf{g}$$

where $\mathbf{L}$ is the same finite difference matrix defined in (2.60), $\boldsymbol{\psi}$ consists of the vectorized values of the adjoint solution ψ at black dots such that $\boldsymbol{\psi}_{\mathcal{I}(i,j)} = \psi(x_i, y_j)$, and

$$\mathbf{g}_{\mathcal{I}(i,j)} = \begin{cases} 0, & (i,j) \in I, \\ g(x_i, y_j), & (i,j) \in B \cup B_c. \end{cases} \tag{2.62}$$

Discretization of the Internal Data Problem. It remains to discretize the internal data problem (2.43) along with the zero Robin boundary condition. This requires discretizing an operator of the form $D\nabla u \cdot \nabla v = D\nabla v \cdot \nabla u$. The staggered grid scheme gives

$$\begin{aligned}
&[D\nabla v \cdot \nabla u]_{i,j} \\
\approx &\frac{[D\partial_x u \partial_x v]_{i+\frac{1}{2},j} + [D\partial_x u \partial_x v]_{i-\frac{1}{2},j}}{2} + \frac{[D\partial_y u \partial_y v]_{i,j+\frac{1}{2}} + [D\partial_y u \partial_y v]_{i,j-\frac{1}{2}}}{2} \\
\approx &\frac{[D\partial_x v]_{i+\frac{1}{2},j}[u_{i+1,j} - u_{i,j}] + [D\partial_x v]_{i-\frac{1}{2},j}[u_{i,j} - u_{i-1,j}]}{2\Delta x} \\
&+ \frac{[D\partial_y v]_{i,j+\frac{1}{2}}[u_{i,j+1} - u_{i,j}] + [D\partial_y v]_{i,j-\frac{1}{2}}[u_{i,j} - u_{i,j-1}]}{2\Delta y} \\
= &\left[\frac{D_{i+\frac{1}{2},j}[v_{i+1,j} - v_{i,j}]}{2\Delta x^2}\right] u_{i+1,j} + \left[\frac{D_{i-\frac{1}{2},j}[v_{i-1,j} - v_{i,j}]}{2\Delta x^2}\right] u_{i-1,j} \\
&+ \left[\frac{D_{i,j+\frac{1}{2}}[v_{i,j+1} - v_{i,j}]}{2\Delta y^2}\right] u_{i,j+1} + \left[\frac{D_{i,j-\frac{1}{2}}[v_{i,j-1} - v_{i,j}]}{2\Delta y^2}\right] u_{i,j-1} \\
&- \left[\frac{D_{i+\frac{1}{2},j}[v_{i+1,j} - v_{i,j}]}{2\Delta x^2} + \frac{D_{i-\frac{1}{2},j}[v_{i-1,j} - v_{i,j}]}{2\Delta x^2} + \frac{D_{i,j+\frac{1}{2}}[v_{i,j+1} - v_{i,j}]}{2\Delta y^2} + \frac{D_{i,j-\frac{1}{2}}[v_{i,j-1} - v_{i,j}]}{2\Delta y^2}\right] u_{i,j},
\end{aligned}$$

The discretization of (2.43) becomes

$$\mathbf{A}_{\boldsymbol{\psi}_0}\boldsymbol{\phi}_0 = \mathbf{h}_{\boldsymbol{\psi}_0}$$

where $\boldsymbol{\phi_0}$ consists of the vectorized values of the forward solution ϕ_0 at black dots such that $\boldsymbol{\phi}_{0\mathcal{I}(i,j)} = \phi(x_i, y_j)$, and

$$(\mathbf{A}_\psi)_{\mathcal{I}(i,j),\mathcal{I}(i',j')} = \begin{cases} -\sum_{(\tilde{i},\tilde{j})\sim(i,j)} \frac{D_{\frac{i+\tilde{i}}{2},\frac{j+\tilde{j}}{2}}[\psi_{i,j}+\frac{2\gamma-1}{2}[\psi_{\tilde{i},\tilde{j}}-\psi_{i,j}]]}{|i-\tilde{i}|\Delta x^2+|j-\tilde{j}|\Delta y^2} + 2\gamma\sigma_{i,j}\psi_{i,j}, & (i',j') = (i,j),\ (i,j)\in I \\ \frac{D_{\frac{i+i'}{2},\frac{j+j'}{2}}[\psi_{i,j}+\frac{2\gamma-1}{2}[\psi_{i',j'}-\psi_{i,j}]]}{|i-i'|\Delta x^2+|j-j'|\Delta y^2}, & (i',j')\sim(i,j),\ (i,j)\in I \\ 1+\ell\sum_{I\ni(\tilde{i},\tilde{j})\sim(i,j)} \frac{D_{\frac{i+\tilde{i}}{2},\frac{j+\tilde{j}}{2}}}{|i-\tilde{i}|\Delta x+|j-\tilde{j}|\Delta y}, & (i',j') = (i,j),\ (i,j)\in B \\ -\ell\frac{D_{\frac{i+i'}{2},\frac{j+j'}{2}}}{|i-i'|\Delta x+|j-j'|\Delta y}, & I\ni(i',j')\sim(i,j)\in B, \\ 1+\frac{\sqrt{2}\ell}{2}\sum_{(\tilde{i},\tilde{j})\sim(i,j)} \frac{D_{\frac{i+\tilde{i}}{2},\frac{j+\tilde{j}}{2}}}{|i-\tilde{i}|\Delta x+|j-\tilde{j}|\Delta y}, & (i',j') = (i,j),\ (i,j)\in B_c, \\ -\frac{\sqrt{2}\ell}{2}\frac{D_{\frac{i+i'}{2},\frac{j+j'}{2}}}{|i-i'|\Delta x+|j-j'|\Delta y}, & (i',j')\sim(i,j),\ (i,j)\in B_c, \\ 0 & \text{others} \end{cases}$$

$$(\mathbf{h}_\psi)_{\mathcal{I}(i,j)} = \begin{cases} (H_\psi)_{i,j}, & (i,j)\in I, \\ 0, & (i,j)\in B\cup B_c. \end{cases}$$

Discrete Uncertainty Quantification Estimate. In parallel to Theorem 2.11, we can derive the following UQ estimate for the discretized model. Note that the uncertainties of the optical parameters (D, σ_a) are implicitly encoded in the difference $\tilde{\mathbf{L}} - \mathbf{L}$ and $\tilde{\mathbf{A}}_{\tilde{\boldsymbol{\phi}}_0} - \mathbf{A}_{\boldsymbol{\phi}_0}$.

Theorem 2.16 ([97]). *Suppose* 0 *is not an eigenvalue of* $\mathbf{A}_{\boldsymbol{\psi}_0}$ *for some* $\boldsymbol{\psi_0} > 0$*, then*

$$\|\tilde{\mathbf{s}} - \mathbf{s}\|_2 \le \|\mathbf{h}_{\boldsymbol{\phi}_0}\|_2(\|\mathbf{A}_{\psi_0}^{-1}\|_2\|\tilde{\mathbf{L}} - \mathbf{L}\|_2 + \|\tilde{\mathbf{L}}\|_2\|\tilde{\mathbf{A}}_{\tilde{\boldsymbol{\phi}}_0}^{-1}\|_2\|\mathbf{A}_{\boldsymbol{\phi}_0}^{-1}\|_2\|\tilde{\mathbf{A}}_{\tilde{\boldsymbol{\phi}}_0} - \mathbf{A}_{\boldsymbol{\phi}_0}\|_2). \tag{2.63}$$

Proof. Under the assumption, the matrix $\mathbf{A}_{\boldsymbol{\psi}_0}$ is invertible for some $\boldsymbol{\psi_0} > 0$. We can represent $\boldsymbol{\phi_0} = \mathbf{A}_{\boldsymbol{\psi}_0}^{-1}\mathbf{h}_{\psi_0}$, then $\mathbf{s} = \mathbf{L}\boldsymbol{\phi_0} = \mathbf{L}\mathbf{A}_{\boldsymbol{\psi}_0}^{-1}\mathbf{h}_{\boldsymbol{\psi}_0}$. Therefore,

$$\begin{aligned} \|\tilde{\mathbf{s}} - \mathbf{s}\|_2 =& \|(\tilde{\mathbf{L}}\tilde{\mathbf{A}}_{\tilde{\boldsymbol{\phi}}_0}^{-1} - \mathbf{L}\mathbf{A}_{\boldsymbol{\phi}_0}^{-1})\mathbf{h}_{\boldsymbol{\phi}_0}\|_2 \\ \le& \|\tilde{\mathbf{L}}\tilde{\mathbf{A}}_{\tilde{\boldsymbol{\phi}}_0}^{-1} - \mathbf{L}\mathbf{A}_{\boldsymbol{\phi}_0}^{-1}\|_2\|\mathbf{h}_{\boldsymbol{\phi}_0}\|_2 \\ \le& (\|(\tilde{\mathbf{L}} - \mathbf{L})\mathbf{A}_{\boldsymbol{\phi}_0}^{-1}\|_2 + \|\tilde{\mathbf{L}}(\tilde{\mathbf{A}}_{\tilde{\boldsymbol{\phi}}_0}^{-1} - \mathbf{A}_{\boldsymbol{\phi}_0}^{-1})\|_2)\|\mathbf{h}_{\boldsymbol{\phi}_0}\|_2 \\ \le& (\|\tilde{\mathbf{L}} - \mathbf{L}\|_2\|\mathbf{A}_{\boldsymbol{\phi}_0}^{-1}\|_2 + \|\tilde{\mathbf{L}}\|_2\|\tilde{\mathbf{A}}_{\tilde{\boldsymbol{\phi}}_0}^{-1} - \mathbf{A}_{\boldsymbol{\phi}_0}^{-1}\|_2)\|\mathbf{h}_{\boldsymbol{\phi}_0}\|_2 \end{aligned} \tag{2.64}$$

where $\|\cdot\|_2$ denotes the vector/matrix 2-norm. Using the relation $A^{-1} - B^{-1} = A^{-1}(B - A)B^{-1}$, we obtain the desired estimate. □

Discretization with Anisotropic D. When D is anisotropic, i.e, a symmetric positive definition matrix-valued function, the operators $\nabla \cdot D\nabla$ and $D\nabla v \cdot \nabla$ can be discretized as follows

$$[\nabla \cdot D\nabla u]_{i,j} = \frac{[(D\nabla u)_1]_{i+\frac{1}{2},j} - [(D\nabla u)_1]_{i-\frac{1}{2},j}}{\Delta x} + \frac{[(D\nabla u)_2]_{i,j+\frac{1}{2}} - [(D\nabla u)_2]_{i,j-\frac{1}{2}}}{\Delta y}$$
$$[D\nabla v \cdot \nabla u]_{i,j} = \frac{[(D\nabla v)_1 \partial_x u]_{i+\frac{1}{2},j} + [(D\nabla v)_2 \partial_x u]_{i-\frac{1}{2},j}}{2} + \frac{[(D\nabla v)_2 \partial_y u]_{i,j+\frac{1}{2}} + [(D\nabla v)_2 \partial_y u]_{i,j-\frac{1}{2}}}{2}$$

where $(D\nabla u)_1$ (resp. $(D\nabla u)_2$) denotes the first (resp. second) component of the vector $D\nabla u$. The discretization now differs from the isotropic case. This is because for an isotropic D

$$(D\nabla u)_1 = D\partial_x u, \qquad (D\nabla u)_2 = D\partial_y u$$

which only requires to compute $[\partial_x u]_{i+\frac{1}{2},j}$ and $[\partial_y u]_{i,j+\frac{1}{2}}$ in the staggered grid. However, for an anisotropic D:

$$(D\nabla u)_1 = D_{11}\partial_x u + D_{12}\partial_y u, \qquad (D\nabla u)_2 = D_{21}\partial_x u + D_{22}\partial_y u$$

which requires to compute two additional terms $[\partial_x u]_{i,j+\frac{1}{2}}$ and $[\partial_y u]_{i+\frac{1}{2},j}$. These additional terms can be discretized as follows:

$$[\partial_y u]_{i+\frac{1}{2},j} = \frac{[\partial_y u]_{i,j} + [\partial_y u]_{i+1,j}}{2} = \frac{u_{i+1,j+1} + u_{i,j+1} - u_{i,j-1} - u_{i+1,j-1}}{4\Delta y},$$
$$[\partial_x u]_{i,j+\frac{1}{2}} = \frac{[\partial_x u]_{i,j} + [\partial_x u]_{i,j+1}}{2} = \frac{u_{i+1,j+1} + u_{i+1,j} - u_{i-1,j} - u_{i-1,j+1}}{4\Delta x},$$

see [45] for the detail. Once discretized, the rest of the steps are similar and one can derive the estimate in Theorem

2.3.3.3 Numerical Experiment

In this section, we demonstrate numerical experiments to validate the reconstruction procedure and quanfity the impact of inaccurate optical coefficients (D, σ_a) to the source recovery. We will restrict the discussion in this section to isotropic D for the ease of notations.

Uncertainty Generation We will utilize the generalized Polynomial Chaos Expansion (PCE) to facilitate generation of uncertainty. PCE approximates a well-behaved random variable using

a series of polynomials under certain probability distribution. Specifically, let $(X, \mathcal{F}, \mathbb{P})$ be a probability space, and let $\xi(\omega)$ be a random variable (where ω is a sample) with probability density function $p(t)$. Suppose a deterministic ground-truth $\mathfrak{u} = \mathfrak{u}(\mathbf{x})$ is given, then the uncertainty generated by PCE takes the form

$$\mathfrak{u}(\mathbf{x}, \xi(\omega)) = \sum_{k=0}^{\infty} \mathfrak{u}_k(\mathbf{x}) \Phi_k(\xi(\omega)), \qquad (x, \omega) \in \Omega \times X \tag{2.65}$$

where $\mathfrak{u}_k(\mathbf{x})$'s are the coefficients, $\mathfrak{u}_0$ is the ground truth, $\Phi_0 = 1$, Φ_k's are orthogonal polynomials, that is,

$$\int_{\mathbb{R}} \Phi_i(t) \Phi_j(t) p(t) \, \mathrm{d}t = \delta_{ij}.$$

For the numerical experiments, ξ is chosen to be uniformly distributed on the sample space $X = [-1, 1]$; Φ_k's are the Legendre polynomials on $[-1, 1]$; the PCE is truncated at $k = K_c$. Then

$$\mathbb{E}[\mathfrak{u}] = \mathfrak{u}_0, \qquad \mathrm{Var}[\mathfrak{u}] = \sum_{k=1}^{K_c} \mathfrak{u}_k^2.$$

In the subsequent numerical experiments, we inject uncertainties into the optical coefficients (D, σ_a) based on the following process:

(1) Generate the coefficients $\mathfrak{u}_{Dk}, \mathfrak{u}_{\sigma_a k}$ using the truncated Fourier series in $\mathbf{x}$:

$$\mathfrak{u}_{Dk} = \sum_{\|\mathbf{n}\|_\infty = k} c_{1\mathbf{n}} \sin(\pi \mathbf{n} \cdot \mathbf{x}) + c_{2\mathbf{n}} \cos(\pi \mathbf{n} \cdot \mathbf{x}),$$

$$\mathfrak{u}_{\sigma_a k} = \sum_{\|\mathbf{n}\|_\infty = k} c_{3\mathbf{n}} \sin(\pi \mathbf{n} \cdot \mathbf{x}) + c_{4\mathbf{n}} \cos(\pi \mathbf{n} \cdot \mathbf{x}).$$

Here $\mathbf{n} \in \mathbb{Z}^n$, the Fourier coefficients $c_{1\mathbf{n}}, c_{2\mathbf{n}}, c_{3\mathbf{n}}, c_{4\mathbf{n}}$ are independently chosen from the uniform distributions on $[-1, 1]$. Once generated, they are fixed so that the coefficients $\mathfrak{u}_{Dk}, \mathfrak{u}_{\sigma_a k}$ are deterministic.

(2) Randomly generate ξ from the uniform distribution on $[-1, 1]$, then construct the uncertainties $\mathfrak{u}_D, \mathfrak{u}_{\sigma_a}$ according to (2.65) with $k = 1, 2, \ldots, 10$:

$$\mathfrak{u}_D \coloneqq \sum_{k=1}^{10} \mathfrak{u}_{Dk} \Phi_k(\xi(\omega)), \qquad \mathfrak{u}_{\sigma_a} \coloneqq \sum_{k=1}^{10} \mathfrak{u}_{\sigma_a k} \Phi_k(\xi(\omega))$$

Note that $\mathbb{E}[\mathfrak{u}_D] = \mathbb{E}[\mathfrak{u}_{\sigma_a}] = 0$.

(3) Once the uncertainties are generated, we rescale the uncertainties based on prescribed relative uncertainty levels e_D, e_{σ_a} to construct the optical coefficients with uncertainty $(\tilde{D}, \tilde{\sigma}_a)$ as follows:

$$\begin{aligned} \tilde{D} &:= D + \frac{\mathfrak{u}_D e_D}{\|\mathfrak{u}_D\|_{H^1}} \|D\|_{H^1}, \\ \tilde{\sigma}_a &:= \sigma_a + \frac{\mathfrak{u}_{\sigma_a} e_{\sigma_a}}{\|\mathfrak{u}_{\sigma_a}\|_{L^2}} \|\sigma_a\|_{L^2}. \end{aligned} \tag{2.66}$$

The impact of the inaccuracy in the optical coefficients will be quantitatively measured by the relative standard deviation defined as follows:

$$\mathcal{E}_S := \frac{\sqrt{\mathbb{E}[\|\tilde{S} - S\|_{L^2}^2]}}{\|S\|_{L^2}}, \quad \mathcal{E}_D := \frac{\sqrt{\mathbb{E}[\|\tilde{D} - D\|_{H^1}^2]}}{\|D\|_{H^1}}, \quad \mathcal{E}_{\sigma_a} := \frac{\sqrt{\mathbb{E}[\|\tilde{\sigma}_a - \sigma_a\|_{L^2}^2]}}{\|\sigma_a\|_{L^2}}. \tag{2.67}$$

Note that $\mathcal{E}_D = e_D$ and $\mathcal{E}_{\sigma_a} = e_{\sigma_a}$ are precisely the relative uncertainty levels that are used to define $(\tilde{D}, \tilde{\sigma}_a)$ in (2.66). This justifies that the relative standard deviation is a reasonable quantity to measure the uncertainty. In the following, we will specify various uncertainty levels e_D, e_{σ_a} and plot $\mathcal{E}_S$ versus them, see Figure 2.12 and Figure 2.17.

Numerical Implementation. We choose the 2D computational domain $\Omega = [-1, 1]^2$, $\ell = 1$. The diffusion equation is solved using the staggered grid scheme as is outlined in Section 2.3.3.2. To avoid the inverse crime, the forward problem is solved on a fine mesh with step size $h = \frac{1}{200}$, while the inverse problem is solved on a coarse mesh with step size $h = \frac{1}{100}$ using re-sampled data. We numerically calculate the noise-free ϕ_0 and ψ_0 using ground truth S and (D, σ_a), here we choose $\psi_0 > 0$ by solving (2.39) with a positive Dirichlet boundary condition. Once we have ϕ_0 and ψ_0, we can calculate the internal data H_{ψ_0} through (2.43). Note that the internal data is derived from the boundary measurement, hence is independent of the uncertainty on the optical coefficients.

Experiment 1. In this experiment, we consider the case that the optical coefficients can be represented using low-frequency Fourier basis. We choose

$$D = \cos^2(x + 2y) - 3\sin^2(3x - 4y) + 5, \qquad \sigma_a = \cos^2(5x) + \sin^2(5y) + 1,$$

and the source S to be the Shepp-Logan phantom, see Figure 2.8.

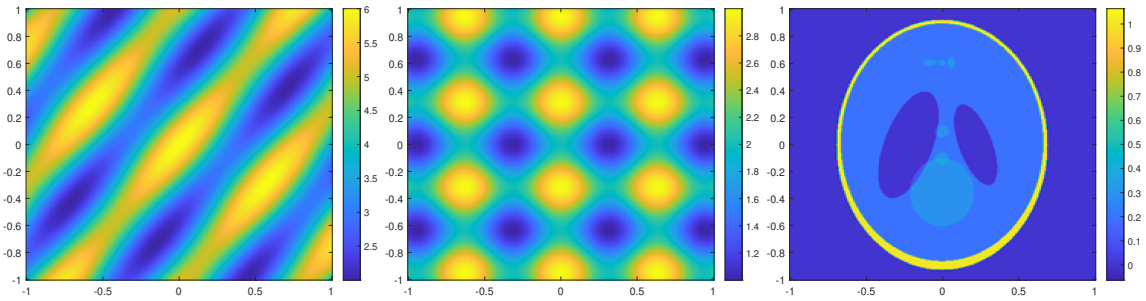

Figure 2.8 Left: Diffusion coefficient D. Middle: Absorption coefficient σ_a. Right: Shepp-Logan Source S.

Using the ground-truth (D, σ_a), we generate the uncertainties according to (2.66) to obtain 1000 samples of the inaccurate optical coefficients $(\tilde{D}, \tilde{\sigma}_a)$. Set $\Delta D := \tilde{D} - D$ and $\Delta\sigma_a = \tilde{\sigma}_a - \sigma_a$. We implemented the reconstruction procedure 1000 times to plot the distribution of $\|\Delta S\|_{L^2}$ versus $\|\Delta D\|_{H^1}$ and $\|\Delta\sigma_a\|_{L^2}$, see Figure 2.9. It is clear that for fixed $\|\Delta D\|_{H^1}$, $\|\Delta S\|_{L^2}$ is more concentrated compared to fixed $\|\Delta\sigma_a\|_{L^2}$, suggesting that the uncertainty in $\tilde{D}$ has larger impact to the reconstruction than the uncertainty in $\tilde{\sigma}_a$. Moreover, the distribution of the scatter plot suggests that $\|\Delta S\|_{L^2}$ is locally Lipschitz stable with respect to $\|\Delta D\|_{H^1}$ for small ΔD, agreeing with the estimates in Theorem 2.11 and Theorem 2.16 One of the reconstructions is illustrated in Figure 2.10, and the average of the 1000 reconstructed sources is illustrated in Figure 2.11. We can see that the averaged $\tilde{S}$ is close to the ground truth S, which means the relation between $\tilde{S}$ and $(\tilde{D}, \tilde{\sigma}_a)$ near (D, σ_a) have no sharp points, see Remark 2.17. It implies that the uncertainty in $\tilde{S}$ have certain regularity with respect to the uncertainties in $(\tilde{D}, \tilde{\sigma}_a)$.

To better understand the relations between $\mathcal{E}_S$ versus $\mathcal{E}_D$ (resp. $\mathcal{E}_S$ versus $\mathcal{E}_{\sigma_a}$), we take $\Delta\sigma_a = 0$ (resp. $\Delta D = 0$) and add $e_D = 2\%, 4\%, 6\%, 8\%, 10\%$ of random noise to D (resp. $e_{\sigma_a} = 2\%, 4\%, 6\%, 8\%, 10\%$ of random noise to σ_a). The plots are shown in Figure 2.12. We observe that $\mathcal{E}_S$ depends linearly or superlinearly on $\mathcal{E}_D$ and $\mathcal{E}_{\sigma_a}$, and the same level of relative uncertainty on D has larger impact than on σ_a. We remark that the plotted curves are nonlinear because the constant factors C_{1ij}, C_2 in Theorem 2.11 also depend on $(\tilde{D}, \tilde{\sigma}_a)$.

Remark 2.17. *Choose random variable* $X \sim N\left(0, \frac{1}{100}\right)$, $f_\alpha(x) = |x|^\alpha$ $(0 < \alpha < 1)$, *we have*

$$0 = f_\alpha(\mathbb{E}[X]) < \mathbb{E}[f_\alpha(X)] = \frac{2^{-\frac{\alpha}{2}} 5^{-\alpha}}{\sqrt{\pi}} \Gamma\left(\frac{\alpha+1}{2}\right) < 1,$$

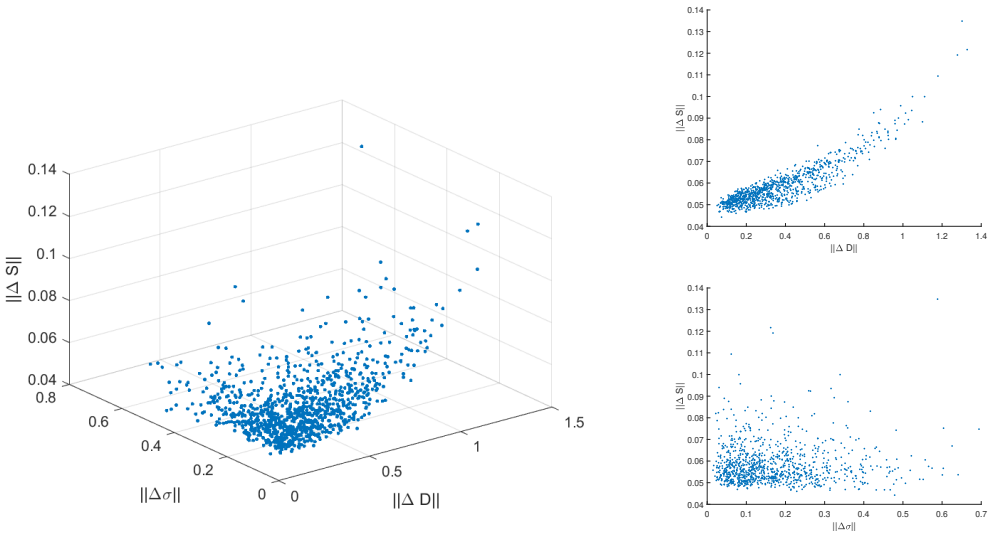

Figure 2.9 The distribution of the error with respect to the inaccuracies in optical coefficients.

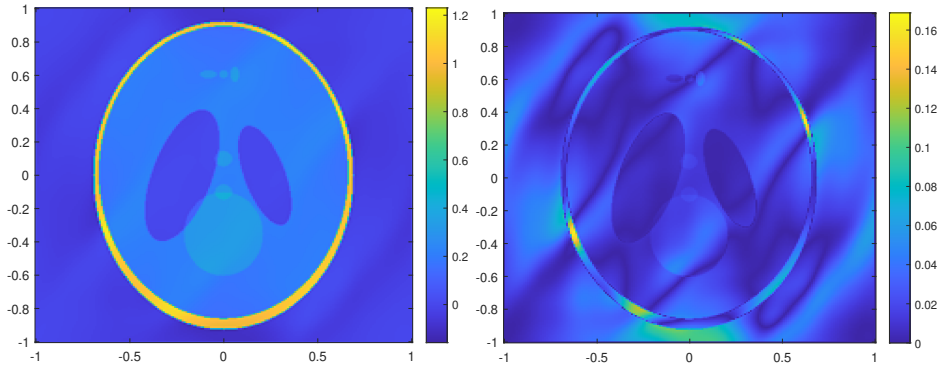

Figure 2.10 Reconstructed source $\tilde{S}$ and its error under 10% Gaussian random noise.

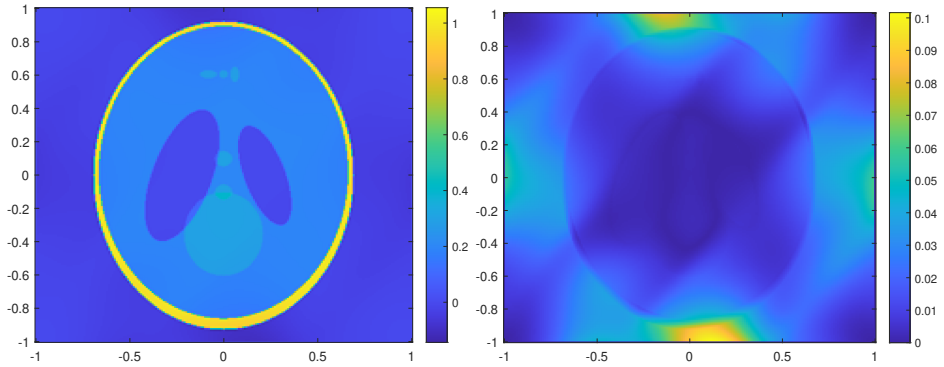

Figure 2.11 Averaged reconstructed source $\tilde{S}$ and its error under 10% Gaussian random noise.

and $\mathbb{E}[f_\alpha(X)]$ *is monotonically converged to* 1 *as* $\alpha \to 0_+$.

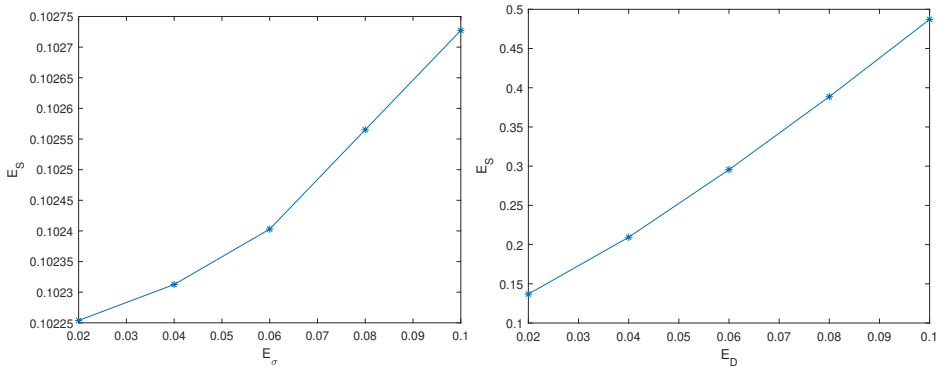

Figure 2.12 Left: $\mathcal{E}_S$ versus $\mathcal{E}_{\sigma_a}$. Right: $\mathcal{E}_S$ versus $\mathcal{E}_D$.

Experiment 2: In this experiment, we consider the case that the optical coefficients can not be represented using the low frequency Fourier basis. We choose

$$D = 3 - \max\{|x|, |y|\}, \qquad \sigma_a = \frac{3}{2} - \frac{1}{2}\mathrm{sgn}\left(x^2 + y^2 - \frac{4}{5}\right),$$

and we choose the source S to be the Shepp-Logan phantom, see Figure 2.13.

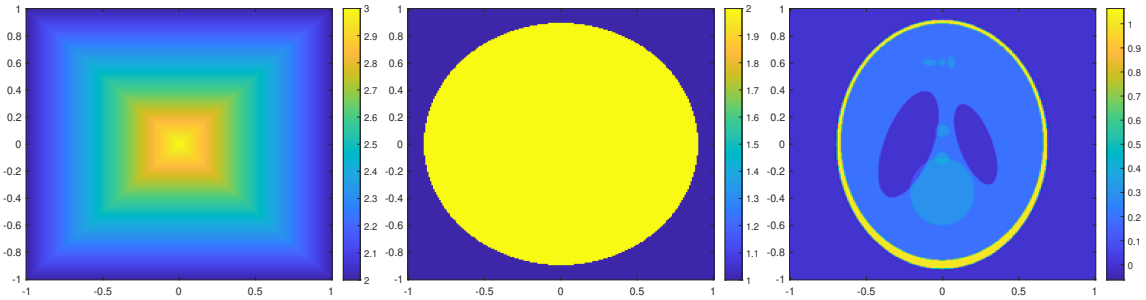

Figure 2.13 Left: Diffusion coefficient D. Middle: Absorption coefficient σ_a. Right: Shepp-Logan Source.

We choose the relative uncertainty level at 10% and run 1000 reconstructions to plot the distribution of $\|\tilde{S} - S\|_{L^2}$ versus $\|\tilde{D} - D\|_{H^1}$ and $\|\tilde{\sigma}_a - \sigma_a\|_{L^2}$, see Figure 2.14. One of the reconstructions is illustrated in Figure 2.15, and the average of 1000 reconstructed sources is illustrated in Figure 2.16.

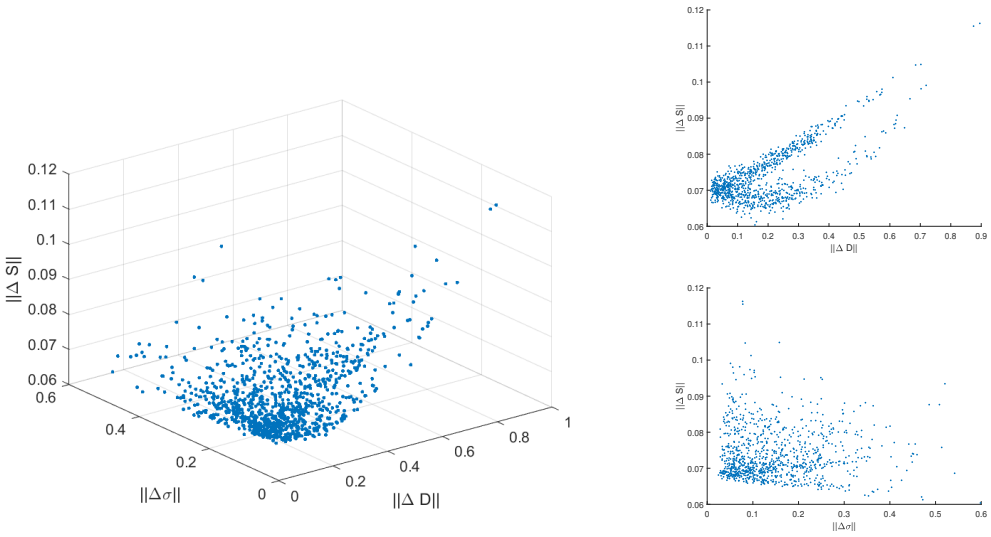

Figure 2.14 The distribution of the error with respect to the inaccuracies in optical coefficients.

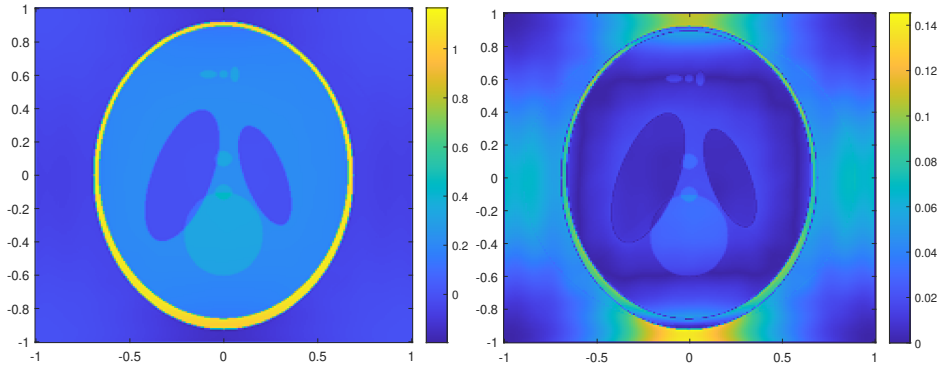

Figure 2.15 Reconstructed source $\tilde{S}$ and its error under 10% Gaussian random noise.

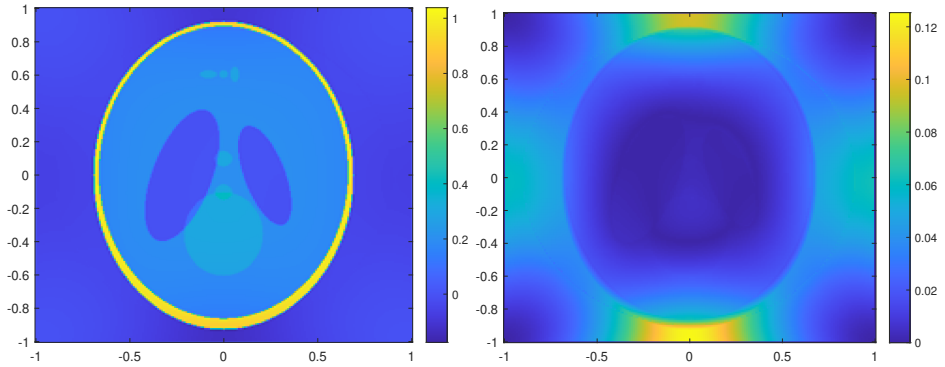

Figure 2.16 Averaged reconstructed source $\tilde{S}$ and its error under 10% Gaussian random noise.

For the relation between the relative standard deviations, we fix D and σ_a respectively and add 2%, 4%, 6%, 8%, 10% Gaussian random noise to another optical coefficient. The relations are shown in Figure 2.17. We can see that the average of $\tilde{S}$ is approximately S and the same relative

uncertainty level on D have larger impact than σ_a on $\tilde{S}$. From the scatter plot, we can see that the uncertainty in $\tilde{S}$ is at least locally Lipschitz boundeded by uncertainties in $(\tilde{D}, \tilde{\sigma}_a)$. The impact $\mathcal{E}_S$ is also linearly or superlinearly depend on $\mathcal{E}_D$ and $\mathcal{E}_{\sigma_a}$.

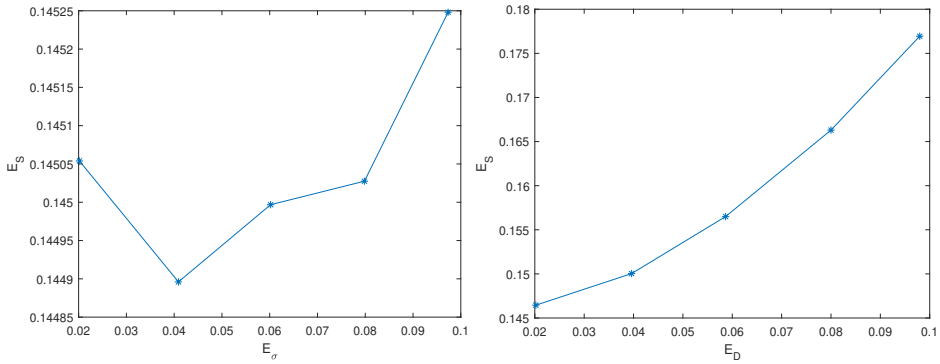

Figure 2.17 Left: $\mathcal{E}_S$ versus $\mathcal{E}_{\sigma_a}$. Right: $\mathcal{E}_S$ versus $\mathcal{E}_D$.

Remark 2.18. *Since we plot the distribution of norms, it is natural to have branches in the result. A simple example is plotting $|y|$ versus $|x|$ with relation $y = (x+1)^2$.*

CHAPTER 3

INVERSE BOUNDARY VALUE PROBLEMS FOR WAVE EQUATIONS

3.1 Introduction

We begin with the formulation of the *Inverse Boundary Value Problem (IBVP)* for the wave equation. Let $T > 0$ be a constant and $\Omega \subset \mathbb{R}^n$ be a bounded open subset with smooth boundary $\partial\Omega$. Consider the following boundary value problem for the acoustic wave equation with potential:

$$\begin{cases} \Box_{\rho,q} u(t,x) &= 0, & \text{in } (0,2T)\times\Omega \\ \partial_\nu u &= f, & \text{on } (0,2T)\times\partial\Omega \\ u(0,x) = \partial_t u(0,x) &= 0 & x \in \Omega. \end{cases} \tag{3.1}$$

Here $\Box_{\rho,q}$ is a linear wave operator defined as

$$\Box_{\rho,q} u(t,x) := \rho(x)\partial_t^2 u(t,x) - \Delta u(t,x) + q(x)u(t,x);$$

$\rho(x) := c^{-2}(x) \in C^\infty(\overline{\Omega})$, where $c(x)$ is a smooth wave speed bounded away from 0 and ∞, $q(x) \in L^\infty(\Omega)$ is a real-valued function referred to as the *potential*. We write the wave solution as $u = u^f(t,x)$ whenever it is necessary to specify the Neumann data.

The wave equation with vanished potential are often used to describe mechanical wave, such as acoustic wave, water wave, and seismic wave, whereas the wave equation with potential arise for example in quantum mechanics in the context of the Klein-Gordon equation. In mathematics, we formulate these equations together as (3.1).

Given $f \in C_c^\infty((0,2T)\times\partial\Omega)$, the well-posedness of this problem is ensured by the standard theory for second order hyperbolic partial differential equations [40]. As a result, the following *Neumann-to-Dirichlet map (ND map)* is well defined:

$$\Lambda_{\rho,q} f := u^f|_{(0,2T)\times\partial\Omega}. \tag{3.2}$$

The IBVP for the acoustic wave equation aims to recover the wave speed $c(x)$ or wave potential $q(x)$ from the knowledge of the ND map $\Lambda_{\rho,q}$.

Many imaging technologies are based on this inverse problem with vanished potential q. The *Ultra-Sound Computed Tomography* (USCT) is one significant example. During USCT, an

acoustic pulse is emitted from a known location outside the tissue by a point-like ultrasound source. A group of nearby ultrasonic transducers records the wave field created when the acoustic wave passes through the tissue. The aim of USCT is to reconstruct the acoustic wave speed throughout the tissue by repeating this process numerous times for a large number of emitter locations. Figure 3.1 shows an example using M transducers. Seismic tomography uses a similar data collection strategy to find oil reservoirs by attempting to recover the underground wave speed. In the continuous formulation of USCT and seismic tomography, the measurement is the boundary values of the Green's function. However, it is well known [71] that such data is equivalent to knowledge of the ND map under mild assumptions.

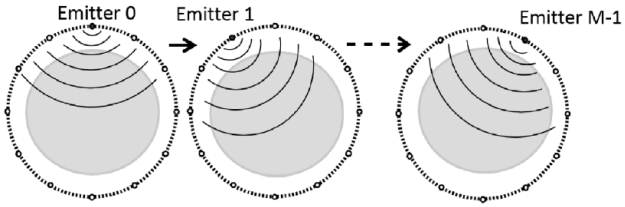

Figure 3.1 Data acquisition scheme in USCT [68].

In the literature, the IBVP for the acoustic wave equation has been thoroughly examined. For variable c and $q \equiv 0$, Belishev [11] demonstrated that c is uniquely determined by combining Tataru's unique continuation result [91] with the boundary control (BC) method. Since then, a great deal of work has been done to extend the result to wave equations on Riemannian manifolds with boundary [16, 36, 37, 38, 39, 43, 46, 49, 54, 55, 59, 62, 78, 81, 87]. Several studies have provided stability estimates: [2, 10, 17, 18, 24, 66, 70, 83, 84, 86].

The wave speed has been numerically reconstructed using the BC method in [12], and later in [15,31,76,96]. The implementations [12,15,31] involve solving unstable control problems, while the implementations [76, 96] are based on solving stable control problems with target functions exhibiting exponential growth or decay. The exponential behaviour leads to instability as well. On the other hand, the linearized approach introduced in [75] is stable. It should be noted that the one-dimensional case can be implemented steadily using the BC method [57]. See [22] on detection

of blockage in networks for an intriguing use of a variant of the method in the one-dimensional case.

Under suitable geometric assumptions, it can be proven that the problem to recover the speed of sound is Hölder stable [83, 84], even when the speed is given by an anisotropic Riemannian metric. Moreover, a low-pass version of c can be recovered in a Lipschitz stable manner [66].

The problem to recover q is Hölder stable assuming, again, that the geometry is nice enough [18, 70, 88]. To our knowledge, the method, based on using high frequency solutions to the wave equation and yielding the latter three results, has not been implemented computationally. Stability results applicable to general geometries have been proven using the BC method in [4], with an abstract modulus continuity, and very recently in [25, 26], with a doubly logarithmic modulus of continuity.

3.2 Nonlinear Inverse Boundary Value Problem

In this section, we consider the IBVP with vanished potential, i.e. $q(x) \equiv 0$. (3.1) can be written as

$$\begin{cases} \partial_t^2 u(t,x) - c^2(x)\Delta u(t,x) &= 0, & \text{in } (0,2T)\times\Omega \\ \partial_\nu u &= f, & \text{on } (0,2T)\times\partial\Omega \\ u(0,x) = \partial_t u(0,x) &= 0 & x\in\Omega. \end{cases} \tag{3.3}$$

This model is frequently used to describe the propagation of mechanical waves, and the inverse problems focus on recovering the wave speed distribution in order to learn about the medium's internal structure.

The ND map is represented as Λ_c, and we aim at recover wave speed $c(x)$ from the ND map [96]. Given function $u(t,x)$, we write $u(t)$ to represent the spatial part $u(t,\cdot)$.

3.2.1 Derivation

Introduce the time reversal operator $R : L^2([0,T]\times\partial\Omega) \to L^2([0,T]\times\partial\Omega)$,

$$Ru(t,\cdot) := u(T-t,\cdot), \qquad 0<t<T; \tag{3.4}$$

the low-pass filter $J : L^2([0,2T] \times \partial\Omega) \to L^2([0,T] \times \partial\Omega)$

$$Jf(t,\cdot) := \frac{1}{2}\int_t^{2T-t} f(\tau,\cdot)\, d\tau, \qquad 0 < t < T. \tag{3.5}$$

the orthogonal projection operator $P_T : L^2((0,2T) \times \partial\Omega) \to L^2((0,T) \times \partial\Omega)$

$$P_T : f \mapsto f|_{(0,T)\times\partial\Omega} \tag{3.6}$$

and its adjoint operator $P_T^* : L^2((0,T) \times \partial\Omega) \to L^2((0,2T) \times \partial\Omega)$, which is the extension by zero from $(0,T)$ to $(0,2T)$. Let $\mathcal{T}_D$ and $\mathcal{T}_N$ be the Dirichlet and Neumann trace operators respectively, that is,

$$\mathcal{T}_D u(t,\cdot) = u(t,\cdot)|_{\partial\Omega}, \qquad \mathcal{T}_N u(t,\cdot) = \partial_\nu u(t,\cdot)|_{\partial\Omega}.$$

Lemma 3.1. *Let u^f be the solution of* (3.3) *with $f \in C_c^\infty((0,2T) \times \partial\Omega)$. Suppose $v(t,x) \in C^\infty((0,2T) \times \Omega)$ satisfies the wave equation*

$$(\partial_t^2 - c^2(x)\Delta)v(t,x) = 0, \qquad \text{in } (0,2T) \times \Omega$$

Then

$$(u^f(T), v(T))_{L^2(\Omega,c^{-2}dx)} = (P_T f, J\mathcal{T}_D v)_{L^2((0,T)\times\partial\Omega)} - (P_T(\Lambda_c f), J\mathcal{T}_N v)_{L^2((0,T)\times\partial\Omega)}.$$

where ν is the unit outer normal vector field on $\partial\Omega$. Here, the weighted space $L^2(\Omega, c_0^{-2}dx)$ is defined as

$$L^2(\Omega, c_0^{-2}dx) := \left\{ u : \int_\Omega |u(x)|^2 c_0^{-2}(x)\, \mathrm{d}x < \infty \right\}.$$

Proof. Define

$$I(t,s) := (u^f(t), v(s))_{L^2(\Omega,c^{-2}dx)}.$$

We compute

$$\begin{aligned} &(\partial_t^2 - \partial_s^2)I(t,s) \\ =&(\Delta u^f(t), v(s))_{L^2(\Omega)} - (u^f(t), \Delta v(s))_{L^2(\Omega)} \\ =&(f(t), \mathcal{T}_D v(s))_{L^2(\partial\Omega)} - (\Lambda_c f(t), \mathcal{T}_N v(s))_{L^2(\partial\Omega)}, \end{aligned} \tag{3.7}$$

where the last equality follows from integration by parts. Since $u^f(0,x) = \partial_t u^f(0,x) = 0$, we have $I(0,s) = \partial_t I(0,s) = 0$, thus (3.7) can be considered as a inhomogeneous 1D wave equation together with initial conditions $I(0,s) = \partial_t I(0,s) = 0$. Solving this PDE gives

$$\begin{aligned}
&I(T,T)\\
=&\frac{1}{2}\int_0^T \int_t^{2T-t} \left[(f(t), \mathcal{T}_D v(\sigma))_{L^2(\partial\Omega)} - (\Lambda_c f(t), \mathcal{T}_N v(\sigma))_{L^2(\partial\Omega)}\right] d\sigma dt\\
=&\int_0^T [(f(t), \frac{1}{2}\int_t^{2T-t} \mathcal{T}_D v(\sigma)\, d\sigma)_{L^2(\partial\Omega)} - (\Lambda_c f(t), \frac{1}{2}\int_t^{2T-t} \mathcal{T}_N v(\sigma)\, d\sigma)_{L^2(\partial\Omega)}]\, dt\\
=&(P_T f, J\mathcal{T}_D v)_{L^2((0,T)\times\partial\Omega)} - (P_T(\Lambda_c f), J\mathcal{T}_N v)_{L^2((0,T)\times\partial\Omega)}.
\end{aligned}$$

□

Lemma 3.1 is used to derive two important results. The first is the Blagoveščenskiĭ's identity. To this end, denote by $\Lambda_{c,T}$ the truncated ND map defined as in (3.2), (3.3) with $2T$ replaced by T. It can be easily verified from integration by parts that its adjoint operator (with respect to the inner product in $L^2((0,T)\times\partial\Omega)$) is $\Lambda_{c,T}^* = R\Lambda_{c,T}R$ where R is the time reversal operator (3.4), see also Appendix B.1.

Introduce the *connecting operator*

$$K := J\Lambda_c P_T^* - R\Lambda_{c,T}RJP_T^*, \tag{3.8}$$

which is the principal object of the boundary control method [14]. The operator K connects inner-products between waves in the interior to measurements on the boundary, see Proposition 3.2. Moreover, K is a compact operator since $\Lambda_{c,T} : L^2((0,T)\times\partial\Omega) \to H^{2/3}((0,T)\times\partial\Omega)$ is smoothing, see [92].

The Blagoveščenskiĭ's identity we will establish is slightly different from its original form [21]. Instead, it is a reformulation that has been previously used in [20, 30, 74].

Proposition 3.2. *Let u^f, u^h be the solutions of* (3.3) *with Neumann traces $f, h \in L^2((0,T)\times\partial\Omega)$, respectively. Then*

$$(u^f(T), u^h(T))_{L^2(\Omega, c^{-2}dx)} = (f, Kh)_{L^2((0,T)\times\partial\Omega)} = (Kf, h)_{L^2((0,T)\times\partial\Omega)}. \tag{3.9}$$

In particular if $h = f$, one has

$$\|u^f(T)\|^2_{L^2(\Omega,c^{-2}dx)} = (f, Kf)_{L^2((0,T)\times\partial\Omega)} = (Kf, f)_{L^2((0,T)\times\partial\Omega)}. \tag{3.10}$$

Proof. We first prove this for $f, h \in C_c^\infty((0,T)\times\partial\Omega)$. Apply Lemma 3.1 to u^f and $v = u^h$ and notice that $\mathcal{T}_D u^h = \Lambda_c P_T^* h$ and $\mathcal{T}_N u^h = P_T^* h$. One has

$$\begin{aligned}
&(u^f(T), u^h(T))_{L^2(\Omega,c^{-2}dx)}\\
=&(P_T f, J\Lambda_c P_T^* h)_{L^2((0,T)\times\partial\Omega)} - (P_T(\Lambda_c f), JP_T^* h)_{L^2((0,T)\times\partial\Omega)}\\
=&(f, J\Lambda_c P_T^* h)_{L^2((0,T)\times\partial\Omega)} - (\Lambda_{c,T} f, JP_T^* h)_{L^2((0,T)\times\partial\Omega)}\\
=&(f, J\Lambda_c P_T^* h)_{L^2((0,T)\times\partial\Omega)} - (f, R\Lambda_{c,T} RJP_T^* h)_{L^2((0,T)\times\partial\Omega)}\\
=&(f, Kh)_{L^2((0,T)\times\partial\Omega)}
\end{aligned}$$

where we have used that $P_T(\Lambda_c f) = \Lambda_{c,T} f$ and that $\Lambda_{c,T}^* = R\Lambda_{c,T}R$ in $L^2((0,T)\times\partial\Omega)$. This establishes the first equality in (3.9). Interchanging f and h yields the second equality in (3.9).

For general $f, h \in L^2((0,T)\times\partial\Omega)$, simply notice that K is a continuous operator and that compactly supported smooth functions are dense in L^2. The proof is completed. □

Notice that harmonic functions can be considered as time independent wave solutions, we can establish an inner product between waves and harmonic functions from boundary data. Introduce an operator B as

$$B := J\mathcal{T}_D - R\Lambda_{c,T}RJ\mathcal{T}_N. \tag{3.11}$$

Proposition 3.3. *Let u^f be the solutions of* (3.3) *with Neumann traces $f \in L^2((0,T)\times\partial\Omega)$. For any harmonic function $\phi \in C^\infty(\Omega)$, one has*

$$(u^f(T), \phi)_{L^2(\Omega,c^{-2}dx)} = (f, B\phi)_{L^2((0,T)\times\partial\Omega)}.$$

Proof. Similar to the proof of Proposition 3.2, let $f \in C_c^\infty((0,T)\times\Omega)$, apply Lemma 3.1 to u^f and

$v = \phi$. One has

$$\begin{aligned}(u^f(T), \phi)_{L^2(\Omega, c^{-2}dx)} =& (f, J\mathcal{T}_D\phi)_{L^2((0,T)\times\partial\Omega)} - (P_T(\Lambda_c f), J\mathcal{T}_N\phi)_{L^2((0,T)\times\partial\Omega)} \\ =& (f, J\mathcal{T}_D\phi)_{L^2((0,T)\times\partial\Omega)} - (\Lambda_{c,T} f, J\mathcal{T}_N\phi)_{L^2((0,T)\times\partial\Omega)} \\ =& (f, J\mathcal{T}_D\phi)_{L^2((0,T)\times\partial\Omega)} - (f, R\Lambda_{c,T}RJ\mathcal{T}_N\phi)_{L^2((0,T)\times\partial\Omega)}.\end{aligned}$$

by the continuity of B and density of compactly supported functions in L^2, we complete the proof. □

Suppose for any harmonic function ψ, one can find an explicit sequence f_α such that $u^{f_\alpha}(T) \to \psi$ as $\alpha \to 0$ in $L^2(\Omega, c^{-2}dx)$, then according to Proposition 3.3:

$$(\psi, \phi)_{L^2(\Omega, c^{-2}dx)} = \lim_{\alpha\to 0}(u^{f_\alpha}(T), \phi)_{L^2(\Omega, c^{-2}dx)} = \lim_{\alpha\to 0}(f_\alpha, B\phi)_{L^2((0,T)\times\partial\Omega)}. \tag{3.12}$$

The right hand side can be computed from Λ_c, see (3.11). Thus the integral

$$(\psi, \phi)_{L^2(\Omega, c^{-2}dx)} = \int_\Omega \psi\phi\, c^{-2}(x)\, dx \tag{3.13}$$

is known for all harmonic functions ψ and ϕ. For any fixed vectors $\xi, \eta \in \mathbb{R}^n$ with $|\xi| = |\eta|$ and $\xi \perp \eta$, choose the complex harmonic functions as

$$\psi(x) := e^{\frac{i}{2}(-\xi + i\eta)\cdot x}, \qquad \phi(x) := e^{\frac{i}{2}(-\xi - i\eta)\cdot x}. \tag{3.14}$$

Then $\psi\phi = e^{i\xi\cdot x}$ and one recovers $\mathcal{F}(c^{-2})$, the Fourier transform of c^{-2}, by varying ξ, the wave speed c is recovered.

In order to construct sequence f_α, we introduce the *control operator*

$$Wf := u^f(T).$$

where u^f is the solution of (3.3). According to [61], $W : L^2((0,T)\times\partial\Omega) \to L^2(\Omega)$ is a bounded linear operator. Moreover, Tataru's theorem in [90] implies that the range of W is dense in $L^2(\Omega)$. It follows from Proposition 3.2 that $K = W^*W$. It is also easy to verify that $W^*\psi = B\psi$ for any harmonic function ψ. The control sequence f_α is constructed using Tikhonov regularization, and the following lemma is used to prove the convergence.

Lemma 3.4 ([74, Lemma 1]). *Let $A : X \to Y$ be a bounded linear operator between two Hilbert spaces X and Y. For any $y \in Y$, let $\alpha > 0$ be a constant and $x_\alpha := (A^*A + \alpha)^{-1}A^*y$. Then*

$$Ax_\alpha \to P_{\overline{Ran(A)}}y \qquad as\ \alpha \to 0$$

where $P_{\overline{Ran(A)}}y$ denotes the orthogonal projection of y onto the closure of the range of A.

Proposition 3.5. *For any harmonic function ψ, the following minimization problem with parameter $\alpha > 0$:*

$$f_\alpha := \arg\min_f \|Wf - \psi\|^2_{L^2(\Omega, c^{-2}dx)} + \alpha\|f\|^2_{L^2(0,T)\times\partial\Omega}.$$

has a unique solution $f_\alpha \in L^2((0,T)\times\partial\Omega)$. This solution satisfies the linear equation

$$(K + \alpha)f_\alpha = B\psi. \tag{3.15}$$

Moreover, $u^{f_\alpha}(T) \to \psi$ as $\alpha \to 0$ in $L^2(\Omega, c^{-2}dx)$.

Proof. The functional to be minimized is

$$F_\alpha(f) := \|Wf - \psi\|^2_{L^2(\Omega, c^{-2}dx)} + \alpha\|f\|^2_{L^2((0,T)\times\partial\Omega)}.$$

As $W : L^2((0,T)\times\partial\Omega) \to L^2(\Omega)$ is bounded and linear, [56, Theorem 2.11] claims that F_α has a unique minimizer, named f_α, in $L^2((0,T)\times\partial\Omega)$.

The functional to be minimized is

$$\begin{aligned}
F_\alpha(f) :=& \|u^f(T) - \psi\|^2_{L^2(\Omega, c^{-2}dx)} + \alpha\|f\|^2_{L^2((0,T)\times\partial\Omega)} \\
=& \|u^f(T)\|^2_{L^2(\Omega, c^{-2}dx)} - 2(u^f(T), \psi)_{L^2(\Omega, c^{-2}dx)} + \|\psi\|^2_{L^2(\Omega, c^{-2}dx)} + \alpha\|f\|^2_{L^2(0,T)\times\partial\Omega}. \\
=& (f, Kf)_{L^2((0,T)\times\partial\Omega)} - 2(f, B\psi)_{L^2((0,T)\times\partial\Omega)} + \|\psi\|^2_{L^2(\Omega, c^{-2}dx)} + \alpha\|f\|^2_{L^2((0,T)\times\partial\Omega)} \\
=& (f, (K + \alpha)f)_{L^2((0,T)\times\partial\Omega)} - 2(f, B\psi)_{L^2((0,T)\times\partial\Omega)} + \|\psi\|^2_{L^2(\Omega, c^{-2}dx)}
\end{aligned}$$

The terms $\|u^f(T)\|^2_{L^2(\Omega, c^{-2}dx)}$ and $(u^f(T), \phi)_{L^2((\Omega, c^{-2}dx))}$ are computed using Proposition 3.2 and Proposition 3.3, respectively. This is a bilinear form of f whose Frechét derivative is

$$F'(f) = 2(K + \alpha)f - 2B\psi.$$

The minimizer satisfies $F'(f_\alpha) = 0$, hence (3.15).

Finally, since $K = W^*W$ and $B\psi = W^*\psi$ (see the content before Proposition 3.5), we conclude from Lemma 3.4 that $Wf_\alpha \to P_{\overline{Ran(W)}}\psi$ in $L^2(\Omega, c^{-2}dx)$ as $\alpha \to 0$. Tataru's theorem [90] claims that the range of W is dense in $L^2(\Omega)$, hence $P_{\overline{Ran(W)}}\psi = \psi$. □

Summarizing the discussion in this section, we have proved global convergence of the following reconstruction algorithm, see Algorithm 3.1.

Input: low-pass filter J, time-reversal operator R, projection operator P_T, ND map Λ_c
Output: wave speed c

---

1. Assemble the connecting operator $K = J\Lambda_c P_T^* - R\Lambda_{c,T}RJP_T^*$ (see (3.8)).
2. Assemble the operator $B = J\mathcal{T}_D - R\Lambda_{c,T}RJ\mathcal{T}_N$ (see (3.11)).
3. Construct the harmonic function $\psi(x) = e^{\frac{i}{2}(-\xi+i\eta)\cdot x}$ (see (3.14)) and solve the linear system $(K+\alpha)f_\alpha = B\psi$, (see (3.15)).
4. Construct the harmonic function $\phi(x) := e^{\frac{i}{2}(-\xi-i\eta)\cdot x}$ (see (3.14)) and compute the Fourier projection
$$\int_\Omega e^{-i\xi\cdot x}c^{-2}(x)\,dx = \lim_{\alpha\to 0}(f_\alpha, B\phi)_{L^2((0,T)\times\partial\Omega)}$$
through the limiting process, (see (3.12)).
5. Repeat the above steps with various ξ to recover the Fourier transform $\mathcal{F}(c^{-2})$.
6. Invert the Fourier transform to recover c^{-2}, and eventually c.

Algorithm 3.1 Non-Iterative Reconstruction Algorithm for Acoustic IBVP.

3.2.2 Algorithm Implementation

In this section, we numerically implement the algorithm using finite difference scheme. We choose the spatial domain to be $\Omega = [-1,1]^2$. For the forward problem, we uniformly discretized Ω into 101×101 grids, i.e. $\Delta x = \Delta y = \frac{1}{50}$. The grid points are represented as (x_i, y_j), where $x_i = -1 + \frac{i}{100}$, $y_j = -1 + \frac{j}{100}$, $0 \le i, j \le 100$. The time step size Δt is chosen as $\Delta t = \frac{2T}{L} \le \frac{\sqrt{2}}{2c_{\max}}\Delta x$ to fulfill the Courant–Friedrichs–Lewy (CFL) condition, where $c_{\max}$ denote the maximum of $c(x)$ over Ω, L is the number of time steps. Then the temporal grid points are labeled using $t_l = l\Delta t$, $l = 0, 1, \ldots, L$. For simplicity, the values of u on the grid points are denoted by

$$u_{ij}^l := u(t_l, x_i, y_j), \qquad l = 0, 1, \ldots, L, \quad i, j = 0, 1, \ldots, 100.$$

3.2.2.1 Discrete Wave Equation Solver

The finite difference solver for (3.3) requires the approximation of operators Δ, ∂_t^2 and ∂_ν. We use the second order approximation for interior grid points:

$$\partial_t^2 u(t_l, x_i, y_j) \approx \frac{u_{i,j}^{l-1} + u_{i,j}^{l+1} - 2u_{i,j}^l}{\Delta t^2};$$

$$\Delta u(t_l, x_i, y_j) \approx \frac{u_{i-1,j}^l + u_{i+1,j}^l + u_{i,j-1}^l + u_{i,j+1}^l - 4u_{i,j}^l}{\Delta x^2},$$

which gives us the update formula for interior points:

$$u_{i,j}^{l+1} = 2u_{i,j}^l - u_{i,j}^{l-1} + c^2(x_i, y_j)\frac{\Delta t^2}{\Delta x^2}[u_{i-1,j}^l + u_{i+1,j}^l + u_{i,j-1}^l + u_{i,j+1}^l - 4u_{i,j}^l].$$

The boundary points are updated from the discretization of Neumann derivatives. For instance $i = 0$, we have

$$\partial_\nu u(t_l, x_0, y_j) \approx -\frac{3u_{0,j}^l - 4u_{1,j}^l + u_{2,j}^l}{2\Delta x}.$$

The initial condition $u(0, x) = u_t(0, x) = 0$ is implemented by setting

$$u_{i,j}^0 = 0, \qquad u_{i,j}^1 = u_{i,j}^{-1}.$$

Notice that all the finite difference approximation above have second order accuracy, we have an discrete wave solver.

3.2.2.2 Implementation of ND Map Λ_c

The spatial boundary $\partial\Omega$ consists of 400 boundary grid points, thus the temporal boundary $[0, T] \times \partial\Omega$ contains $400(L + 1)$ boundary grid points in total. These boundary grid points are ordered in the lexicographical order to form a column vector, that is, a boundary grid point (t_l, x_i, y_j) is ahead of another $(t_{l'}, x_{i'}, y_{j'})$ if and only if (1) $l < l'$; or (2) $l = l'$ and $i < i'$; or (3) $l = l', i = i', j < j'$. In this way, the discretized ND map is a $400(L + 1) \times 400(L + 1)$ square matrix, denoted by $[\Lambda_c] \in \mathbb{R}^{400(L+1)\times 400(L+1)}$.

In order to find the matrix representation $[\Lambda_c]$, we place a unit source f_{ij}^l on each boundary grid point as the Neumann data and utilize the forward solver to obtain the resulting Dirichlet data on all

the boundary grid points. Here f_{ij}^{l} takes the value 1 on (t_l, x_i, y_j) and 0 on all the other boundary grid points.

Once the matrices are generated, we re-sample the ND map on a coarser grid of size $(L+1)\times 51\times 51$ and implement Algorithm 3.1 to avoid the inverse crime, i.e. the spatial grid size changed to $\Delta x = \Delta y = \frac{1}{25}$. Thus the ND map matrices are $[\Lambda_{c,T}] \in \mathbb{R}^{200\lceil\frac{L+1}{2}\rceil\times 200\lceil\frac{L+1}{2}\rceil}$ and $[\Lambda_c] \in \mathbb{R}^{200(L+1)\times 200(L+1)}$.

3.2.2.3 Implementation of Connecting Operator K

In order to discretize K, we need to discretize J first. The integration is calculated using trapezoidal rule, which is

$$\int_{t_l}^{2T-t_l} f(\tau,\cdot)\,d\tau \approx \sum_{k=l}^{L-l-1} \frac{f(t_k,\cdot)+f(t_{k+1},\cdot)}{2}\Delta t.$$

Since we rearrange the grid points into lexicographical order, the discretized filtering operator can be written as a blocking matrix $[J] \in \mathbb{R}^{200\lceil\frac{L+1}{2}\rceil\times 200(L+1)}$, whose blocks are all 200×200 diagonal matrix. Here $\lceil\frac{L+1}{2}\rceil$ denote the smallest integer which is greater or equal to $\frac{L+1}{2}$.

Specifically, if L is odd,

$$[J] = \frac{\Delta t}{2}\begin{pmatrix} [I] & 2[I] & 2[I] & \dots & \dots & \dots & \dots & 2[I] & 2[I] & [I] \\ & [I] & 2[I] & \dots & \dots & \dots & \dots & 2[I] & [I] & \\ & & \ddots & \ddots & & & \iddots & \iddots & & \\ & & & [I] & 2[I] & 2[I] & [I] & & & \\ & & & & [I] & [I] & & & & \end{pmatrix},$$

If L is even,

$$[J] = \frac{\Delta t}{2}\begin{pmatrix} [I] & 2[I] & 2[I] & \dots & \dots & \dots & 2[I] & 2[I] & [I] \\ & [I] & 2[I] & \dots & \dots & \dots & 2[I] & [I] & \\ & & \ddots & \ddots & & \iddots & \iddots & & \\ & & & [I] & 2[I] & [I] & & & \\ & & & & [O] & & & & \end{pmatrix},$$

where $[I]$ denote the identity matrix and $[O]$ denote the zero matrix.

Similarly the discretized time reversal operator $[R] \in \mathbb{R}^{200\lceil\frac{L+1}{2}\rceil\times 200\lceil\frac{L+1}{2}\rceil}$ and discretized restriction operator $[P_T] \in \mathbb{R}^{200\lceil\frac{L+1}{2}\rceil\times 200(L+1)}$ can be represented as

$$[P_T] = \left([I]_{200\lceil\frac{L+1}{2}\rceil\times 200\lceil\frac{L+1}{2}\rceil} \quad [O]\right), \qquad [R] = \begin{pmatrix} & & [I] \\ & \iddots & \\ [I] & & \end{pmatrix}.$$

The discrete extension operator $[P_T^*]$ is taken to be $[P_T]^t$, the transpose of $[P_T]$. It is obvious that $[\Lambda_{c,T}] = [P_t][\Lambda_c][P_T^*]$, which implies $[\Lambda_{c,T}]$ is simply the top left submatrix of $[\Lambda_c]$. Finally, the discretized K is the following matrix product, according to (3.8):

$$[K] = [J][\Lambda_c][P_T]^t - [R][\Lambda_{c,T}][R][J][P_T]^t \qquad \in \mathbb{R}^{200\lceil\frac{L+1}{2}\rceil\times 200\lceil\frac{L+1}{2}\rceil}.$$

3.2.2.4 Implementation of the Operator B

The implementation of operator B requires to calculate $\mathcal{T}_D, \mathcal{T}_N$. Since the harmonic function ψ is handcrafted and time independent, we can analytically calculate Dirichlet and Neumann value of the known harmonic function and make $L+1$ copies to form vector $[\mathcal{T}_D\psi], [\mathcal{T}_N\psi] \in \mathbb{R}^{200(L+1)\times 1}$.

3.2.2.5 Solve Boundary Control Sequence f_α

Following The next step is to solve for $[f_\alpha]$ from the discretized version of (3.15):

$$([K] + \alpha)[f_\alpha] = [B][\psi|_{\partial\Omega}]. \tag{3.16}$$

Here $[f_\alpha]$ is the discretized version of f_α in (3.15); ψ is an arbitrary harmonic function and $[\psi|_{\partial\Omega}] \in \mathbb{R}^{200(L+1)\times 1}$ denotes the vectorized boundary restriction $\psi|_{\partial\Omega}$. Both $[f_\alpha]$ and $\psi|_{\partial\Omega}$ are in the lexicographical order as before. Since $[K]$ is calculated using matrix multiplication, it is not guaranteed to be positive semidefinite. Instead of solving (3.15) with Tikhonov regularization, the equation that we solve is

$$([K]^t[K] + \alpha)[f_\alpha] = [K]^t[B][\psi|_{\partial\Omega}] \tag{3.17}$$

where $[K]^t$ is the transpose of $[K]$.

3.2.2.6 Solve Wave Speed c

In Algorithm 3.1, c is recovered by creating appropriate complex exponential harmonic functions (3.14) and inverting the Fourier transform. However, due to their propensity for explosive growth in some directions, such harmonic functions are not appropriate for numerical implementation.

We build harmonic functions using the fundamental solutions method (FSM) as an alternative to selecting complex exponential harmonic functions. Kupradze [58] was the first to propose this method, which has the advantage of being easily implemented numerically. There has been research on its suitability for elliptic boundary value problems in general [23]; additionally, see also the review paper [42]. In FSM, the harmonic functions are of the form

$$\sum_{j=1}^{N} a_j \Phi(|x - x^{(j)}|) \tag{3.18}$$

Here Φ is the fundamental solution of the Laplace operator, i.e. $\Phi(r) = \log r$ for $n = 2$ and $\Phi(r) = \frac{1}{r}$ for $n \geq 3$, and a_j are real scalar coefficients. These functions are harmonic in $\mathbb{R}^n$ except at the singularities $x^{(j)}$, which are chosen to be outside the computational domain. It has been shown [67] that an arbitrary 2D function which is harmonic inside the unit disk and continuous up to the boundary can be approximated to any prescribed accuracy using functions of the form (3.18).

Under such construction, for a fixed sufficiently small $\alpha > 0$, the right-hand side of (3.12) can be approximate using the trapezoidal rule:

$$(f_\alpha, B\phi)_{L^2((0,T)\times\partial\Omega)} \approx \sum_{j=1}^{200\lceil\frac{L+1}{2}\rceil} w_j [f_\alpha]_j [B\phi]_j \Delta x \Delta t \tag{3.19}$$

where $[f_\alpha]$ has been obtained from (3.17), $[B\phi]$ is computed from the matrix multiplication, and $w \in \mathbb{R}^{200\lceil\frac{L+1}{2}\rceil}$ is the weight coefficient vector from the trapezoidal rule, whose first and last 200 elements are $\frac{1}{2}$ and others are 1.

On the left-hand side of (3.12), we approximate the interior integral over Ω by successively applying the trapezoidal rule first to y and then to x. If we write $\tilde{w} = (\frac{1}{2}, 1, \ldots, 1, \frac{1}{2}) \in \mathbb{R}^{51}$ for the

coefficient vector of the trapezoidal rule, then

$$(\psi, \phi)_{L^2(\Omega, c^{-2}dx)} = \int_{-1}^{1}\int_{-1}^{1} \psi(x,y)\phi(x,y)c^{-2}(x,y)\,dxdy$$
$$\approx \sum_{j,k=0}^{I} \tilde{w}_j\tilde{w}_k\psi(x_j,y_k)\phi(x_j,y_k)c^{-2}(x_j,y_k)(\Delta x)^2. \tag{3.20}$$

Equating (3.19) and (3.20) and inserting various harmonic functions of the form (3.18) gives rise to a system of linear equations on the unknowns $c^{-2}(x_j, y_k)$, $j, k = 0, 1, \ldots, 50$. Depending on the number of harmonic functions, the linear system can be over determined or under determined, we can apply different regression methods, such as least square regression, Tikhonov regularization, to solve for the regularized unknowns.

3.2.3 Numerical Experiment

In this section, following (3.18), we choose harmonic basis to be

$$\phi^{(1)} = \ln((x-2.3)^2 + (y-2.2)^2), \qquad \phi^{(2)} = \ln((x+2.5)^2 + (y-2.1)^2),$$
$$\phi^{(3)} = \ln((x-2.7)^2 + (y+1.9)^2), \qquad \phi^{(4)} = \ln((x+1.5)^2 + (y+2.5)^2),$$
$$\phi^{(5)} = \ln((x+1.2)^2 + (y+2.5)^2), \qquad \phi^{(6)} = 1.$$

We denote the vector space generated by the products of these harmonic functions by S_6, that is,

$$S_6 := \text{span}\{\phi^{(i)}\phi^{(j)} : i, j = 1, \ldots, 6\}.$$

If c^{-2} is in the vector space S_6, we have following representation

$$c^{-2} = \sum_{1\le i\le j\le 6} c_{ij}\phi^{(i)}\phi^{(j)}.$$

Take the inner product $(\cdot,\cdot)_{L^2(\Omega)}$ with $\phi^{(k)}\phi^{(l)}$ respectively, $1 \le k \le l \le 6$, to obtain the following linear system

$$\mathbf{A}\cdot\begin{bmatrix} c_{11} \\ c_{12} \\ \vdots \\ c_{66} \end{bmatrix} = \begin{bmatrix} (c^{-2}, {\phi^{(1)}}^2)_{L^2(\Omega)} \\ (c^{-2}, \phi^{(1)}\phi^{(2)})_{L^2(\Omega)} \\ \vdots \\ (c^{-2}, {\phi^{(7)}}^2)_{L^2(\Omega)} \end{bmatrix}. \tag{3.21}$$

where the 21×21 coefficient matrix $\mathbf{A}$ is

$$\begin{bmatrix} (\phi^{(1)^2}, \phi^{(1)^2})_{L^2(\Omega)} & (\phi^{(1)^2}, \phi^{(1)}\phi^{(2)})_{L^2(\Omega)} & \dots & (\phi^{(1)^2}, \phi^{(6)^2})_{L^2(\Omega)} \\ (\phi^{(1)}\phi^{(2)}, \phi^{(1)^2})_{L^2(\Omega)} & (\phi^{(1)}\phi^{(2)}, \phi^{(1)}\phi^{(2)})_{L^2(\Omega)} & \dots & (\phi^{(1)}\phi^{(2)}, \phi^{(6)^2})_{L^2(\Omega)} \\ \vdots & \vdots & \ddots & \vdots \\ (\phi^{(6)^2}, \phi^{(1)^2})_{L^2(\Omega)} & (\phi^{(6)^2}, \phi^{(1)}\phi^{(2)})_{L^2(\Omega)} & \dots & (\phi^{(6)^2}, \phi^{(6)^2})_{L^2(\Omega)} \end{bmatrix}$$

The coefficient matrix on the left-hand side can be analytically computed, and the components of the vector on the right-hand side are exactly the inner products on the left hand side of (3.20). We then solve the discretized version of this linear system to obtain the coefficients c_{ij}.

The orthogonal projection of c^{-2} onto S_6 is implied by the inner products on the right side of (3.21) if c^{-2} is not in the vector space S_6. The linear system can be solved to obtain an orthogonal projection. Since harmonic function products are dense in $L^2(\Omega)$, the orthogonal projection should better approximate c^{-2} as the number of harmonic functions $\phi^{(j)}$ increases.

3.2.3.1 Experiment 1: $c \equiv 1, c^{-2} \in S_6$.

We start our experiment by evaluating the reconstruction for the simplest case, the wave speed $c_1 \equiv 1$. Notice that $c_1^{-2} \equiv 1 \in S_6$ since $\phi^{(6)} = 1$. Figure 3.2 shows the reconstructed speed and errors in the presence of 0%, 5%, and 50% of Gaussian random noises with zero mean and unit variance, respectively. It is observed that the reconstructed wave speed are little affected by the presence of random noise. This is because, in the definition (3.8) of K, the low-pass filter J and the ND map Λ_c tend to smooth out the Gaussian random noise.

3.2.3.2 Experiment 2: c is variable, $c^{-2} \in S_6$.

The algorithm is then tested with a variable speed c_2, where $c_2^{-2} \in S_6$. In this experiment, the random Gaussian noise is fixed at 5%. The ground-truth speed is generated as

$$c_2^{-2} = \sum_{i=1}^{6} \frac{i}{10} \phi^{(i)},$$

see the leftmost of Figure 3.3.

We execute the reconstructions using the first 2, 4, and 6 harmonic functions $\phi^{(i)}$, correspondingly, to demonstrate how the quality of the images improves with an increase in the number of basis

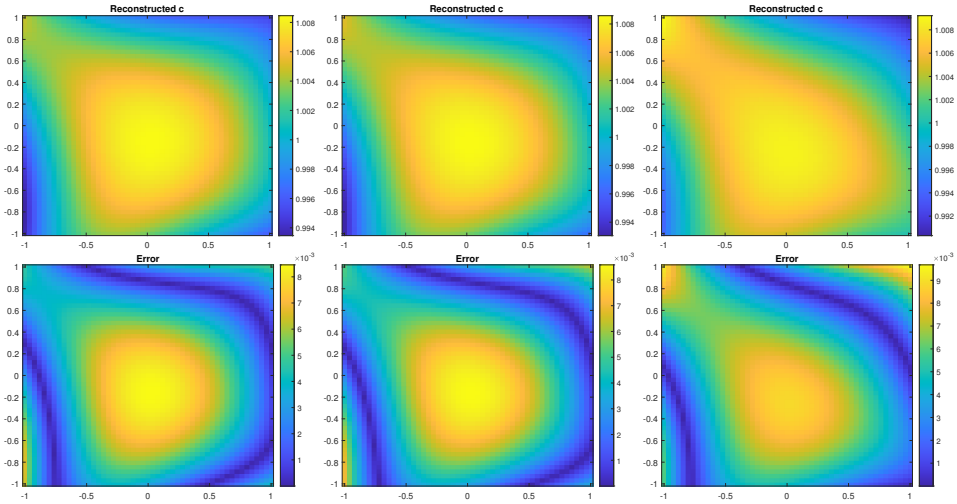

Figure 3.2 Experiment 1. Top row: reconstructed c. Bottom row: error between the reconstruction and the ground truth. First column: 0% noise; the relative L^2-error is 0.4769%. Second column: 5% noise; the relative L^2-error is 0.4873%. Third column: 50% noise; the relative L^2-error is 0.5454%. Grid: $283 \times 51 \times 51$.

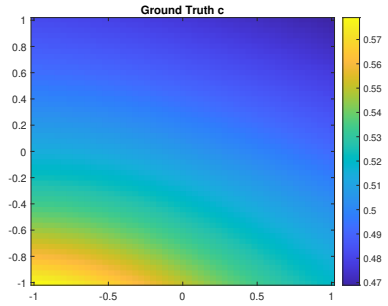

Figure 3.3 The variable speed c_2.

functions. As the number of harmonic functions rises, we find that the reconstruction becomes more accurate; Figure 3.4 provides numerical evidence for this observation.

3.2.3.3 Experiment 3: c is variable, $c^{-2} \notin S_6$.

Next, we test the ability of the algorithm in recovering a variable speed

$$c_3(x, y) = 1 + 0.08 \sin \pi x + 0.06 \cos \pi y,$$

with $c_3^{-2} \notin S_6$. The wave speed c_3 and its orthogonal projection on S_6 are illustrated in Figure 3.5.

The reconstructions with the first 2, 4, and 6 harmonic functions $\phi^{(i)}$ are shown in Figure 3.6. It is not possible to recover the exact discrete version of c^{-2} in this scenario. The L^2-orthogonal projection of c^{-2} onto the subspace S_6 is what the algorithm produces instead. This is because, in

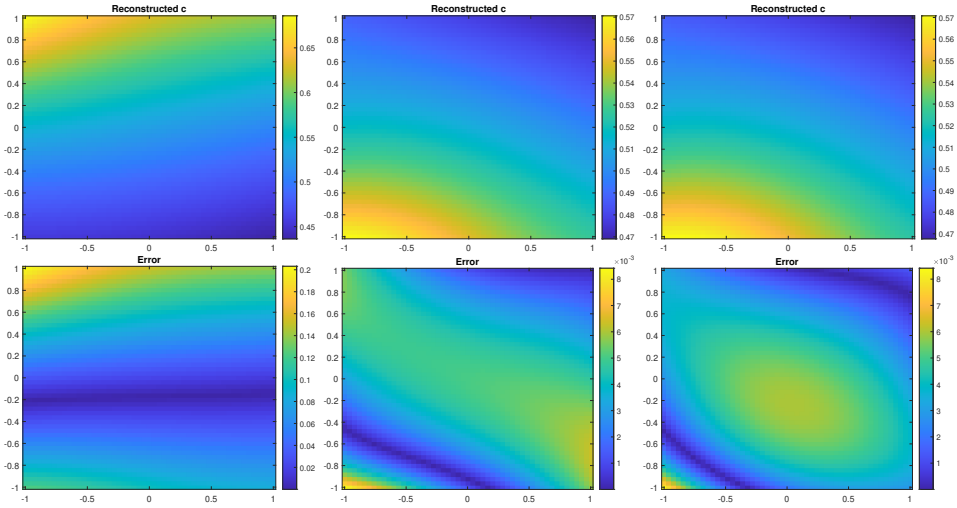

Figure 3.4 Experiment 2. Top row: reconstructed c. Bottom row: error between the reconstruction and the ground truth. First column: First 2 harmonic functions; the relative L^2-error is 15.6987%. Second column: First 4 harmonic functions; the relative L^2-error is 0.7939%. Third column: All 6 harmonic functions; the relative L^2-error is 0.7907%. Grid: $323 \times 51 \times 51$.

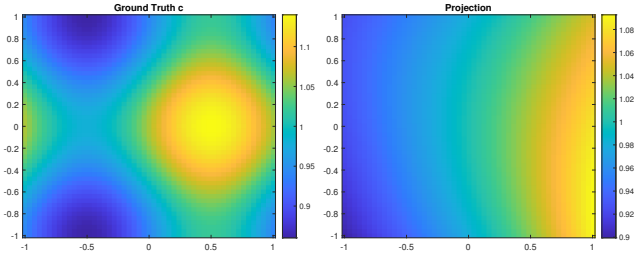

Figure 3.5 Left: the variable speed c_3. Right: orthogonal projection of c_3 on S_6.

order to solve for $[c^{-2}]$, Tikhonov regularization was used. You can view the numerical validation in Figure 3.6.

3.2.3.4 More Experiments

We also test the performance of the inversion formulae in different cases, such as discontinuous wave speed $c(x)$ or partial data case, i.e. the NP map is set to zero at the region can not be measured. See [96] for details.

3.3 Linearized Inverse Boundary Value Problem

Linearization, such as Born approximation, Kirchhoff approximation, is a method to give linear approximation of a nonlinear model. It is widely used to solve nonlinear inverse problems [3, 19, 60, 98]. The linearized inverse problems consider the model as a perturbation of a (known) background model. One can construct a perturbed model which is linearly depend on the unknown

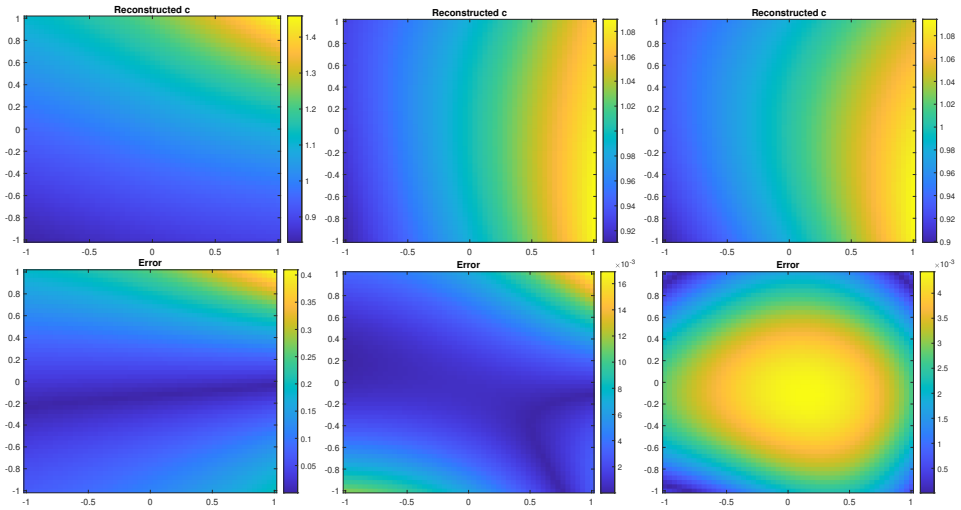

Figure 3.6 Experiment 3. Top row: reconstructed c. Bottom row: error between the reconstruction and the orthogonal projection of the ground truth. First column: First 2 harmonic functions; the relative L^2-error is 12.3535%. Second column: First 4 harmonic functions; the relative L^2-error is 0.4139%. Third column: All 6 harmonic functions; the relative L^2-error is 0.3104%. Grid: $323 \times 51 \times 51$.

parameters. In this section, we introduce linearized IBVP algorithms for both wave speed and wave potential reconstruction.

3.3.1 Reconstruct Wave Speed through Linearization

In Section 3.2, we introduce an algorithm to reconstruct wave speed with full nonlinear treatment. In this section, we apply linearization to the nonlinear IBVP to reconstruct the wave speed. We assume the wave potential $q = q_0(x) \in C^\infty(\overline{\Omega})$ is known, and we want to recover $c(x)$ from the ND map Λ_{ρ,q_0}. For simplicity, we use Λ_ρ to represent Λ_{ρ,q_0} in this section.

We use the linearization to solve the IBVP. For the formal derivation, we write

$$\rho(x) = \rho_0(x) + \varepsilon\dot{\rho}(x), \qquad u(t,x) = u_0(t,x) + \varepsilon\dot{u}(t,x)$$

where $\rho_0 = c_0^{-2}$ from a known background wave speed and u_0 is the background solution. Substitute these into (3.1). Equating the $O(1)$-terms gives

$$\begin{cases} \Box_{\rho_0,q_0} u_0(t,x) &= 0, & \text{in } (0,2T)\times\Omega \\ \partial_\nu u_0 &= f, & \text{on } (0,2T)\times\partial\Omega \\ u_0(0,x) = \partial_t u_0(0,x) &= 0, & x\in\Omega. \end{cases} \tag{3.22}$$

Equating the $O(\varepsilon)$-terms gives

$$\begin{cases} \Box_{\rho_0,q_0}\dot{u}(t,x) &= -\dot{\rho}(x)\partial_t^2 u_0(t,x), & \text{in } (0,2T)\times\Omega \\ \partial_\nu \dot{u} &= 0, & \text{on } (0,2T)\times\partial\Omega \\ \dot{u}(0,x) = \partial_t\dot{u}(0,x) &= 0 & x\in\Omega. \end{cases} \tag{3.23}$$

Write the ND map $\Lambda_\rho = \Lambda_{\rho_0} + \varepsilon\dot{\Lambda}_{\dot{\rho}}$, where Λ_{ρ_0} denote the ND map for the unperturbed boundary value problem (3.22), and $\dot{\Lambda}_{\dot{\rho}}$ is defined as

$$\dot{\Lambda}_{\dot{\rho}} : f \mapsto \dot{u}|_{(0,2T)\times\partial\Omega}. \tag{3.24}$$

Since ρ_0 and q_0 are known, the unperturbed problem (3.22) can be explicitly solved to obtain u_0 and Λ_{ρ_0}. As in the previous section, we will write $\dot{u} = \dot{u}^f$ if it is necessary to specify the Neumann data f. Then the linearized IBVP concerns recovery of the speed $\dot{\rho}$ from $\dot{\Lambda}_{\dot{\rho}}$.

3.3.1.1 Derivation

Similar to Section 3.2, introduce the time reversal operator R, see (3.4), the low-pass filter J, see (3.5). the orthogonal projection operator P_T, see (3.6) and its adjoint operator P_T^* as the extension by zero from $(0,T)$ to $(0,2T)$. Let $\mathcal{T}_D$ and $\mathcal{T}_N$ be the Dirichlet and Neumann trace operators respectively, that is,

$$\mathcal{T}_D u(t,\cdot) = u(t,\cdot)|_{\partial\Omega}, \qquad \mathcal{T}_N u(t,\cdot) = \partial_\nu u(t,\cdot)|_{\partial\Omega}.$$

Introduce the *connecting operator*

$$K := J\Lambda_q P_T^* - R\Lambda_{q,T} RJP_T^*$$

Similarly, the following Blagoveščenskiĭ's identity holds.

Proposition 3.6. *Let u^f, u^h be the solutions of* (3.1) *with Neumann traces $f, h \in L^2((0,T)\times\partial\Omega)$, respectively. Then*

$$(u^f(T), u^h(T))_{L^2(\Omega, c_0^{-2}dx)} = (f, Kh)_{L^2((0,T)\times\partial\Omega)} = (Kf, h)_{L^2((0,T)\times\partial\Omega)}. \tag{3.25}$$

Proof. The proof is similar to the proof of Proposition 3.2. We first prove this for $f, h \in C_c^\infty((0,T)\times \partial\Omega)$. Define

$$I(t,s) := (u^f(t), u^h(s))_{L^2(\Omega, c_0^{-2}dx)}.$$

We compute

$$\begin{aligned}
&(\partial_t^2 - \partial_s^2) I(t,s) \\
=&((\Delta+q)u^f(t), u^h(s))_{L^2(\Omega)} - (u^f(t), (\Delta+q)u^h(s))_{L^2(\Omega)} \\
=&(f(t), \Lambda_\rho P_T^* h(s))_{L^2(\partial\Omega)} - (\Lambda_\rho P_T^* f(t), h(s))_{L^2(\partial\Omega)},
\end{aligned} \tag{3.26}$$

where the last equality follows from integration by parts.

Notice that the expression in (3.26) is exactly the same as in (3.7), the following proof are exactly the same as the proof of Proposition 3.2. □

Corollary 3.7. *Suppose $f, h \in C_c^\infty((0,T]\times\partial\Omega)$. Then*

$$(\Delta u^f(T) - q u^f(T), u^h(T))_{L^2(\Omega, c_0^{-2}dx)} = (\partial_t^2 f, Kh)_{L^2((0,T)\times\partial\Omega)} = (K\partial_t^2 f, h)_{L^2((0,T)\times\partial\Omega)}. \tag{3.27}$$

Proof. Replacing f by $\partial_t^2 f$ in (3.25), we get

$$(u^{\partial_t^2 f}(T), u^h(T))_{L^2(\Omega, c_0^{-2}dx)} = (\partial_t^2 f, Kh)_{L^2((0,T)\times\partial\Omega)} = (K\partial_t^2 f, h)_{L^2((0,T)\times\partial\Omega)}.$$

As both $u^{\partial_t^2 f}$ and $\partial_t^2 u^f$ satisfy (3.1) with f replaced by $\partial_t^2 f$, the well-posedness of the boundary value problem ensures that

$$\rho u^{\partial_t^2 f} = \rho \partial_t^2 u^f = \Delta u^f - q u^f.$$

□

Remember that we write $\Lambda_\rho = \Lambda_{\rho_0} + \varepsilon \dot{\Lambda}_{\dot{\rho}}$ in the linearization setting, we have the following linearization $K = K_0 + \varepsilon \dot{K}$. Here K_0 is the connecting operator for the background wave equation (3.22):

$$K_0 := J\Lambda_{\rho_0} P_T^* - R\Lambda_{\rho_0, T} R J P_T^*. \tag{3.28}$$

K_0 can be explicitly computed since Λ_{ρ_0,q_0} is known. $\dot{K}$ is the resulting perturbation in the connecting operator:

$$\dot{K} := J\dot{\Lambda}_{\dot{\rho}}P_T^* - R\dot{\Lambda}_{\dot{\rho},T}RJP_T^*. \tag{3.29}$$

$\dot{K}$ can be explicitly computed once $\dot{\Lambda}_{\dot{\rho}}$ is given.

We write $\dot{\Lambda}$ for $\dot{\Lambda}_{\dot{\rho}}$ when there is no risk of confusion. Linearizing (3.25) and (3.27) gives the following integral identity, which is essential to the development of the reconstruction procedure:

Proposition 3.8. *Let $0 \neq \lambda \in \mathbb{R}$ be a nonzero real number. If $f, h \in C_c^\infty((0,T] \times \partial\Omega)$ satisfy*

$$[\Delta - q_0 + \lambda\rho_0]u_0^f(T) = [\Delta - q_0 + \lambda\rho_0]u_0^h(T) = 0 \quad \text{in } \Omega, \tag{3.30}$$

then the following identity holds:

$$-(\dot{\rho}u_0^f(T), u_0^h(T))_{L^2(\Omega)} = \frac{1}{\lambda}[(\partial_t^2 f + \lambda f, \dot{K}h)_{L^2((0,T)\times\partial\Omega)} + (\dot{\Lambda}f(T), h(T))_{L^2(\partial\Omega)}]. \tag{3.31}$$

Proof. For $f, h \in C_c^\infty((0,T) \times \partial\Omega)$, we will make use of (3.25) (3.27) to obtain some identities. First, we substitute all linearizations into (3.25). Equating $O(1)$-terms gives

$$(\rho_0 u_0^f(T), u_0^h(T))_{L^2(\Omega)} = (f, K_0 h)_{L^2((0,T)\times\partial\Omega)} = (K_0 f, h)_{L^2((0,T)\times\partial\Omega)}.$$

Equating $O(\varepsilon)$-terms gives

$$\begin{aligned}&(f, \dot{K}h)_{L^2((0,T)\times\partial\Omega)} = (\dot{K}f, h)_{L^2((0,T)\times\partial\Omega)}\\ =&(\dot{\rho}u_0^f(T), u_0^h(T))_{L^2(\Omega)} + (\rho_0\dot{u}^f(T), u_0^h(T))_{L^2(\Omega)} + (\rho_0 u_0^f(T), \dot{u}^h(T))_{L^2(\Omega)}.\end{aligned} \tag{3.32}$$

Similarly, we substitute all linearizations into (3.27). Equating $O(1)$-terms gives

$$(\Delta u_0^f(T) - q u_0^f(T), u_0^h(T))_{L^2(\Omega)} = (\partial_t^2 f, K_0 h)_{L^2((0,T)\times\partial\Omega)} = (K_0\partial_t^2 f, h)_{L^2((0,T)\times\partial\Omega)}.$$

Equating $O(\varepsilon)$-terms gives

$$\begin{aligned}&(\partial_t^2 f, \dot{K}h)_{L^2((0,T)\times\partial\Omega)} = (\dot{K}\partial_t^2 f, h)_{L^2((0,T)\times\partial\Omega)}\\ =&((\Delta - q_0)\dot{u}^f(T), u_0^h(T))_{L^2(\Omega)} + ((\Delta - q_0)u_0^f(T), \dot{u}^h(T))_{L^2(\Omega)}\\ =&(\dot{u}^f(T), (\Delta - q_0)u_0^h(T))_{L^2(\Omega)} - (\dot{\Lambda}f(T), h(T))_{L^2(\partial\Omega)} + ((\Delta - q_0)u_0^f(T), \dot{u}^h(T))_{L^2(\Omega)}\end{aligned}$$

where the last inequality use the integration by parts and the fact that $\dot{u}^f|_{(0,2T)\times\partial\Omega} = \dot{\Lambda} f$ and $\partial_\nu \dot{u} = 0$. Add (3.32) multiplied by $\lambda \in \mathbb{R}$ to get

$$\begin{aligned}
&(\partial_t^2 f + \lambda f, \dot{K} h)_{L^2((0,T)\times\partial\Omega)} + (\dot{\Lambda} f(T), h(T))_{L^2(\partial\Omega)} \\
=&(\partial_t^2 f, \dot{K} h)_{L^2((0,T)\times\partial\Omega)} + (\dot{\Lambda} f(T), h(T))_{L^2(\partial\Omega)} + (\lambda f, \dot{K} h)_{L^2((0,T)\times\partial\Omega)} \\
=&(\dot{u}^f(T), [\Delta - q_0 + \lambda\rho_0] u_0^h(T))_{L^2(\Omega)} + ([\Delta - q_0 + \lambda\rho_0] u_0^f(T), \dot{u}^h(T))_{L^2(\Omega)} \\
&+ \lambda(\dot{\rho} u_0^f(T), u_0^h(T))_{L^2(\Omega)}.
\end{aligned}$$

If $[\Delta - q_0 + \lambda\rho_0] u_0^f(T) = [\Delta - q_0 + \lambda\rho_0] u_0^h(T) = 0$ in Ω, the first term and second term on the right-hand side vanish, resulting in (3.31). □

Notice that all parameters in (3.30) are known. For each $\lambda \in \mathbb{R}$, we can construct functions ϕ, ψ satisfy (3.30). According to Proposition 3.8, once we find control sequence f_α, h_α such that $u^{f_\alpha}(T) \to \phi$, $u^{h_\alpha}(T) \to \psi$, we have the weighted inner product $(\phi, \psi)_{L^2(\Omega, \dot{\rho}\,\mathrm{d}x)}$ from (3.31). The following proposition ensures the existance of such boundary controls:

Proposition 3.9. *Let $c_0 \in C^\infty(\overline{\Omega})$ be strictly positive and $q_0 \in C^\infty(\overline{\Omega})$. Suppose that all maximal[1] geodesics on $(\overline{\Omega}, c_0^{-2}\,\mathrm{d}x^2)$ have length strictly less than some fixed $T > 0$. Then for any $\phi \in C^\infty(\overline{\Omega})$, there is $f \in C_c^\infty((0,T] \times \partial\Omega)$ such that*

$$u_0^f(T) = \phi \quad \text{in } \Omega, \tag{3.33}$$

where u_0 is the solution of (3.22)*. Moreover, there is $C > 0$, independent of ϕ, such that*

$$\|f\|_{H^2((0,T)\times\partial\Omega)} \le C \|\phi\|_{H^4(\Omega)}. \tag{3.34}$$

Proof. See [75, Proposition 4]. □

3.3.1.2 Stability and Reconstruction

The following reconstruction is mostly based on (3.30) (3.31).

[1]For a maximal geodesic $\gamma : [a,b] \to \overline{\Omega}$ there may exists $t \in (a,b)$ such that $\gamma(t) \in \partial\Omega$. The geodesics are maximal on the closed set $\overline{\Omega}$.

Case 1: ρ_0 is constant Without loss of generality, we assume $\rho_0 = 1$. When q_0 is constant, we choose $\lambda \geq q_0$. The equation (3.30) becomes the Helmholtz equation

$$[\Delta + (\lambda - q_0)]u_0^f(T) = [\Delta + (\lambda - q_0)]u_0^f(T) = 0 \quad \text{in } \Omega.$$

Without loss of generality, we take $q_0 = 0$. Then the Helmholtz solutions are $e^{i\sqrt{\lambda}\theta\cdot x}$, where $\theta \in \mathbb{S}^{n-1}$ is an arbitrary unit vector. Furthermore, Proposition 3.9 guarantees the existence of $f, h \in C_c^\infty((0,T] \times \partial\Omega)$ such that

$$u_0^f(T) = u_0^h(T) = e^{i\sqrt{\lambda}\theta\cdot x}. \tag{3.35}$$

Theorem 3.10. *Suppose $\lambda > 0$, $c_0 = 1$ and $q_0 = 0$. Then the Fourier transform $\hat{\dot\rho}$ of $\dot\rho$ can be reconstructed as follows:*

$$\hat{\dot\rho}(2\sqrt{\lambda}\theta) = -\frac{1}{\lambda}[(\partial_t^2 f + \lambda f, \dot K h)_{L^2((0,T)\times\partial\Omega)} + (\dot\Lambda f(T), h(T))_{L^2(\partial\Omega)}] \tag{3.36}$$

where $f, h \in C_c^\infty((0,T] \times \partial\Omega)$ are solutions to (3.35)*.*

Proof. The formula is obtained by substitute (3.35) into (3.31). Since $\theta \in \mathbb{S}^{n-1}$ and $\lambda \geq 0$ are arbitrary, it gives the Fourier transform of $\dot\rho$ everywhere. See also Algorithm 3.2. □

Remark 3.11. *An explicit procedure to solve for f and h from* (3.15) *is explained in Section 3.3.1.3.*

Input: low-pass filter J, time-reversal operator R, projection operator P_T, linearized ND map $\dot\Lambda_{\dot\rho}$
Output: sound speed perturbation $\dot\rho$

---

1. Choose $\lambda > 0$ and $\theta \in \mathbb{S}^{n-1}$.
2. Solve the boundary control equations $u_0^f(T) = u_0^h(T) = e^{i\sqrt{\lambda}\theta\cdot x}$ for f and h.
3. Construct the linearized connecting operator $\dot K$ by $\dot K := J\dot\Lambda P_T^* - R\dot\Lambda_T RJP_T^*$.
4. Compute $\mathcal{F}[\dot\rho](2\sqrt{\lambda}\theta)$ by

$$\mathcal{F}[\dot\rho](2\sqrt{\lambda}\theta) = -\frac{1}{\lambda}\left[(\partial_t^2 f + \lambda f, \dot K h)_{L^2((0,T)\times\partial\Omega)} + (\dot\Lambda f(T), h(T))_{L^2(\partial\Omega)}\right]. \tag{3.37}$$

5. Repeat the above steps with various $\lambda > 0$ and $\theta \in \mathbb{S}^{n-1}$ to recover the Fourier transform $\mathcal{F}[\dot\rho]$.
6. Invert the Fourier transform to recover $\dot\rho$.

Algorithm 3.2 Linearized Boundary Control Reconstruction of $\dot\rho$ when $q \equiv 0$.

Theorem 3.12. *Suppose $\lambda > 0$, $c_0 = 1$ and $q_0 = 0$. There exists a constant $C > 0$, independent of λ, such that*

$$\left|\hat{\dot{\rho}}(\sqrt{2\lambda}\theta)\right| \leq C(1+\sqrt{2}T(1+\lambda))\lambda^3 \|\dot{\Lambda}\|_{H^2((0,T)\times\partial\Omega)\to H^1((0,T)\times\partial\Omega)}$$

Proof. For a bounded linear operator $T : \mathcal{X} \to \mathcal{Y}$ between two Hilbert spaces $\mathcal{X}$ and $\mathcal{Y}$, we write $\|T\|_{\mathcal{X}\to\mathcal{Y}}$ for the operator norm of T. Let $f, h \in C_c^\infty((0,T]\times\partial\Omega)$ be solutions of (3.35) obtained from Proposition 3.9. We employ (3.36) to estimate:

$$\begin{aligned}
\lambda\left|\mathcal{F}[\dot{\rho}](\sqrt{2\lambda}\theta)\right| \leq & \|\partial_t^2 f + \lambda f\|_{L^2((0,T)\times\partial\Omega)} \|h\|_{L^2((0,T)\times\partial\Omega)} \|\dot{K}\|_{L^2((0,T)\times\partial\Omega)\to L^2((0,T)\times\partial\Omega)} \\
& + \|\dot{\Lambda} f(T)\|_{L^2(\partial\Omega)} \|h(T)\|_{L^2(\partial\Omega)} \\
\leq & (1+\lambda)\|f\|_{H^2((0,T)\times\partial\Omega)} \|h\|_{L^2((0,T)\times\partial\Omega)} \|\dot{K}\|_{L^2((0,T)\times\partial\Omega)\to L^2((0,T)\times\partial\Omega)} \\
& + \|\dot{\Lambda} f\|_{H^1((0,T)\times\partial\Omega)} \|h\|_{H^1((0,T)\times\partial\Omega)}
\end{aligned}$$

by the continuity of the trace operator.

In order to estimate $\|\dot{\Lambda} f\|_{H^1((0,T)\times\partial\Omega)}$, we extend $f \in H^2((0,T)\times\partial\Omega)$ to a function $F \in H^{2+\frac{3}{2}}((0,T)\times\Omega)$ so that $\partial_\nu F|_{(0,T)\times\partial\Omega} = f$ and $F(t,x) = 0$ for $x \in \Omega$ and t close to 0 (recall that $f(t,x) = 0$ for t near 0). Such F can be chosen to fulfill

$$\|F\|_{H^{3+\frac{1}{2}}((0,T)\times\Omega)} \leq C\|f\|_{H^2((0,T)\times\partial\Omega)}$$

Set $v := F - u_0$ where u_0 is the solution of (3.63), then v satisfies

$$\begin{cases}
\Box_{\rho_0,q_0} v &= \Box_{\rho_0,q_0} F, & \text{in } (0,2T)\times\Omega \\
\partial_\nu v &= 0, & \text{on } (0,2T)\times\partial\Omega \\
v|_{t=0} = \partial_t v|_{t=0} &= 0, & x \in \Omega.
\end{cases}$$

The regularity estimate for the wave equation [40] implies

$$\|v\|_{H^{2+\frac{1}{2}}((0,T)\times\Omega)} \leq C\|\Box_{\rho_0,q_0} F\|_{H^{1+\frac{1}{2}}((0,T)\times\Omega)} \leq C\|F\|_{H^{3+\frac{1}{2}}((0,T)\times\Omega)}$$

We conclude $u_0 \in H^{2+\frac{1}{2}}((0,T)\times\Omega)$ and $\dot{\rho}\partial_t^2 u_0 \in H^{\frac{1}{2}}((0,T)\times\Omega)$. The same regularity estimate for the wave equation applied to (3.23) implies

$$\|\dot{u}\|_{H^{1+\frac{1}{2}}((0,T)\times\Omega)} \leq C\|\dot{\rho}\partial_t^2 u_0\|_{H^{\frac{1}{2}}((0,T)\times\Omega)} \leq C\|u_0\|_{H^{2+\frac{1}{2}}((0,T)\times\Omega)}$$

These inequalities together with the trace estimate yield

$$\|\dot{\Lambda} f\|_{H^1((0,T)\times\partial\Omega)} \leq C\|\dot{u}\|_{H^{1+\frac{1}{2}}((0,T)\times\Omega)} \leq C\|f\|_{H^2((0,T)\times\partial\Omega)}$$

where the constant $C > 0$ is independent of f. Hence $\dot{\Lambda} : H^2((0,T)\times\partial\Omega) \to H^1((0,T)\times\partial\Omega)$ is a bounded linear operator.

It remains to estimate $\|\dot{K}\|_{L^2((0,T)\times\partial\Omega)\to L^2((0,T)\times\partial\Omega)}$. Consider the norms of each operator in (3.29). It is clear that

$$\|P_T^*\|_{L^2((0,T)\times\partial\Omega)\to L^2((0,2T)\times\partial\Omega)} = 1,$$

$$\|P_T\|_{L^2((0,2T)\times\partial\Omega)\to L^2((0,T)\times\partial\Omega)} = 1,$$

$$\|R\|_{L^2((0,T)\times\partial\Omega)\to L^2((0,T)\times\partial\Omega)} = 1.$$

Since $\dot{\Lambda}_T = P_T\dot{\Lambda}P_T^*$,

$$\|\dot{\Lambda}_T\|_{L^2((0,T)\times\partial\Omega)\to L^2((0,T)\times\partial\Omega)} \leq \|\dot{\Lambda}\|_{L^2((0,2T)\times\partial\Omega)\to L^2((0,2T)\times\partial\Omega)}.$$

To estimate operator J, it is important to observe that

$$\begin{aligned}
\|Jf\|^2_{L^2((0,T)\times\partial\Omega)} =& \int_0^T \int_{\partial\Omega} \left|\frac{1}{2}\int_t^{2T-t} f(\tau,x)\,\mathrm{d}\tau\right|^2 \mathrm{d}x\,\mathrm{d}t \\
\leq& \frac{1}{4}\int_0^T \int_{\partial\Omega} \left(\int_t^{2T-t} |f(\tau,x)|\,\mathrm{d}\tau\right)^2 \mathrm{d}x\,\mathrm{d}t \\
\leq& \frac{1}{4}\int_0^T \int_{\partial\Omega} \left(\int_0^{2T} |f(\tau,x)|\,\mathrm{d}\tau\right)^2 \mathrm{d}x\,\mathrm{d}t \\
\leq& \frac{1}{4}\int_0^T \int_{\partial\Omega} 2T\int_0^{2T} |f(\tau,x)|^2\,\mathrm{d}\tau\,\mathrm{d}x\,\mathrm{d}t \\
=& \frac{T^2}{2}\|f\|^2_{L^2((0,2T)\times\partial\Omega)},
\end{aligned}$$

we have

$$\|J\|_{L^2((0,2T)\times\partial\Omega)\to L^2((0,T)\times\partial\Omega)} \leq \frac{T}{\sqrt{2}},$$

Thus, we conclude

$$\|\dot{K}\|_{L^2((0,T)\times\partial\Omega)\to L^2((0,T)\times\partial\Omega)} \leq \sqrt{2}T\|\dot{\Lambda}\|_{L^2((0,2T)\times\partial\Omega)\to L^2((0,2T)\times\partial\Omega)}.$$

Finally, we can complete the stability estimate:

$$\begin{aligned}
&\left|\mathcal{F}[\dot{\rho}](\sqrt{2\lambda}\theta)\right| \\
\leq&\frac{1+\lambda}{\lambda}\|f\|_{H^2((0,T)\times\partial\Omega)}\|h\|_{H^1((0,T)\times\partial\Omega)}\|\dot{K}\|_{L^2((0,T)\times\partial\Omega)\to L^2((0,T)\times\partial\Omega)} \\
+&\frac{1}{\lambda}\|\dot{\Lambda}f\|_{H^3((0,T)\times\partial\Omega)}\|h\|_{H^1((0,T)\times\partial\Omega)} \\
\leq&\frac{\sqrt{2}T(1+\lambda)}{\lambda}\|f\|_{H^2((0,T)\times\partial\Omega)}\|h\|_{H^1((0,T)\times\partial\Omega)}\|\dot{\Lambda}\|_{L^2((0,T)\times\partial\Omega)\to L^2((0,T)\times\partial\Omega)} \\
+&\frac{1}{\lambda}\|f\|_{H^2((0,T)\times\partial\Omega)}\|\dot{\Lambda}\|_{H^2((0,T)\times\partial\Omega)\to H^1((0,T)\times\partial\Omega)}\|h\|_{H^1((0,T)\times\partial\Omega)} \\
\leq&C_\lambda\|\dot{\Lambda}\|_{H^2((0,T)\times\partial\Omega)\to H^1((0,T)\times\partial\Omega)}
\end{aligned}$$

where the constant C_λ satisfies (see (3.34))

$$\begin{aligned}
C_\lambda :=&\frac{1+\sqrt{2}T(1+\lambda)}{\lambda}\|f\|_{H^2((0,T)\times\partial\Omega)}\|h\|_{H^1((0,T)\times\partial\Omega)} \\
\leq&C\frac{1+\sqrt{2}T(1+\lambda)}{\lambda}\|e^{i\sqrt{\lambda}\theta\cdot x}\|^2_{H^4(\Omega)} \leq C(1+\sqrt{2}T(1+\lambda))\lambda^3
\end{aligned}$$

for some constant $C > 0$ independent of λ. □

When q_0 is variable, choose $\lambda \geq 0$, then (3.30) becomes the perturbed Helmholtz equation

$$[\Delta + \lambda - q_0]u_0^f(T) = [\Delta + \lambda - q_0]u_0^h(T) = 0 \quad \text{in } \Omega.$$

A class of solutions are total waves of the form

$$\phi(x) = e^{i\sqrt{\lambda}\theta\cdot x} + r(x;\lambda) \tag{3.38}$$

with $\theta \in \mathbb{S}^{n-1}$ and the scattered wave $r(x;\lambda)$ satisfying

$$(\Delta + \lambda - q_0)r = q_0 e^{i\sqrt{\lambda}\theta\cdot x} \qquad \text{in } \Omega. \tag{3.39}$$

According to [75, Lemma 13],

$$\|r\|_{H^s(\mathbb{R}^n)} = O(\lambda^{\frac{s-1}{2}}) \qquad \text{as } \lambda \to \infty \tag{3.40}$$

for any $s \geq 0$.

One dimension: In one dimension (1D), $\theta = \pm 1$. Let us take $\theta = 1$ and choose (3.38) to be the value of $u_0^f(T)$ and $u_0^h(T)$. Substituting into (3.31) gives

$$\begin{aligned}&\hat{\dot{\rho}}(2\sqrt{\lambda}) + 2(\dot{\rho}e^{i\sqrt{\lambda}\theta\cdot x}, r)_{L^2(\Omega)} + (\dot{\rho}r, r)_{L^2(\Omega)}\\ =&-\frac{1}{\lambda}[(\partial_t^2 f + \lambda f, \dot{K}h)_{L^2((0,T)\times\partial\Omega)} + (\dot{\Lambda}f(T), h(T))_{L^2(\partial\Omega)}]\end{aligned} \tag{3.41}$$

Since

$$|(\dot{\rho}e^{i\sqrt{\lambda}\theta\cdot x}, r)_{L^2(\Omega)}| \le C\|\dot{\rho}\|_{L^\infty(\Omega)}\|r\|_{L^2(\Omega)}, \qquad |(\dot{\rho}r, r)_{L^2(\Omega)}| \le C\|\dot{\rho}\|_{L^\infty(\Omega)}\|r\|^2_{L^2(\Omega)}.$$

The left hand side of (3.41) decay like $O(\lambda^{-\frac{1}{2}})$ as $\lambda \to \infty$ according to (3.40). The approximate reconstruction follows in the high-frequency regime. Moreover, an approximate stability estimate can be provided in the same way as in the proof of Theorem 3.12 with an extra $O(\lambda^{-\frac{1}{2}})$ term:

$$\left|\hat{\dot{\rho}}(\sqrt{2\lambda}\theta)\right| \le C(1+\sqrt{2}T(1+\lambda))\lambda^3\|\dot{\Lambda}\|_{H^2((0,T)\times\partial\Omega)\to H^1((0,T)\times\partial\Omega)} + O(\lambda^{-\frac{1}{2}}). \tag{3.42}$$

High Dimension: In dimension $n \ge 2$, more freedom is available in choosing the wave vectors. Let $\theta, \omega \in \mathbb{R}^n$ be two vectors such that $\theta \perp \omega$. We take the following solutions:

$$\begin{aligned}\phi(x) :=&\phi_0(x) + r_1(x;\lambda), \qquad \phi_0(x) := e^{i(k\theta+l\omega)\cdot x}\\ \psi(x) :=&\psi_0(x) + r_2(x;\lambda), \qquad \psi_0(x) := e^{i(k\theta-l\omega)\cdot x}\end{aligned}$$

where r_1, r_2 satisfy (3.40). Choose $k^2+l^2 = \lambda$ such that $(\Delta+\lambda)\phi_0 = (\Delta+\lambda)\psi_0 = 0$. Proposition 3.9 asserts that there are $f, h \in C_c^\infty((0,T]\times\partial\Omega)$ such that

$$u_0^f(T) = \phi = \phi_0 + r_1, \qquad u_0^h(T) = \psi = \psi_0 + r_2. \tag{3.43}$$

Inserting (3.43) into (3.31) gives

$$\begin{aligned}&-\hat{\dot{\rho}}(2k\theta) - (\dot{\rho}e^{i(k\theta+l\omega)\cdot x}, r_2)_{L^2(\Omega)} - (\dot{\rho}e^{i(k\theta-l\omega)\cdot x}, r_1)_{L^2(\Omega)} - (\dot{\rho}r_1, r_2)_{L^2(\Omega)}\\ =&\frac{1}{\lambda}[(\partial_t^2 f + (k^2+l^2)f, \dot{K}h)_{L^2((0,T)\times\partial\Omega)} + (\dot{\Lambda}f(T), h(T))_{L^2(\partial\Omega)}]\end{aligned} \tag{3.44}$$

If we fix k and let $l \to \infty$, then $\lambda \to \infty$. Due to the decay property (3.40), $\|r_1\|_{L^2(\Omega)}, \|r_2\|_{L^2(\Omega)} \to 0$. We obtain the reconstruction formula for any $k \ge 0$ and any $\theta \in \mathbb{S}^{n-1}$:

$$\hat{\dot{\rho}}(2k\theta) = -\lim_{l\to\infty}\frac{1}{k^2+l^2}\left[(\partial_t^2 f + (k^2+l^2)f, \dot{K}h)_{L^2((0,T)\times\partial\Omega)} + (\dot{\Lambda}f(T), h(T))_{L^2(\partial\Omega)}\right].$$

Moreover, we can obtain a Hölder-type stability estimate for $\|\dot{\rho}\|_{H^{-s}(\mathbb{R}^n)}$, where $s > 0$ is an arbitrary real number and $H^{-s}(\mathbb{R}^n)$ is the L^2-based Sobolev space of order $-s$ over $\mathbb{R}^n$.

Theorem 3.13. *Suppose $c_0 = 1$, $q_0 \in C^\infty(\overline{\Omega})$ and q_0 is not identically zero. For any $s > 0$, there exists a constant $C > 0$ independent of λ such that*

$$\|\dot{\rho}\|_{H^{-s}(\mathbb{R}^n)} \leq C\|\dot{\Lambda}\|^{\frac{2s}{9(n+2s)}}_{H^2((0,T)\times\partial\Omega)\to H^1((0,T)\times\partial\Omega)}.$$

Proof. Write $\xi := 2k\theta$ and

$$\delta := \|\dot{\Lambda}\|_{H^2((0,T)\times\partial\Omega)\to H^1((0,T)\times\partial\Omega)}.$$

Let $\xi_0 > 0$ be a sufficiently large number that is to be determined. We decompose

$$\|\dot{\rho}\|^2_{H^{-s}(\mathbb{R}^n)} = \int_{|\xi|\leq\xi_0} \frac{|\hat{\dot{\rho}}(\xi)|^2}{(1+|\xi|^2)^s}\, d\xi + \int_{|\xi|>\xi_0} \frac{|\hat{\dot{\rho}}(\xi)|^2}{(1+|\xi|^2)^s}\, d\xi.$$

For the integral over high frequencies, we have

$$\int_{|\xi|>\xi_0} \frac{|\hat{\dot{\rho}}(\xi)|^2}{(1+|\xi|^2)^s}\, d\xi \leq \frac{1}{(1+\xi_0^2)^s}\int_{|\xi|>\xi_0} |\hat{\dot{\rho}}(\xi)|^2\, d\xi \leq \frac{\|\dot{\rho}\|^2_{L^2(\mathbb{R}^n)}}{(1+\xi_0^2)^s} \leq C\frac{1}{\xi_0^{2s}}.$$

For the integral over low frequencies, it is easy to see that:

$$\int_{|\xi|\leq\xi_0} \frac{|\hat{\dot{\rho}}(\xi)|^2}{(1+|\xi|^2)^s}\, d\xi \leq \int_{|\xi|\leq\xi_0} |\hat{\dot{\rho}}(\xi)|^2\, d\xi \leq C\xi_0^n \|\hat{\dot{\rho}}\|^2_{L^\infty(B(0,\xi_0))}.$$

The norm $\|\hat{\dot{\rho}}\|_{L^\infty(B(0,\xi_0))}$ can be estimated using (3.82). Indeed, for $|\xi| \leq \xi_0$, we have

$$\begin{aligned}
|\hat{\dot{\rho}}(\xi)| &\leq \frac{1}{\lambda}|(\partial_t^2 f + (k^2+l^2)f, \dot{K}h)_{L^2((0,T)\times\partial\Omega)} + (\dot{\Lambda}f(T), h(T))_{L^2(\partial\Omega)}| + \frac{C}{\sqrt{\lambda}} \\
&\leq C\frac{1+\sqrt{2}T(1+\lambda)}{\lambda}\|\phi\|_{H^4(\Omega)}\|\psi\|_{H^4(\Omega)}\delta + \frac{C}{\sqrt{\lambda}} \\
&\leq C\frac{1+\sqrt{2}T(1+\lambda)}{\lambda}\left(\|\phi_0\|_{H^4(\Omega)} + \|r_1\|_{H^4(\Omega)}\right)\left(\|\psi_0\|_{H^4(\Omega)} + \|r_2\|_{H^4(\Omega)}\right)\delta + \frac{C}{\sqrt{\lambda}} \\
&\leq C\frac{1+\sqrt{2}T(1+\lambda)}{\lambda}\left(\lambda^2 + \lambda^{\frac{3}{2}}\right)^2\delta + \frac{C}{\sqrt{\lambda}}
\end{aligned}$$

where the first and the last inequality is a consequence of (3.40), the second inequality follows from the proof of Proposition 3.12. Utilizing the relation $\lambda = k^2 + l^2$, we conclude

$$\|\hat{\dot{\rho}}\|^2_{L^\infty(B(0,\xi_0))} \leq C\left[(1+\sqrt{2}T(1+\lambda))^2\lambda^4(1+\sqrt{\lambda})^4\delta^2 + \frac{1}{\lambda}\right] \leq C\left[(\xi_0^2+l^2)^8\delta + \frac{1}{l^2}\right]$$

provided $\xi_0 > 0$ is sufficiently large. Combining these estimates, we see that

$$\|\dot{\rho}\|^2_{H^{-s}(\mathbb{R}^n)} \leq C\left[\xi_0^n(\xi_0^2 + l^2)^8\delta^2 + \frac{\xi_0^n}{l^2} + \frac{1}{\xi_0^{2s}}\right].$$

Choosing $l^2 = \xi_0^{n+2s}$ and $\xi_0 = \delta^{-\frac{2}{9(n+2s)}}$ yields

$$\|\dot{\rho}\|^2_{H^{-s}(\mathbb{R}^n)} \leq C\delta^{\frac{4s}{9(n+2s)}},$$

where C is a constant independent of λ and δ is sufficiently small.

□

Case2: ρ_0 is variable When $\rho_0 = \rho_0(x) > 0$ is non-constant, the equations (3.30) are no longer perturbed Helmholtz equations, but Schrödinger's equations with the potential $-q + \lambda\rho_0 \in L^\infty(\Omega)$. The idea is to employ Schrödinger solutions to probe based on the identity (3.31).

The class of solutions we will resort to are the *complex geometric optics (CGO) solutions* that were first proposed in [89] for dimension $n \geq 3$. A CGO solution ϕ is a function of the form

$$\phi(x) := e^{i\zeta\cdot x}(1 + r(x)). \tag{3.45}$$

where $\zeta \in \mathbb{C}^n$ is a complex vector with $\zeta \cdot \zeta = 0$, and the remainder term $r(x)$ satisfies

$$\Delta r + 2\zeta \cdot \nabla r - (q - \lambda\rho_0)r = q - \lambda\rho_0. \tag{3.46}$$

Moreover, $r \to 0$ in a certain function space as $|\zeta| \to \infty$.

The following proposition is a direct application of [89, Theorem 2.3 and Corollary 2.4] to the Schrödinger's equation $(\Delta - q + \lambda\rho_0)\phi = 0$.

Lemma 3.14 ([89, Theorem 2.3 and Corollary 2.4])**.** *Let $n \geq 3$ and $s \in \mathbb{R}$ a real number such that $s > \frac{n}{2}$. Let $\zeta \in \mathbb{C}^n$ be a complex vector with $\zeta \cdot \zeta = 0$ and $|\zeta| \geq \varepsilon_0 > 0$ for some positive constant ε_0. There exist positive constants C_0, C_1, depending on s, n, ε_0 and Ω, such that if*

$$C_0\|q - \lambda\rho_0\|_{H^s(\Omega)} < |\zeta|,$$

then $\phi = \phi(x)$ defined in (3.45) *satisfies $(\Delta - q + \lambda\rho_0)\phi = 0$; moreover*

$$\|r\|_{H^s(\Omega)} \leq \frac{C_1}{|\zeta|}\|q - \lambda\rho_0\|_{H^s(\Omega)} \tag{3.47}$$

We now construct specific CGO solutions that are useful for our purpose. Let $\xi \in \mathbb{R}^n (n \geq 3)$ be an arbitrary non-zero vector, and let $e^{(1)}, e^{(2)} \in \mathbb{S}^{n-1}$ be two real unit vectors such that $\{\xi, e^{(1)}, e^{(2)}\}$ forms an orthogonal set. Choose a positive number R with $R \geq \frac{|\xi|}{\sqrt{2}}$. Define

$$\zeta^{(1)} := -\frac{1}{2}\xi + i\frac{R}{\sqrt{2}}e^{(1)} + \sqrt{\frac{R^2}{2} - \frac{|\xi|^2}{4}}e^{(2)}, \qquad \zeta^{(2)} := -\frac{1}{2}\xi - i\frac{R}{\sqrt{2}}e^{(1)} - \sqrt{\frac{R^2}{2} - \frac{|\xi|^2}{4}}e^{(2)}.$$

It is easy to verify that

$$\zeta^{(1)} + \zeta^{(2)} = -\xi, \quad \zeta^{(j)} \cdot \zeta^{(j)} = 0, \quad |\zeta^{(j)}| = R, \quad \text{for } j = 1, 2.$$

If R is sufficiently large, by Lemma 3.14, we can construct CGO solutions

$$\phi_j(x) = e^{i\zeta^{(j)}\cdot x}(1 + r_j(x)) \tag{3.48}$$

where the remainder term r_j satisfies

$$\|r_j\|_{H^s(\Omega)} \leq \frac{C_1}{|\zeta^{(j)}|}\|q - \lambda\rho_0\|_{H^s(\Omega)} \leq \frac{C_1}{C_0}. \tag{3.49}$$

(Here, C_0 is the constant in Lemma 3.14.)

Thus for $s > \frac{n}{2}$,

$$\|\phi_j\|_{H^s(\Omega)} \leq \|e^{i\zeta^{(j)}\cdot x}\|_{H^s(\Omega)}\|1 + r_j\|_{H^s(\Omega)} \leq \left(|\Omega|^{\frac{1}{2}} + \frac{C_1}{C_0}\right)\|e^{i\zeta^{(j)}\cdot x}\|_{H^s(\Omega)}.$$

By choosing λ_0 such that for any $\lambda > \lambda_0$, we have

$$C_0\|q - \lambda\rho_0\|_{H^s(\Omega)} \geq \frac{1}{\sqrt{n}},$$

then $|\zeta^{(j)}| \geq \frac{1}{\sqrt{n}}$. Noticing that for integer $k \geq 0$,

$$\begin{aligned}\|e^{i\zeta^{(j)}\cdot x}\|^2_{H^k(\Omega)} =& \sum_{i=0}^{k}\sum_{|\alpha|=i}\|D^\alpha e^{i\zeta^{(j)}\cdot x}\|^2_{L^2(\Omega)} = \sum_{i=0}^{k}\sum_{\sum_{m=1}^n \alpha_m = i}\left(\prod_{m=1}^{n}|\zeta_m^{(j)}|^{\alpha_m}\right)\|e^{\mathrm{Im}\zeta^{(j)}\cdot x}\|^2_{L^2(\Omega)} \\ \leq& C\sum_{i=0}^{k}\|\zeta^{(j)}\|_1^i e^{\sqrt{2}R} \leq C\sum_{i=0}^{k}(\sqrt{n}\|\zeta^{(j)}\|_2)^i e^{\sqrt{2}R} = C\sum_{i=0}^{k}(\sqrt{n}R)^i e^{\sqrt{2}R} \leq CR^k e^{\sqrt{2}R}\end{aligned}$$

where C only depend on k, n, Ω. Thus from interpolation formula, we have

$$\|\phi_j\|_{H^s(\Omega)} \leq \left(|\Omega|^{\frac{1}{2}} + \frac{C_1}{C_0}\right)\|e^{i\zeta^{(j)}\cdot x}\|_{H^s(\Omega)} \leq CR^{\frac{s}{2}}e^{\frac{R}{\sqrt{2}}}. \tag{3.50}$$

We begin with a pointwise estimate for $\dot{\rho}$ in the Fourier domain. For simplicity, we denote

$$\delta := \|\dot{\Lambda}\|_{H^2((0,T)\times\partial\Omega)\to H^1((0,T)\times\partial\Omega)}.$$

Lemma 3.15. *Let $s > \frac{n}{2}$ with $n \geq 3$. Suppose there exists a constant $M > 0$ such that*

$$\|q\|_{H^{\max(s,4)}(\Omega)} \leq M, \quad \|\rho_0\|_{H^{\max(s,4)}(\Omega)} \leq M.$$

Then there exists a constant C, independent of λ and δ, such that

$$|\hat{\dot{\rho}}(\xi)| \leq \begin{cases} C\left[\frac{\lambda+1}{\lambda}(\lambda+1)^{\max(s,4)} e^{\sqrt{2}a_0(\lambda+1)}\delta + \frac{1}{a_0}\|\dot{\rho}\|_{H^{-s}(\Omega)}\right] & |\xi| \leq \sqrt{2}a_0(\lambda+1) \\ C\left[\frac{\lambda+1}{\lambda}|\xi|^{\max(s,4)} e^{|\xi|}\delta + \frac{\lambda+1}{|\xi|}\|\dot{\rho}\|_{H^{-s}(\Omega)}\right] & |\xi| \geq \sqrt{2}a_0(\lambda+1) \end{cases} \tag{3.51}$$

for any $\lambda > 0$ and sufficiently small δ. Here, a_0 is a constant satisfying $a_0 \geq C_0 M$, where C_0 is the constant in Lemma 3.14.

Proof. From Proposition 3.9, there exist boundary controls f_j such that $u_0^{f_j}(T) = \phi_j$ for the CGO solutions ϕ_j defined in (3.45). With similar estimation as in the proof of Theorem 3.12,

$$\left|\int_\Omega \dot{\rho}\phi_1\phi_2 \,\mathrm{d}x\right| \leq C_\lambda \delta$$

where the constant C_λ is

$$\begin{aligned} C_\lambda :=& \frac{1+\sqrt{2}T(1+\lambda)}{\lambda}\|f_1\|_{H^2((0,T)\times\partial\Omega)}\|f_2\|_{H^2((0,T)\times\partial\Omega)} \\ \leq& C\frac{1+\lambda}{\lambda}\|\phi_1\|_{H^4(\Omega)}\|\phi_2\|_{H^4(\Omega)} \\ \leq& C\frac{1+\lambda}{\lambda}\|\phi_1\|_{H^{\max(s,4)}(\Omega)}\|\phi_2\|_{H^{\max(s,4)}(\Omega)} \\ \leq& C\frac{1+\lambda}{\lambda}R^{\max(s,4)}e^{\sqrt{2}R}. \end{aligned} \tag{3.52}$$

where the last inequality comes from (3.50). We obtain the estimate

$$\begin{aligned} |\hat{\dot{\rho}}(\xi)| \leq& \left|\int_\Omega \dot{\rho}\phi_1\phi_2 \,\mathrm{d}x\right| + \left|\int_\Omega \dot{\rho}e^{-i\xi\cdot x}(r_1 + r_2 + r_1 r_2)\,\mathrm{d}x\right| \\ \leq& C_\lambda\delta + \|\dot{\rho}\|_{H^{-s}(\Omega)}\|r_1 + r_2 + r_1 r_2\|_{H^s(\Omega)} \\ \leq& C_\lambda\delta + \|\dot{\rho}\|_{H^{-s}(\Omega)}(\|r_1\|_{H^s(\Omega)} + \|r_2\|_{H^s(\Omega)} + \|r_1\|_{H^s(\Omega)}\|r_2\|_{H^s(\Omega)}) \\ \leq& C_\lambda\delta + C\|\dot{\rho}\|_{H^{-s}(\Omega)}\left(\frac{2}{R}\|q-\lambda\rho_0\|_{H^s(\Omega)} + \frac{1}{R^2}\|q-\lambda\rho_0\|^2_{H^s(\Omega)}\right) \\ \leq& C_\lambda\delta + C(\lambda+1)R^{-1}\|\dot{\rho}\|_{H^{-s}(\Omega)}, \end{aligned} \tag{3.53}$$

where in the last inequality we used the estimate (3.49). This derivation holds for any $R \geq \frac{|\xi|}{\sqrt{2}}$. In particular, we choose $R = \frac{|\xi|}{\sqrt{2}}$ when $|\xi| > \sqrt{2}a_0(\lambda+1)$, and $R = \sqrt{2}a_0(\lambda+1)$ when $|\xi| \leq \sqrt{2}a_0(\lambda+1)$ to obtain (3.51).

The condition $a_0 \geq C_0 M$ arises since

$$C_0\|q - \lambda\rho_0\|_{H^s(\Omega)} \leq C_0(\|q\|_{H^s(\Omega)} + \lambda\|\rho_0\|_{H^s(\Omega)}) \leq C_0 M(\lambda + 1)$$

is a natural upper bound, thus we require $|\zeta^{(j)}| = R > C_0 M(\lambda + 1)$ to fulfill the assumption of Lemma 3.14. For either choice of R above, it holds that $R > a_0(\lambda + 1)$. It remains to require $a_0 \geq C_0 M$. □

With the help of Lemma 3.15, the following stability estimate can be established for $\dot{\rho}$.

Theorem 3.16. *Let $s > \frac{n}{2}$ with $n \geq 3$. Suppose there exists a constant $M > 0$ such that*

$$\|q\|_{H^{\max(s,4)}(\Omega)} \leq M, \quad \|\rho_0\|_{H^{\max(s,4)}(\Omega)} \leq M, \quad \|\dot{\rho}\|_{H^s(\Omega)} \leq M.$$

and $\dot{\rho}$ is compact supported in Ω, then there exist a constant C (independent of λ and δ) and a positive constant $\lambda_0 > 0$ such that

$$\|\dot{\rho}\|_{L^\infty(\Omega)} \leq C\left[(\lambda+1)^{\max(s,4)} e^{C(\lambda+1)}\delta + \left(\lambda + \ln\frac{1}{\delta}\right)^{\frac{n-2s}{2}}\right]^{\frac{2s-n}{8s}}$$

for any $\lambda > \lambda_0 > 0$ and $0 < \delta \leq e^{-1}$ ($e = 2.71828\ldots$ is the Euler's number).

Remark 3.17. *For any fixed $\delta > 0$, it is clear that $\left(\lambda + \ln\frac{1}{\delta}\right)^{\frac{n-2s}{2}} \to 0$ as $\lambda \to \infty$ since $n - 2s < 0$. Therefore, for a large $\lambda > 0$, the estimate in Proposition 3.16 becomes a nearly Hölder-type stability.*

Proof. We follow the idea in the proof of the increasing stability result [72] and name all the constants that are independet of λ and δ as C.

Let ξ_0 be a constant such that $\xi_0 \geq \sqrt{2}a_0(\lambda+1)$, then

$$\begin{aligned}\|\dot{\rho}\|^2_{H^{-s}(\Omega)} &= \int_{\mathbb{R}^n} (1+|\xi|^2)^{-s}|\hat{\dot{\rho}}(\xi)|^2 \,\mathrm{d}\xi \\ &= \int_{|\xi|>\xi_0} (1+|\xi|^2)^{-s}|\hat{\dot{\rho}}(\xi)|^2 \,\mathrm{d}\xi + \int_{\sqrt{2}a_0(\lambda+1)\leq|\xi|\leq\xi_0} (1+|\xi|^2)^{-s}|\hat{\dot{\rho}}(\xi)|^2 \,\mathrm{d}\xi \\ &\quad + \int_{|\xi|\leq\sqrt{2}a_0(\lambda+1)} (1+|\xi|^2)^{-s}|\hat{\dot{\rho}}(\xi)|^2 \,\mathrm{d}\xi \\ &=: I_1 + I_2 + I_3.\end{aligned} \tag{3.54}$$

We estimate I_1, I_2, I_3 as follows. For I_1, as $\dot{\rho}$ is compact supported in Ω, Hölder's inequality gives $|\hat{\dot{\rho}}(\xi)| \leq \int_\Omega \left|\dot{\rho}(x)e^{i\xi\cdot x}\right| \mathrm{d}x \leq C\|\dot{\rho}\|_{L^2(\Omega)}$. Thus,

$$\begin{aligned}I_1 &:= \int_{|\xi|>\xi_0} (1+|\xi|^2)^{-s}|\hat{\dot{\rho}}(\xi)|^2 \,\mathrm{d}\xi \\ &\leq C\|\dot{\rho}\|^2_{L^2(\Omega)} \int_{|\xi|>\xi_0} (1+|\xi|^2)^{-s} \,\mathrm{d}\xi \\ &\leq C\|\dot{\rho}\|^2_{H^s(\Omega)}\xi_0^{n-2s} \leq \underbrace{C\xi_0^{n-2s}}_{:=\Phi_1(\xi_0)}\end{aligned}$$

where the last inequality follows from $\|\dot{\rho}\|_{H^s(\Omega)} \leq M$. The function $\Phi_1(\xi_0)$ denotes an upper bound of I_1.

For I_3, we use $|\hat{\dot{\rho}}(\xi)| \leq \|\hat{\dot{\rho}}\|_{L^\infty(B(0,\sqrt{2}a_0(\lambda+1)))}$ (here $B(0,t)$ means the unit ball of center 0 and radius t) to get

$$\begin{aligned}I_3 &:= \int_{|\xi|\leq\sqrt{2}a_0(\lambda+1)} (1+|\xi|^2)^{-s}|\hat{\dot{\rho}}(\xi)|^2 \,\mathrm{d}\xi \\ &\leq \|\hat{\dot{\rho}}\|^2_{L^\infty(B(0,\sqrt{2}a_0(\lambda+1)))} \int_{\mathbb{R}^n} (1+|\xi|^2)^{-s} \,\mathrm{d}\xi \\ &\leq C\|\hat{\dot{\rho}}\|^2_{L^\infty(B(0,\sqrt{2}a_0(\lambda+1)))} \\ &\leq C\left[\frac{(\lambda+1)^2}{\lambda^2}(\lambda+1)^{2\max(s,4)}e^{2\sqrt{2}a_0(\lambda+1)}\delta^2 + \frac{1}{a_0^2}\|\dot{\rho}\|^2_{H^{-s}(\Omega)}\right].\end{aligned} \tag{3.55}$$

where the last inequality is a consequence of (3.51) combined with the estimate $(a+b)^2 \leq 2a^2+2b^2$.

For I_2, we apply the estimate (3.51) to get

$$\begin{aligned}
I_2 &:= \int_{\sqrt{2}a_0(\lambda+1)\le|\xi|\le\xi_0} (1+|\xi|^2)^{-s}|\hat{\dot\rho}(\xi)|^2\,\mathrm{d}\xi \\
&\le C\int_{\sqrt{2}a_0(\lambda+1)\le|\xi|\le\xi_0} (1+|\xi|^2)^{-s}\left|\frac{\lambda+1}{\lambda}|\xi|^{\max(s,4)}e^{|\xi|}\delta + \frac{\lambda+1}{|\xi|}\|\dot\rho\|_{H^{-s}(\Omega)}\right|^2\mathrm{d}\xi \\
&\le C\int_{\sqrt{2}a_0(\lambda+1)\le|\xi|\le\xi_0} (1+|\xi|^2)^{-s}\left[\frac{(\lambda+1)^2}{\lambda^2}|\xi|^{2\max(s,4)}e^{2|\xi|}\delta^2 + \frac{(\lambda+1)^2}{|\xi|^2}\|\dot\rho\|^2_{H^{-s}(\Omega)}\right]\mathrm{d}\xi \\
&= I_{21}+I_{22}
\end{aligned}$$

Let $t := |\xi|$ be the radial variable, then

$$\begin{aligned}
I_{21} &:= C\int_{\sqrt{2}a_0(\lambda+1)\le|\xi|\le\xi_0} (1+|\xi|^2)^{-s}\frac{(\lambda+1)^2}{\lambda^2}|\xi|^{2\max(s,4)}e^{2|\xi|}\delta^2\,\mathrm{d}\xi \\
&\le C\frac{(\lambda+1)^2}{\lambda^2}\delta^2\int_{\sqrt{2}a_0(\lambda+1)}^{\xi_0}(1+t^2)^{-s}t^{2\max(s,4)+n-1}e^{2t}\,dt \\
&\le C\frac{(\lambda+1)^2}{\lambda^2}e^{2\xi_0}\delta^2\int_0^{\xi_0} t^{2\max(s,4)+n-1-2s}\,dt \\
&= C\frac{(\lambda+1)^2}{\lambda^2}\xi_0^{2\max(s,4)+n-2s}e^{2\xi_0}\delta^2;
\end{aligned}$$

and

$$\begin{aligned}
I_{22} &:= C\int_{\sqrt{2}a_0(\lambda+1)\le|\xi|\le\xi_0} (1+|\xi|^2)^{-s}\frac{(\lambda+1)^2}{|\xi|^2}\|\dot\rho\|^2_{H^{-s}(\Omega)}\,\mathrm{d}\xi \\
&= C(\lambda+1)^2\|\dot\rho\|^2_{H^{-s}(\Omega)}\int_{\sqrt{2}a_0(\lambda+1)}^{\xi_0}(1+t^2)^{-s}t^{n-3}\,dt \\
&\le C(\lambda+1)^2\|\dot\rho\|^2_{H^{-s}(\Omega)}\int_{\sqrt{2}a_0(\lambda+1)}^{\infty} t^{n-3-2s}\,dt \\
&\le C(\lambda+1)^2\|\dot\rho\|^2_{H^{-s}(\Omega)}[\sqrt{2}a_0(\lambda+1)]^{n-2-2s} \\
&\le C(\lambda_0+1)^{n-2s}a_0^{n-2s}\frac{1}{a_0^2}\|\dot\rho\|^2_{H^{-s}(\Omega)} \\
&= \frac{C}{a_0^2}\|\dot\rho\|^2_{H^{-s}(\Omega)}.
\end{aligned}$$

Put together, we have the following upper bound for I_2:

$$I_2 \le I_{21}+I_{22} \le \underbrace{C\frac{(\lambda+1)^2}{\lambda^2}\xi_0^{2\max(s,4)+n-2s}e^{2\xi_0}\delta^2}_{:=\Phi_2(\xi_0)} + \frac{C}{a_0^2}\|\dot\rho\|^2_{H^{-s}(\Omega)}. \tag{3.56}$$

Combining the estimate for I_1, I_2, I_3, we conclude

$$\begin{aligned}\|\dot{\rho}\|^2_{H^{-s}(\Omega)} =& I_1 + I_2 + I_3 \\ \leq& \Phi_1(\xi_0) + \left[\Phi_2(\xi_0) + \frac{C}{a_0^2}\|\dot{\rho}\|^2_{H^{-s}(\Omega)}\right] \\ &+ \left[C\frac{(\lambda+1)^2}{\lambda^2}(\lambda+1)^{2\max(s,4)}e^{2\sqrt{2}a_0(\lambda+1)}\delta^2 + \frac{C}{a_0^2}\|\dot{\rho}\|^2_{H^{-s}(\Omega)}\right]\end{aligned} \tag{3.57}$$

where the right hand side has been combined into three groups which are the upper bounds of I_1, I_2, I_3, respectively. By choosing a_0 sufficiently large, the H^{-s} norm can be absorbed by the left hand side to yield

$$\|\dot{\rho}\|^2_{H^{-s}(\Omega)} \leq \Phi_1(\xi_0) + \Phi_2(\xi_0) + C\frac{(\lambda+1)^2}{\lambda^2}(\lambda+1)^{2\max(s,4)}e^{2\sqrt{2}a_0(\lambda+1)}\delta^2 \tag{3.58}$$

The estimate will henceforth be split into two cases: $\frac{1}{2}\ln\frac{1}{\delta} \geq \sqrt{2}a_0(\lambda+1)$ and $\frac{1}{2}\ln\frac{1}{\delta} < \sqrt{2}a_0(\lambda+1)$. When $\frac{1}{2}\ln\frac{1}{\delta} \geq \sqrt{2}a_0(\lambda+1)$, we choose $\xi_0 = \frac{1}{2}\ln\frac{1}{\delta}$ to get

$$\begin{aligned}\Phi_1(\xi_0) + \Phi_2(\xi_0) =& C\xi_0^{n-2s} + C\frac{(\lambda+1)^2}{\lambda^2}\xi_0^{2\max(s,4)+n-2s}e^{2\xi_0}\delta^2 \\ =& C\left[1 + \frac{(\lambda+1)^2}{\lambda^2}\xi_0^{2\max(s,4)}e^{2\xi_0}\delta^2\right]\xi_0^{n-2s} \\ \leq& C\left[1 + \frac{(\lambda+1)^2}{\lambda^2}\left(\ln\frac{1}{\delta}\right)^{2\max(s,4)}\delta\right]\left(\ln\frac{1}{\delta}\right)^{n-2s}.\end{aligned}$$

As $\lim_{\delta\to 0_+}\delta\left(\ln\frac{1}{\delta}\right)^{2\max(s,4)} = 0$ and $\lim_{\lambda\to\infty}\frac{(\lambda+1)^2}{\lambda^2} = 1$, the square parenthesis is bounded whenever $\delta \in (0, e^{-1}]$ and $\lambda \geq \lambda_0$ for some $\lambda_0 > 0$. Hence,

$$\begin{aligned}\Phi_1(\xi_0) + \Phi_2(\xi_0) \leq& C\left(\ln\frac{1}{\delta}\right)^{n-2s} = C\left(\frac{\ln\frac{1}{\delta}}{\lambda + \ln\frac{1}{\delta}}\right)^{n-2s}\left(\lambda + \ln\frac{1}{\delta}\right)^{n-2s} \\ \leq& C\left(\frac{2\sqrt{2}a_0}{2\sqrt{2}a_0+1}\right)^{n-2s}\left(\lambda + \ln\frac{1}{\delta}\right)^{n-2s} \\ \leq& C\left(\lambda + \ln\frac{1}{\delta}\right)^{n-2s}\end{aligned}$$

where the second but last inequality holds since the function $(\frac{t}{\lambda+t})^{n-2s}$ is decreasing in $t > 0$. When $\frac{1}{2}\ln\frac{1}{\delta} < \sqrt{2}a_0(\lambda+1)$, we choose $\xi_0 = \sqrt{2}a_0(\lambda+1)$, then $I_2 = 0$. As a result, we can simply choose

$\Phi_2(\xi_0) = 0$ as an upper bound of I_2, hence

$$\begin{aligned}\Phi_1(\xi_0) + \Phi_2(\xi_0) = \Phi_1(\xi_0) = C\xi_0^{n-2s} = C(\lambda+1)^{n-2s} \\ = C\left(\frac{\lambda+1}{\lambda+\ln\frac{1}{\delta}}\right)^{n-2s}\left(\lambda+\ln\frac{1}{\delta}\right)^{n-2s} \leq C\left(\frac{1}{1+2\sqrt{2}a_0}\right)^{n-2s}\left(\lambda+\ln\frac{1}{\delta}\right)^{n-2s}.\end{aligned}$$

In either case, we have

$$\Phi_1(\xi_0) + \Phi_2(\xi_0) \leq C\left(\lambda+\ln\frac{1}{\delta}\right)^{n-2s}$$

for some constant $C > 0$ that is independent of $\lambda \in [\lambda_0, \infty)$ and $\delta \in (0, e^{-1}]$. In view of (3.58), we conclude

$$\begin{aligned}\|\dot{\rho}\|^2_{H^{-s}(\Omega)} \leq & C\frac{(\lambda+1)^2}{\lambda^2}(\lambda+1)^{2\max(s,4)}e^{2\sqrt{2}a_0(\lambda+1)}\delta^2 + C\left(\lambda+\ln\frac{1}{\delta}\right)^{n-2s} \\ \leq & C(\lambda+1)^{2\max(s,4)}e^{C(\lambda+1)}\delta^2 + C\left(\lambda+\ln\frac{1}{\delta}\right)^{n-2s}.\end{aligned} \tag{3.59}$$

Finally, we interpolate to obtain an estimate for the infinity norm. Let $\eta > 0$ such that $s = \frac{n}{2}+2\eta$, choose $k_0 = -s$, $k_1 = s$, $k = \frac{n}{2}+\eta = s-\eta$. Then

$$k = (1-p)k_0 + pk_1, \text{ where } p = \frac{2s-\eta}{2s}.$$

Using the interpolation theorem and the Sobolev embedding, we have

$$\begin{aligned}\|\dot{\rho}\|_{L^\infty(\Omega)} \leq & C\|\dot{\rho}\|_{H^k(\Omega)} \leq C\|\dot{\rho}\|^{1-p}_{H^{-s}(\Omega)}\|\dot{\rho}\|^p_{H^s(\Omega)} \leq C\|\dot{\rho}\|^{\frac{2s-n}{8s}}_{H^{-s}(\Omega)} \\ \leq & C\left[(\lambda+1)^{2\max(s,4)}e^{C(\lambda+1)}\delta^2 + C\left(\lambda+\ln\frac{1}{\delta}\right)^{n-2s}\right]^{\frac{2s-n}{16s}} \\ \leq & C\left[(\lambda+1)^{\max(s,4)}e^{C(\lambda+1)}\delta + C\left(\lambda+\ln\frac{1}{\delta}\right)^{\frac{n-2s}{2}}\right]^{\frac{2s-n}{8s}}\end{aligned} \tag{3.60}$$

□

3.3.1.3 Numerical Experiment

This section demonstrates the numerical implementation and validation of the reconstruction formula (3.36) in a one-dimensional (1D) context, where $\rho_0 = 1$ and $q_0 = 0$.

Computing Boundary Controls with Time Reversal Notice that there is a second order derivative of f in (3.36), the boundary controls should have at least second order differentiable. The ∂_t^2 operator will magnify the error caused by solving f using similar methods as in Section 3.2.2.5.

In this section, we introduce an analytic method to construct boundary control with high-order smoothness. In order to find boundary control f such that $u_0^f(T) = \phi$, we consider the following backward initial value problem

$$\begin{cases} \Box_{1,0} v(t,x) &= 0, \qquad \text{in } (0,T)\times\mathbb{R}^n \\ v(T) &= \tilde{\phi}, \qquad \text{in } \mathbb{R}^n \\ \partial_t v(T) &= 0, \qquad \text{in } \mathbb{R}^n. \end{cases}$$

where $\tilde{\phi}$ is the extension with compact support from Ω to $\mathbb{R}^n$. If $T > 0$ is sufficiently large and dimension n is odd, we would have $v(0) = \partial_t v(0) = 0$ by the Huygen's principle. This implies

$$u_0^{f-\partial_\nu v}(T) = u_0^f(T) - v(T) = 0 \text{ in } \Omega.$$

As a result, we can take $f = \partial_\nu v|_{[0,T]\times\partial\Omega}$. Note that v can be explictly expressed using the Kirchhoff's formula [40], thus $\partial_t^2 f = \partial_\nu \partial_t^2 v|_{[0,T]\times\partial\Omega}$ can be analytically computed.

Recall that $n = 1$, we take $\Omega = (a,b)$. D'Alembert's formula gives

$$v(t,x) = \frac{1}{2}[\tilde{\phi}(x+t-T) + \tilde{\phi}(x+T-t)]. \tag{3.61}$$

Thus

$$\partial_t^2 f = \partial_\nu \partial_t^2 v|_{[0,T]\times\partial\Omega} = \pm\frac{1}{2}[\tilde{\phi}'''(x+t-T) + \tilde{\phi}'''(x+T-t)]|_{x=a,b},$$

where we take + when $x = b$ and − when $x = a$. We choose the following extension:

$$\tilde{\phi} := \begin{cases} \phi & x \in [a,b], \\ \phi\cdot\exp\{1 - \frac{1}{1-(x-a)^{2p}}\} & x \in (a-1,a), \\ \phi\cdot\exp\{1 - \frac{1}{1-(x-b)^{2p}}\} & x \in (b,b+1), \\ 0 & x \notin (a-1,b+1), \end{cases}$$

where $p \geq 1$ is a positive integer. It is easy to verify that $\tilde{\phi}$ is C^∞ almost everywhere, except for two boundary points $x = a, b$, where it only have C^{2p-1} continuity. To guarantee the existence of the second derivative of f, we take $p \geq 2$.

Numerical Experiment We choose the spatial domain to be $\Omega = [-1, 1]$ with $T = 5$. Since we can analytically give the boundary control for each Helmholtz solution $e^{i\sqrt{\lambda}\theta\cdot x}$, we do not have to write all operators into matrices as in Section 3.2.2.

The solution of (3.22) is given by (3.61), and the forward problem (3.23) is solved using the second order central difference scheme on a temporal-spatial grid of size 24999×501, i.e. the linearized ND map (3.24) is implemented by solving (3.23) with background solution (3.61).

Then (3.35) are inserted into (3.36) to recover the Fourier transform of $\dot{q}$ at $2\sqrt{\lambda}\theta$, where f and h are computed using the time revesal method as in Section 3.3.1.3. The basis functions for the prescribed Helmholtz solution ϕ in our experiments are

$$1, \sin\left(\frac{\pi}{2}x\right), \cos\left(\frac{\pi}{2}x\right), \ldots, \sin\left(\frac{N\pi}{2}x\right), \cos\left(\frac{N\pi}{2}x\right) \tag{3.62}$$

with $N = 10$. They correspond to Helmholtz solutions with $\sqrt{\lambda} = 0, \frac{\pi}{2}, \ldots, \frac{N\pi}{2}$.

Noticing that the right hand side of (3.31) involves $\frac{1}{\lambda}$, we can not directly compute $\mathcal{F}[\dot{\rho}](0)$. Instead, we can take an arbitrary positive eigenvalue $\lambda_j = \frac{j^2\pi^2}{4}$ for some j, compute the inner products $(\dot{\rho}, \cos^2(\frac{j\pi}{2}x))_{L^2(-1,1)}$ and $(\dot{\rho}, \sin^2(\frac{j\pi}{2}x))_{L^2(-1,1)}$ using (3.31), then add them to get

$$\mathcal{F}[\dot{\rho}](0) = (\dot{\rho}, 1)_{L^2(-1,1)} = (\dot{\rho}, \cos^2(\frac{j\pi}{2}x))_{L^2(-1,1)} + (\dot{\rho}, \sin^2(\frac{j\pi}{2}x))_{L^2(-1,1)}.$$

Experiment 1. We start with a continuous perturbation

$$\dot{\rho} = \sin(\pi x) + \sin(2\pi x) - \cos(5\pi x) + \cos(7\pi x) - 1,$$

which is in the span of the Fourier basis functions (3.62). The graph of $\dot{\rho}$ is shown in Figure 3.7. The Gaussian random noise are added to the measurement $\dot{\Lambda}$ by adding to the numerical solutions on the boundary nodes. The reconstructions and corresponding errors with noise level 0%, 1%, 5% are illustrated in Figure 3.8.

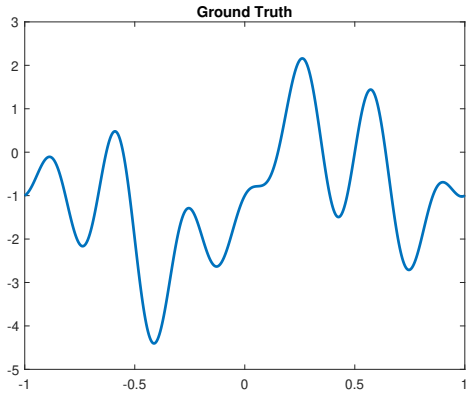

Figure 3.7 Ground truth $\dot{\rho}$.

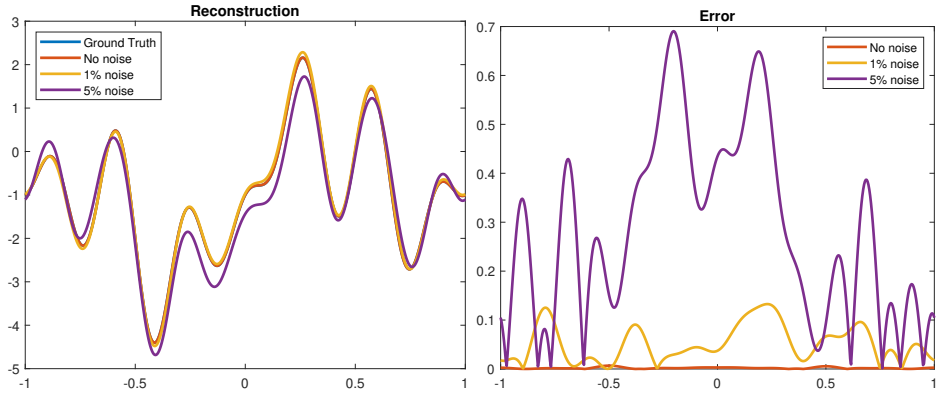

Figure 3.8 Left: Reconstructed $\dot{\rho}$ with 0%, 1%, 5% Gaussian noise and the ground truth. Right: The corresponding error between the reconstruction result and the ground truth. The relative L^2-errors are 0.14%, 3.66% and 19.37%, respectively.

Experiment 2. In this experiment, we consider a discontinuous perturbation

$$\dot{\rho} = \chi_{[-1,-\frac{1}{6}]} - \chi_{[-\frac{1}{6},\frac{1}{4}]},$$

where χ is the characteristic function. The Fourier series of $\dot{\rho}$ is given by

$$\dot{\rho} = \frac{5}{24} + \sum_{n=1}^{\infty} \left[-\frac{\sin\left(\frac{n\pi}{4}\right) + 2\sin\left(\frac{n\pi}{6}\right)}{n\pi} \cos(n\pi x) + \frac{\cos(n\pi) + \cos\left(\frac{n\pi}{4}\right) + 2\cos\left(\frac{n\pi}{6}\right)}{n\pi} \sin(n\pi x) \right].$$

With the choice of the basis functions (3.62), we can only expect to reconstruct the orthogonal projection:

$$\dot{\rho}_N := \frac{5}{24} + \sum_{n=1}^{N} \left[-\frac{\sin\left(\frac{n\pi}{4}\right) + 2\sin\left(\frac{n\pi}{6}\right)}{n\pi} \cos(n\pi x) + \frac{\cos(n\pi) + \cos\left(\frac{n\pi}{4}\right) + 2\cos\left(\frac{n\pi}{6}\right)}{n\pi} \sin(n\pi x) \right],$$

see Figure 3.9. We plot the reconstruction result and the corresponding error with respect to the orthogonal projection $\dot{\rho}_N$ with different noise level in Figure 3.10.

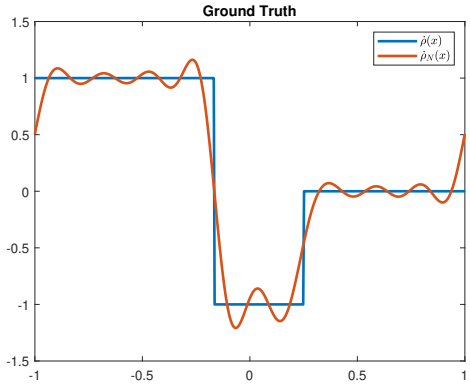

Figure 3.9 Ground truth $\dot{\rho}$.

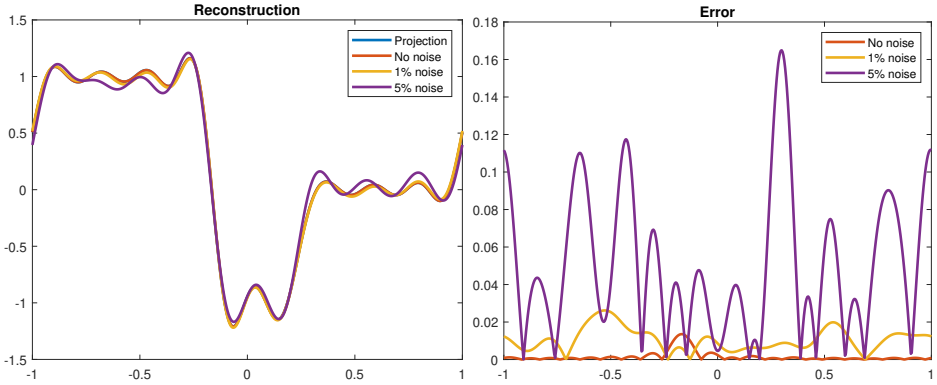

Figure 3.10 Left: Reconstructed $\dot{\rho}$ with 0%, 1%, 5% Gaussian noise and the ground truth. Right: The corresponding error between the reconstruction result and the ground truth. The relative L^2-errors are 0.39%, 1.57% and 8.15%, respectively.

Experiment 3. In this experiment, we apply the algorithm to the non-linear IBVP where

$$\rho = \rho_0 + \varepsilon\dot{\rho} + \varepsilon^2\ddot{\rho},$$

with $\varepsilon = 0.001$ and

$$\dot{\rho} = \sin(\pi x) + \sin(2\pi x) - \cos(5\pi x) + \cos(7\pi x) - 1, \qquad \ddot{\rho} = 200\sin(25\pi x).$$

See Figure 3.11 for the graph of ρ. Since

$$\Lambda_\rho - \Lambda_{\rho_0} \approx \varepsilon\dot{\Lambda}_{\dot{\rho}} = \dot{\Lambda}_{\varepsilon\dot{\rho}}$$

when ε is small, we can use $\varepsilon^{-1}(\Lambda_\rho - \Lambda_{\rho_0})$ as an approximation of $\dot{\Lambda}_{\dot{\rho}}$ in (3.31). In this case, $\Lambda_\rho f$ and $\Lambda_{\rho_0} f$ are computed by numerically solving the forward problem (3.22) with ρ and $\rho_0 \equiv 1$. We then apply Algorithm 3.2 to find $\dot{\rho}$, and view $1 + \dot{\rho}$ as an approximation of the ground truth ρ. In

the experiment, we added the Gaussian noise to the difference $\Lambda_\rho - \Lambda_{\rho_0}$ rather than to $\Lambda_\rho f$ and $\Lambda_{\rho_0} f$ individually, see [75] for discussion of the difference. The reconstruction and the respective errors with 0%, 1%, 5% Gaussian noise are illustrated in Figure 3.12.

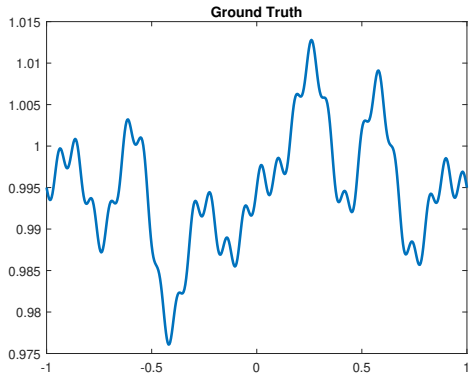

Figure 3.11 Ground truth ρ.

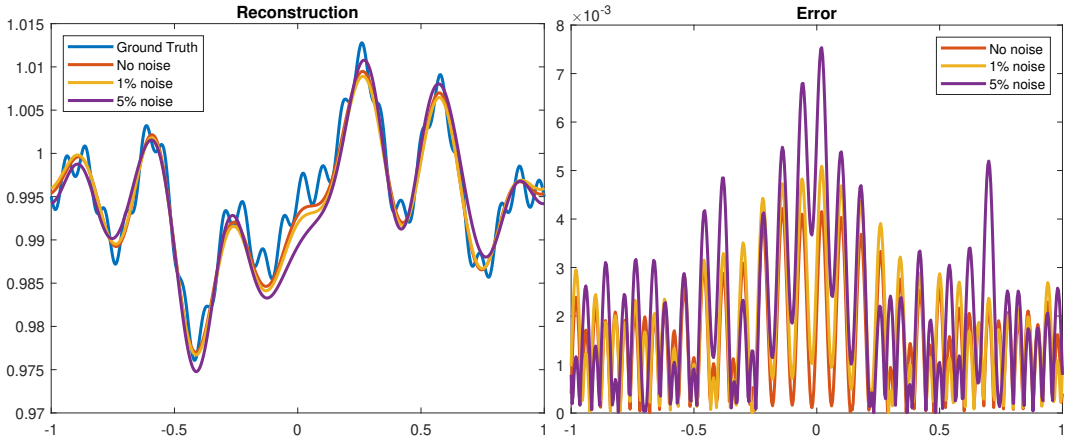

Figure 3.12 Left: Reconstructed ρ with 0%, 1%, 5% Gaussian noise and the ground truth. Right: The corresponding error between the reconstruction result and the ground truth. The relative L^2-errors are 18.09%, 20.95% and 26.46%, respectively.

3.3.2 Reconstruct Wave Potential through Linearization

The wave potential q, similar to the potential energy function of quantum mechanics, describes the reflection and transmission characteristics of the system [44]. However, the full nonlinear treatment introduced in Section 3.2 is not sufficient for the potential reconstruction. In the algorithm for reconstructing wave speed $c(x)$, the most important step is to construct a series of boundary controls f_α such that $u^{f_\alpha}(T)$ converge to a handcrafted time independent wave solution ψ as $\alpha \to 0$.

However, for unknown q, the time independent wave solution ψ of (3.1) satisfies equation

$$[-\Delta + q(x)]\psi(x) = 0,$$

which can not be construct explicitly. With linearization, the background potential q_0 would give us a series of time independent background wave solutions, which can help reconstructing the perturbed wave potential [75]. In this section, we assume the wave speed $c = c_0(x) \in C^\infty(\overline{\Omega})$ is known, and we want to recover $q(x)$ from the ND map $\Lambda_{\rho_0,q}$. For simplicity, we use Λ_q to represent $\Lambda_{\rho_0,q}$ in this section.

We use the linearization to solve the IBVP. For the formal derivation, we write

$$q(x) = q_0(x) + \varepsilon\dot{q}(x), \qquad u(t,x) = u_0(t,x) + \varepsilon\dot{u}(t,x)$$

where q_0 is a known background potential and u_0 is the background solution. Substitute these into (3.1). Equating the $O(1)$-terms gives

$$\begin{cases} \Box_{\rho_0,q_0} u_0(t,x) &= 0, & \text{in } (0,2T)\times\Omega \\ \partial_\nu u_0 &= f, & \text{on } (0,2T)\times\partial\Omega \\ u_0(0,x) = \partial_t u_0(0,x) &= 0, & x\in\Omega. \end{cases} \tag{3.63}$$

Equating the $O(\varepsilon)$-terms gives

$$\begin{cases} \Box_{\rho_0,q_0} \dot{u}(t,x) &= -u_0(t,x)\dot{q}(x), & \text{in } (0,2T)\times\Omega \\ \partial_\nu \dot{u} &= 0, & \text{on } (0,2T)\times\partial\Omega \\ \dot{u}(0,x) = \partial_t \dot{u}(0,x) &= 0 & x\in\Omega. \end{cases} \tag{3.64}$$

Write the ND map $\Lambda_q = \Lambda_{q_0} + \varepsilon\dot{\Lambda}_{\dot{q}}$, where Λ_{q_0} denote the ND map for the unperturbed boundary value problem (3.63), and $\dot{\Lambda}_{\dot{q}}$ is defined as

$$\dot{\Lambda}_{\dot{q}} : f \mapsto \dot{u}|_{(0,2T)\times\partial\Omega}. \tag{3.65}$$

Since c_0 and q_0 are known, the unperturbed problem (3.63) can be explicitly solved to obtain u_0 and Λ_{q_0}. As in the previous section, we will write $\dot{u} = \dot{u}^f$ if it is necessary to specify the Neumann data f. Then the linearized IBVP concerns recovery of the potential $\dot{q}$ from $\dot{\Lambda}_{\dot{q}}$.

3.3.2.1 Derivation

The derivation of the Blagoveščenskiĭ's identity is exactly the same. Introduce the *connecting operator*

$$K := J\Lambda_q P_T^* - R\Lambda_{q,T} RJP_T^*.$$

Similar to the proof of Proposition 3.6 and Corollary 3.7, we have

$$(u^f(T), u^h(T))_{L^2(\Omega, c_0^{-2}dx)} = (f, Kh)_{L^2((0,T)\times\partial\Omega)} = (Kf, h)_{L^2((0,T)\times\partial\Omega)}. \tag{3.66}$$

$$(\Delta u^f(T) - qu^f(T), u^h(T))_{L^2(\Omega, c_0^{-2}dx)} = (\partial_t^2 f, Kh)_{L^2((0,T)\times\partial\Omega)} = (K\partial_t^2 f, h)_{L^2((0,T)\times\partial\Omega)}. \tag{3.67}$$

Remember that we write $\Lambda_q = \Lambda_{q_0} + \varepsilon\dot{\Lambda}_{\dot{q}}$ in the linearization setting, we have the following linearization $K = K_0 + \varepsilon\dot{K}$. Here K_0 is the connecting operator for the background wave equation (3.63):

$$K_0 := J\Lambda_{q_0} P_T^* - R\Lambda_{q_0,T} RJP_T^*. \tag{3.68}$$

K_0 can be explicitly computed since Λ_{ρ_0,q_0} is known. $\dot{K}$ is the resulting perturbation in the connecting operator:

$$\dot{K} := J\dot{\Lambda}_{\dot{q}} P_T^* - R\dot{\Lambda}_{\dot{q},T} RJP_T^*. \tag{3.69}$$

$\dot{K}$ can be explicitly computed once $\dot{\Lambda}_{\dot{q}}$ is given.

We write $\dot{\Lambda}$ for $\dot{\Lambda}_{\dot{q}}$ when there is no risk of confusion. Linearizing (3.66) and (3.67) gives the following integral identity, which is essential to the development of the reconstruction procedure:

Proposition 3.18. *Let $\lambda \in \mathbb{R}$ be a real number. If $f, h \in C_c^\infty((0,T]\times\partial\Omega)$ satisfy*

$$[\Delta - q_0 + \lambda]u_0^f(T) = [\Delta - q_0 + \lambda]u_0^h(T) = 0 \quad \text{in } \Omega, \tag{3.70}$$

then the following identity holds:

$$-(\dot{q}u_0^f(T), u_0^h(T))_{L^2(\Omega)} = (\partial_t^2 f + \lambda f, \dot{K}h)_{L^2((0,T)\times\partial\Omega)} + (\dot{\Lambda}f(T), h(T))_{L^2(\partial\Omega)} \tag{3.71}$$

Proof. Similar to the proof of Proposition 3.8, substitute all linearizations into (3.66) and (3.67). Equating $O(1)$-terms gives

$$(u_0^f(T), u_0^h(T))_{L^2(\Omega, c_0^{-2}dx)} = (f, K_0 h)_{L^2((0,T)\times\partial\Omega)} = (K_0 f, h)_{L^2((0,T)\times\partial\Omega)}.$$

$$(\Delta u_0^f(T) - q_0 u_0^f(T), u_0^h(T))_{L^2(\Omega, c_0^{-2}dx)} = (\partial_t^2 f, K_0 h)_{L^2((0,T)\times\partial\Omega)} = (K_0 \partial_t^2 f, h)_{L^2((0,T)\times\partial\Omega)}.$$

Equating $O(\varepsilon)$-terms gives

$$\begin{aligned}
&(f, \dot{K}h)_{L^2((0,T)\times\partial\Omega)} = (\dot{K}f, h)_{L^2((0,T)\times\partial\Omega)} \\
=&(\dot{u}^f(T), u_0^h(T))_{L^2(\Omega, c_0^{-2}dx)} + (u_0^f(T), \dot{u}^h(T))_{L^2(\Omega, c_0^{-2}dx)}.
\end{aligned} \tag{3.72}$$

$$\begin{aligned}
&(\partial_t^2 f, \dot{K}h)_{L^2((0,T)\times\partial\Omega)} = (\dot{K}\partial_t^2 f, h)_{L^2((0,T)\times\partial\Omega)} \\
=&(\Delta\dot{u}^f(T) - \dot{q}u_0^f(T) - q_0\dot{u}^f(T), u_0^h(T))_{L^2(\Omega, c_0^{-2}dx)} \\
&+ (\Delta u_0^f(T) - q_0 u_0^f(T), \dot{u}^h(T))_{L^2(\Omega, c_0^{-2}dx)} \\
=&\underbrace{(\Delta\dot{u}^f(T), u_0^h(T))_{L^2(\Omega)} - (q_0\dot{u}^f(T), u_0^h(T))_{L^2(\Omega)}}_{:=I_1} \\
&- (\dot{q}u_0^f(T), u_0^h(T))_{L^2(\Omega)} \\
&+ \underbrace{(\Delta u_0^f(T), \dot{u}^h(T))_{L^2(\Omega)} - (q_0 u_0^f(T), \dot{u}^h(T))_{L^2(\Omega)}}_{:=I_2}.
\end{aligned} \tag{3.73}$$

Notice that

$$\begin{aligned}
I_1 =&(\Delta\dot{u}^f(T), u_0^h(T))_{L^2(\Omega)} - (q_0\dot{u}^f(T), u_0^h(T))_{L^2(\Omega)} \\
=&(\dot{u}^f(T), \Delta u_0^h(T))_{L^2(\Omega)} - (\dot{\Lambda}f(T), \partial_\nu u_0^h(T))_{L^2(\partial\Omega)} - (q_0\dot{u}^f(T), u_0^h(T))_{L^2(\Omega)} \\
=&(\dot{u}^f(T), [\Delta - q_0]u_0^h(T))_{L^2(\Omega)} - (\dot{\Lambda}f(T), h(T))_{L^2(\partial\Omega)}.
\end{aligned}$$

Here we use the integration by parts and use the fact that $\dot{u}^f|_{(0,2T)\times\partial\Omega} = \dot{\Lambda}f$ and $\partial_\nu \dot{u} = 0$.

On the other hand, combing the terms in I_2 gives

$$I_2 = ([\Delta - q_0]u_0^f(T), \dot{u}^h(T))_{L^2(\Omega)}.$$

Insert these expressions for I_1 and I_2 into (3.73), then add (3.72) multiplied by $\lambda \in \mathbb{R}$ to get

$$\begin{aligned}
&(\partial_t^2 f + \lambda f, \dot{K}h)_{L^2((0,T)\times\partial\Omega)} + (\dot{\Lambda}f(T), h(T))_{L^2(\partial\Omega)} \\
=&(\dot{u}^f(T), [\Delta - q_0 + \lambda]u_0^h(T))_{L^2(\Omega)} - (\dot{q}u_0^f(T), u_0^h(T))_{L^2(\Omega)} \\
&+ ([\Delta - q_0 + \lambda]u_0^f(T), \dot{u}^h(T))_{L^2(\Omega)}.
\end{aligned} \tag{3.74}$$

If $[\Delta - q_0 + \lambda]u_0^f(T) = [\Delta - q_0 + \lambda]u_0^h(T) = 0$ in Ω, the first term and last term on the right-hand side vanish, resulting in (3.71). □

Notice that all parameters in (3.70) are known. For each $\lambda \in \mathbb{R}$, we can construct functions ϕ, ψ satisfy (3.70). Proposition 3.9 ensures that we can find control sequence f, h such that $u^f(T) = \phi$, $u^h(T) = \psi$, therefore, we have the weighted inner product $(\phi, \psi)_{L^2(\Omega, \dot{q}\,\mathrm{dx})}$ from (3.71).

3.3.2.2 Stability and Reconstruction

Observing that the right hand side of (3.31) and (3.71) differ only by a constant λ, the discussion is almost the same as in Section 3.3.1.2, see also [75].

Case 1: q_0 is constant Without loss of generality, we take $q_0 = 0$. By choosing $\lambda \geq 0$, the equation (3.70) becomes the Helmholtz equation

$$[\Delta + \lambda]u_0^f(T) = [\Delta + \lambda]u_0^f(T) = 0 \quad \text{in } \Omega.$$

Let $\theta \in \mathbb{S}^{n-1}$ be an arbitrary unit vector, Proposition 3.9 guarantees the existence of $f, h \in C_c^\infty((0,T] \times \partial\Omega)$ such that

$$u_0^f(T) = u_0^h(T) = e^{i\sqrt{\lambda}\theta \cdot x}, \tag{3.75}$$

which is the Helmholtz solution. Similarly, we have following results:

Theorem 3.19. *Suppose $c_0 = 1$ and $q_0 = 0$. Then the Fourier transform $\hat{\dot{q}}$ of $\dot{q}$ can be reconstructed as follows:*

$$\hat{\dot{q}}(2\sqrt{\lambda}\theta) = -(\partial_t^2 f + \lambda f, \dot{K}h)_{L^2((0,T)\times\partial\Omega)} - (\dot{\Lambda}f(T), h(T))_{L^2(\partial\Omega)} \tag{3.76}$$

where $f, h \in C_c^\infty((0,T] \times \partial\Omega)$ are solutions to (3.75).

Proof. The formula is obtained by substitute (3.75) into (3.71). Since $\theta \in \mathbb{S}^{n-1}$ and $\lambda \geq 0$ are arbitrary, it gives the Fourier transform of $\dot{q}$ everywhere. □

Theorem 3.20. *Suppose $c_0 = 1$ and $q_0 = 0$. There exists a constant $C > 0$, independent of λ, such that*

$$\left|\hat{\dot{q}}(\sqrt{2\lambda}\theta)\right| \leq C(1 + \sqrt{2}T(1+\lambda))\lambda^4 \|\dot{\Lambda}\|_{H^2((0,T)\times\partial\Omega)\to H^3((0,T)\times\partial\Omega)}$$

Proof. The proof is nearly a word-by-word repetition of Theorem 3.12, see also [75]. □

Case 2: q_0 is variable Let $\lambda \geq 0$, then (3.70) becomes the perturbed Helmholtz equation

$$[\Delta + \lambda - q_0]u_0^f(T) = [\Delta + \lambda - q_0]u_0^h(T) = 0 \quad \text{in } \Omega.$$

For any $\theta \in \mathbb{S}^{n-1}$, we choose the solution to be

$$\phi(x) = e^{i\sqrt{\lambda}\theta\cdot x} + r(x;\lambda) \tag{3.77}$$

the residual $r(x;\lambda)$ satisfies

$$(\Delta + \lambda - q_0)r = q_0 e^{i\sqrt{\lambda}\theta\cdot x} \qquad \text{in } \Omega. \tag{3.78}$$

According to [75, Lemma 13],

$$\|r\|_{H^s(\mathbb{R}^n)} = O(\lambda^{\frac{s-1}{2}}) \qquad \text{as } \lambda \to \infty \tag{3.79}$$

for any $s \geq 0$.

One dimension: In one dimension (1D), $\theta = \pm 1$. Let us take $\theta = 1$ and choose (3.77) to be the value of $u_0^f(T)$ and $u_0^h(T)$. Substituting into (3.71) gives

$$\begin{aligned} &-\hat{\dot{q}}(2\sqrt{\lambda}) - 2(\dot{q}e^{i\sqrt{\lambda}\theta\cdot x}, r)_{L^2(\Omega)} - (\dot{q}r, r)_{L^2(\Omega)} \\ =&(\partial_t^2 f + \lambda f, \dot{K}h)_{L^2((0,T)\times\partial\Omega)} + (\dot{\Lambda}f(T), h(T))_{L^2(\partial\Omega)} \end{aligned} \tag{3.80}$$

With similar analysis as (3.42), we have

$$\left|\hat{\dot{q}}(\sqrt{2\lambda}\theta)\right| \leq C(1+\sqrt{2}T(1+\lambda))\lambda^4\|\dot{\Lambda}\|_{H^2((0,T)\times\partial\Omega)\to H^3((0,T)\times\partial\Omega)} + O(\lambda^{-\frac{1}{2}}).$$

High Dimension: In dimension $n \geq 2$, let $\lambda \geq 0$, $\theta, \omega \in \mathbb{R}^n$ be two vectors such that $\theta \perp \omega$. We take the following solutions:

$$\begin{aligned} \phi(x) :=& \phi_0(x) + r_1(x;\lambda), \qquad \phi_0(x) := e^{i(k\theta + l\omega)\cdot x} \\ \psi(x) :=& \psi_0(x) + r_2(x;\lambda), \qquad \psi_0(x) := e^{i(k\theta - l\omega)\cdot x} \end{aligned}$$

where r_1, r_2 satisfy (3.79), $k^2 + l^2 = \lambda$ such that $(\Delta + \lambda)\phi_0 = (\Delta + \lambda)\psi_0 = 0$. Proposition 3.9 asserts that there are $f, h \in C_c^\infty((0,T] \times \partial\Omega)$ such that

$$u_0^f(T) = \phi = \phi_0 + r_1, \qquad u_0^h(T) = \psi = \psi_0 + r_2. \tag{3.81}$$

Inserting (3.81) into (3.71) gives

$$\begin{aligned} &- \hat{\dot{q}}(2k\theta) - (\dot{q}e^{i(k\theta+l\omega)\cdot x}, r_2)_{L^2(\Omega)} - (\dot{q}e^{i(k\theta-l\omega)\cdot x}, r_1)_{L^2(\Omega)} - (\dot{q}r_1, r_2)_{L^2(\Omega)} \\ =&(\partial_t^2 f + (k^2+l^2)f, \dot{K}h)_{L^2((0,T)\times\partial\Omega)} + (\dot{\Lambda}f(T), h(T))_{L^2(\partial\Omega)} \end{aligned} \tag{3.82}$$

If we fix k and let $l \to \infty$, we obtain the reconstruction formula for any $k \geq 0$ and any $\theta \in \mathbb{S}^{n-1}$:

$$\hat{\dot{q}}(2k\theta) = -\lim_{l\to\infty} \left[(\partial_t^2 f + (k^2+l^2)f, \dot{K}h)_{L^2((0,T)\times\partial\Omega)} + (\dot{\Lambda}f(T), h(T))_{L^2(\partial\Omega)}\right].$$

Similarly, we can obtain a Hölder-type stability estimate for $\|\dot{q}\|_{H^{-s}(\mathbb{R}^n)}$.

Theorem 3.21. *Suppose $c_0 = 1$, $q_0 \in C^\infty(\overline{\Omega})$ and q_0 is not identically zero. For any $s > 0$, there exists a constant $C > 0$ independent of λ such that*

$$\|\dot{q}\|_{H^{-s}(\mathbb{R}^n)} \leq C\|\dot{\Lambda}\|^{\frac{2s}{11(n+2s)}}_{H^2((0,T)\times\partial\Omega)\to H^3((0,T)\times\partial\Omega)}.$$

Proof. Write $\xi := 2k\theta$ and

$$\delta := \|\dot{\Lambda}\|_{H^2((0,T)\times\partial\Omega)\to H^3((0,T)\times\partial\Omega)}.$$

Let $\rho > 0$ be a sufficiently large number that is to be determined. We decompose

$$\|\dot{q}\|^2_{H^{-s}(\mathbb{R}^n)} = \int_{|\xi|\leq\rho} \frac{|\hat{\dot{q}}(\xi)|^2}{(1+|\xi|^2)^s}\, d\xi + \int_{|\xi|>\rho} \frac{|\hat{\dot{q}}(\xi)|^2}{(1+|\xi|^2)^s}\, d\xi.$$

For the integral over high frequencies, we have

$$\int_{|\xi|>\rho} \frac{|\hat{\dot{q}}(\xi)|^2}{(1+|\xi|^2)^s}\, d\xi \leq \frac{1}{(1+\rho^2)^s} \int_{|\xi|>\rho} |\hat{\dot{q}}(\xi)|^2\, d\xi \leq \frac{\|\dot{q}\|^2_{L^2(\mathbb{R}^n)}}{(1+\rho^2)^s} \leq C\frac{1}{\rho^{2s}}.$$

For the integral over low frequencies, it is easy to see that:

$$\int_{|\xi|\leq\rho} \frac{|\hat{\dot{q}}(\xi)|^2}{(1+|\xi|^2)^s}\, d\xi \leq \int_{|\xi|\leq\rho} |\hat{\dot{q}}(\xi)|^2\, d\xi \leq C\rho^n \|\hat{\dot{q}}\|^2_{L^\infty(B(0,\rho))}.$$

The norm $\|\hat{\dot{q}}\|_{L^\infty(B(0,\rho))}$ can be estimated using (3.82). Indeed, for $|\xi| \le \rho$, we have

$$\begin{aligned}
|\hat{\dot{q}}(\xi)| &\le |(\partial_t^2 f + (k^2+l^2)f, \dot{K}h)_{L^2((0,T)\times\partial\Omega)} + (\dot{\Lambda}f(T), h(T))_{L^2(\partial\Omega)}| + \frac{C}{\sqrt{\lambda}} \\
&\le C(1+\sqrt{2}T(1+\lambda))\|\phi\|_{H^4(\Omega)}\|\psi\|_{H^4(\Omega)}\delta + \frac{C}{\sqrt{\lambda}} \\
&\le C(1+\sqrt{2}T(1+\lambda))\left(\|\phi_0\|_{H^4(\Omega)} + \|r_1\|_{H^4(\Omega)}\right)\left(\|\psi_0\|_{H^4(\Omega)} + \|r_2\|_{H^4(\Omega)}\right)\delta + \frac{C}{\sqrt{\lambda}} \\
&\le C(1+\sqrt{2}T(1+\lambda))\left(\lambda^2 + \lambda^{\frac{3}{2}}\right)^2\delta + \frac{C}{\sqrt{\lambda}}
\end{aligned}$$

where the first and the last inequality is a consequence of (3.79), the second inequality follows from the proof of Proposition 3.20. Utilizing the relation $\lambda = k^2 + l^2$, we conclude

$$\|\hat{\dot{q}}\|^2_{L^\infty(B(0,\rho))} \le C\left[(1+\sqrt{2}T(1+\lambda))^2\lambda^6(1+\sqrt{\lambda})^4\delta^2 + \frac{1}{\lambda}\right] \le C\left[(\rho^2+l^2)^{10}\delta + \frac{1}{l^2}\right]$$

provided $\rho > 0$ is sufficiently large. Combining these estimates, we see that

$$\|\dot{q}\|^2_{H^{-s}(\mathbb{R}^n)} \le C\left[\rho^n(\rho^2+l^2)^{10}\delta^2 + \frac{\rho^n}{l^2} + \frac{1}{\rho^{2s}}\right].$$

Choosing $l^2 = \rho^{n+2s}$ and $\rho = \delta^{-\frac{2}{11(n+2s)}}$ yields

$$\|\dot{q}\|^2_{H^{-s}(\mathbb{R}^n)} \le C\delta^{\frac{4s}{11(n+2s)}},$$

where C is a constant independent of λ and δ is sufficiently small.

□

3.3.2.3 Numerical Experiment

This section demonstrates the numerical implementation and validation of the reconstruction formula (3.76) in a one-dimensional (1D) context, where $c_0 = 1$ and $q_0 = 0$.

The setting is the same as in Section 3.3.1.3. We choose the spatial domain to be $\Omega = [-1, 1]$ with $T = 5$. The forward problem (3.64) is solved using the second order central difference scheme on a temporal-spatial grid of size 24999×501. The basis functions for the prescribed Helmholtz solution ϕ in our experiments are

$$1, \sin\left(\frac{\pi}{2}x\right), \cos\left(\frac{\pi}{2}x\right), \ldots, \sin\left(\frac{N\pi}{2}x\right), \cos\left(\frac{N\pi}{2}x\right)$$

with $N = 10$. They correspond to Helmholtz solutions with $\sqrt{\lambda} = 0, \frac{\pi}{2}, \ldots, \frac{N\pi}{2}$. Boundary controls are computed using the time revesal method as in Section 3.3.1.3.

Experiment 1. The first experiment aims to reconstruct the following smooth $\dot{q}$ using the formula (3.76):

$$\dot{q} = \sin(\pi x) + 2\cos(2\pi x) + 4\sin(4\pi x) - 3.$$

The graph of $\dot{q}$ is shown in Figure 3.13. The measurement $\dot{\Lambda}_{\dot{q}}$ is added with 0%, 1%, and 5% of Gaussian noise, respectively. The reconstructions and the corresponding errors are illustrated in Figure 3.14. Notice that the reconstruction error with 5% noise is relatively larger, as can be expected. When multiple measurements are available, we can repeat the reconstruction several times and then take the average. This strategy effectively reduces the error, since the inverse problem is linear and the Gaussian noise has zero mean, see Figure 3.15.

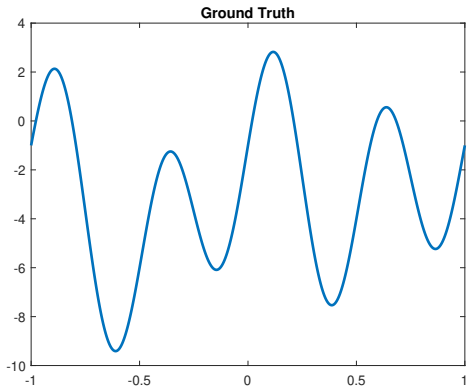

Figure 3.13 Ground truth $\dot{q} = \sin(\pi x) + 2\cos(2\pi x) + 4\sin(4\pi x) - 3$.

Experiment 2. The second experiment tests reconstruction of a discontinuous $\dot{q}$. we choose $\dot{q}$ to be the Heaviside function

$$H(x) = \begin{cases} 1 & x \geq 0, \\ 0 & x < 0. \end{cases}$$

The Fourier series of $H(x)$ on $\Omega = [-1, 1]$ is

$$H(x) = \frac{1}{2} + \sum_{n=1}^{\infty} \frac{2}{(2n-1)\pi} \sin((2n-1)\pi x).$$

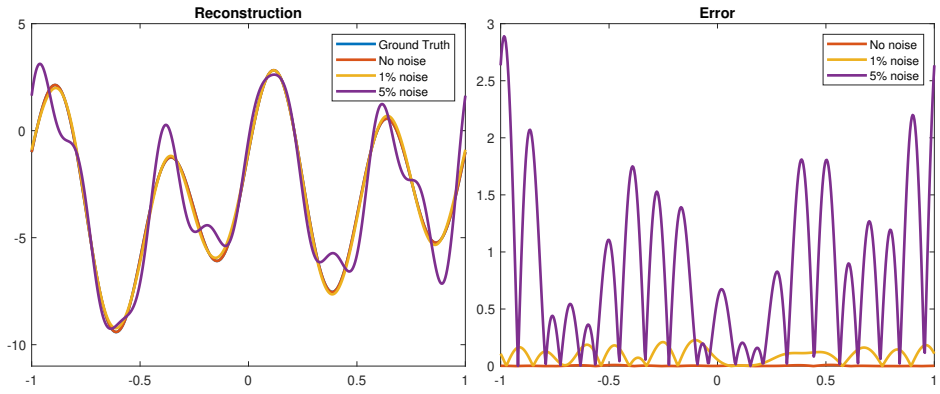

Figure 3.14 Left: Reconstructed $\dot{q}$ with 0%, 1%, 5% Gaussian noise and the ground truth. Right: The corresponding error between the reconstruction and the ground truth. The relative L^2-errors are 0.1%, 2.5%, and 23.9% respectively.

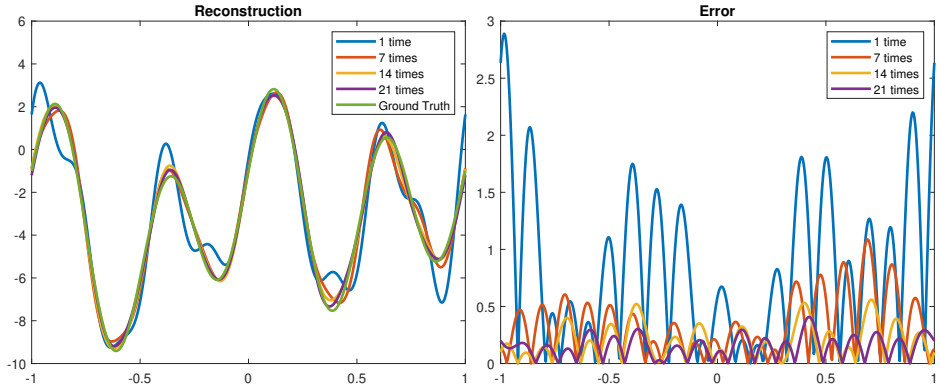

Figure 3.15 Left: Reconstructed $\dot{q}$ under $1, 7, 14, 21$ times repetition with 5% Gaussian noise and the ground truth. Right: The corresponding error between the reconstruction and the ground truth. The relative L^2-errors are 23.9%, 9.4%, 5.5%, and 4.0% respectively.

With the choice of the finite computational basis, we can only expect to reconstruct the following orthogonal projection:

$$H_N(x) := \frac{1}{2} + \sum_{n=1}^{\lceil \frac{N}{2} \rceil} \frac{2}{(2n-1)\pi} \sin((2n-1)\pi x),$$

see Figure 3.16 for the graph of $H(x)$ and $H_N(x)$. The reconstruction formula (3.76) is implemented with $0\%, 1\%$, and 5% of Gaussian noise added to $\dot{\Lambda}_{\dot{q}}$, respectively. The reconstructions and corresponding errors with a single measurement are illustrated in Figure 3.17. The averaged reconstruction with 5% of Gaussian noise and multiple repeated measurements are illustrated in Figure 3.18.

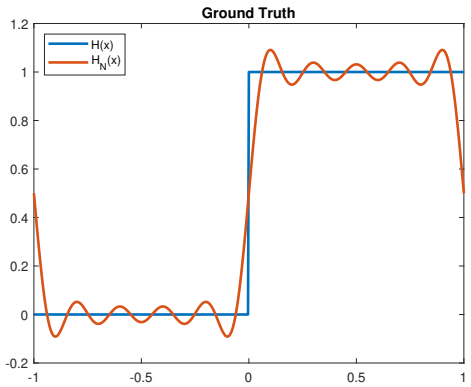

Figure 3.16 Ground truth $\dot{q} = H(x)$ and its projection $H_N(x)$.

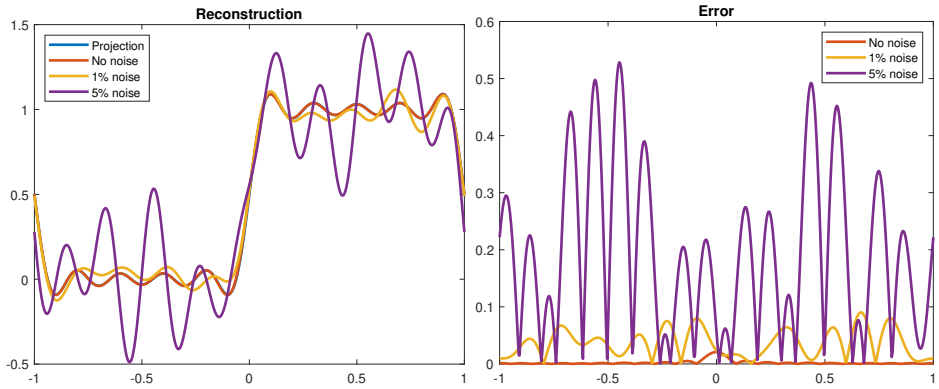

Figure 3.17 Left: Reconstructed $\dot{q}$ with 0%, 1%, 5% Gaussian noise and the projection of the ground truth. Right: The corresponding error between the reconstruction and the projection of the ground truth. The relative L^2-errors are 0.6%, 6.2%, and 33.8%, respectively.

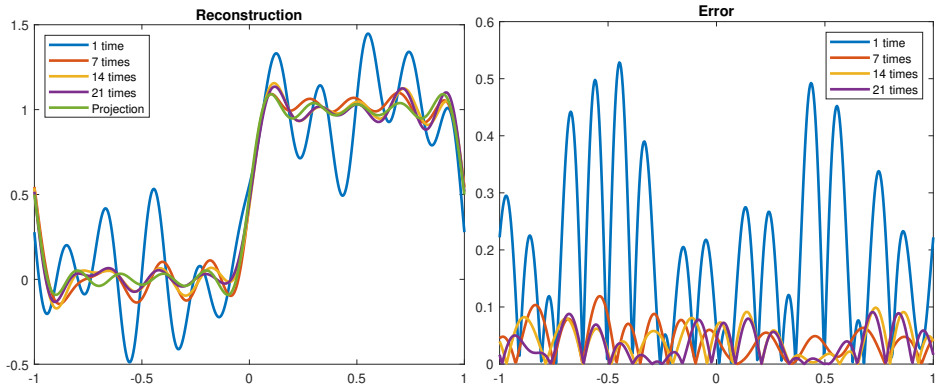

Figure 3.18 Left: Reconstructed $\dot{q}$ under $1, 7, 14, 21$ times repetition with 5% Gaussian noise and the projection of the ground truth. Right: The corresponding error between the reconstruction and the projection of the ground truth. The relative L^2-errors are 33.8%, 7.2%, 6.9%, and 6.1% respectively.

Experiment 3. This experiment aims to test the reconstruction in the case $c_0 = 1$ and a small $q_0 \neq 0$. We choose

$$q_0 = \frac{1}{10}\sin(\pi x),$$

and $\dot{q}$ to be the same Heaviside function as in Experiment 2, see Figure 3.19. We attempt to reconstruct an approximate $\dot{q}$ based on (3.80) by neglecting the terms involving r. A computational challenge is that we cannot find explicit form of $\partial_t^2 f$ when $q_0 \neq 0$. Instead, we make use of the smallness of q_0 to approximately construct $\partial_t^2 f$ as if $q_0 = 0$. In the meanwhile, the operator $\dot{K}$ and $\dot{\Lambda}_{\dot{q}}$ are still implemented using the exact q_0 and $\dot{q}$. The reconstructions and corresponding errors with a single measurement under 0%, 1%, and 5% of Gaussian noise are illustrated in Figure 3.20. The averaged reconstruction with 5% of Gaussian noise and multiple repeated measurements are illustrated in Figure 3.21. This experiment confirms that approximate reconstruction using (3.80) remains possible for $q_0 \neq 0$ as long as it is small.

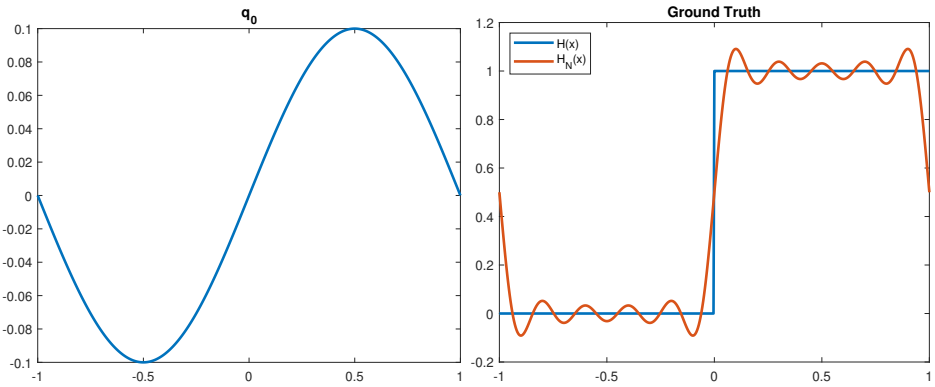

Figure 3.19 Left: $q_0 = \frac{1}{10}\sin(\pi x)$. Right: Ground truth $\dot{q} = H(x)$ and its projection $H_N(x)$.

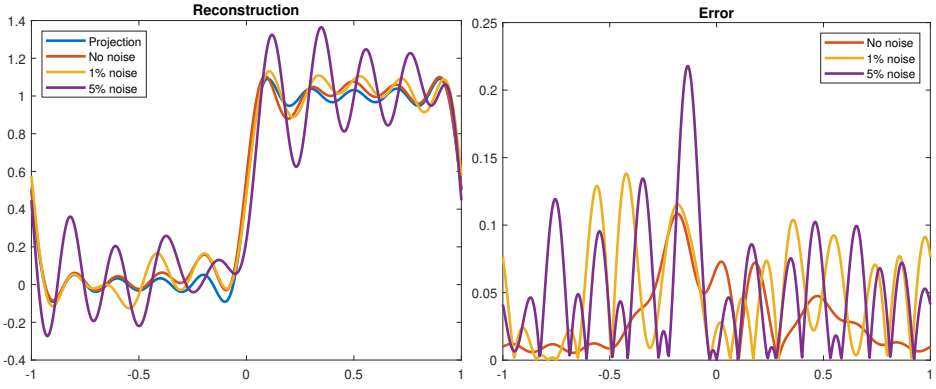

Figure 3.20 Left: Reconstructed $\dot{q}$ with 0%, 1%, 5% Gaussian noise and the projection of the ground truth. Right: The corresponding error between the reconstruction and the projection of the ground truth. The relative L^2-errors are 5.8%, 8.9%, and 24.2%, respectively.

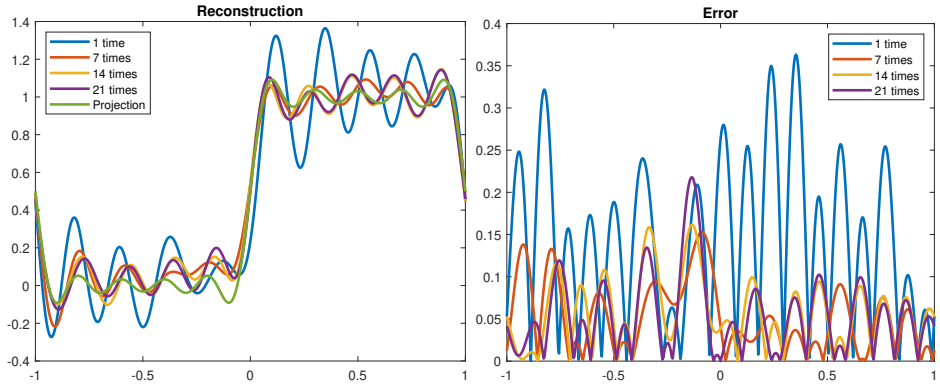

Figure 3.21 Left: Reconstructed $\dot{q}$ under $1, 7, 14, 21$ times repetition with 5% Gaussian noise and the projection of the ground truth. Right: The corresponding error between the reconstruction and the projection of the ground truth. The relative L^2-errors are 24.2%, 9.38%, 9.87% and 9.93%, respectively.

More Experiments We also apply the reconstruction formula (3.76) to measurement from the non-linear IBVP, see [75] for more details.

CHAPTER 4

CONCLUSION

In Chapter 2, we introduce several algorithms for UMBLT. For UMBLT under transport regime, see Section 2.2, we proposed an algorithm to reconstruct isotropic sources, which reduce the measurement requirement and computational demand. However, our proposed algorithm still based on the measurement over entire outgoing boundary, and the source are limited to isotropic source. In future, we can generalize the algorithm to the partial data case similar to the partial data case in diffusive regime. We can choose the adjoint outgoing boundary condition to be supported on the measurement area and we can prove that we can choose such boundary condition to make the adjoint RTE solution positive. For UMBLT under diffusive regime, see Section 2.3, we generalize the algorithm from full data case to partial data case, and give uncertainty quantification based on PDE theory. However, the numerical experiment start from the internal functional and lack of real world data. In future, we could try to numerically recover internal functional from boundary measurement to test the algorithm.

In Chapter 3, we introduce nonlinear IBVP for wave speed reconstruction, see Section 3.2, and linearized IBVP for wave speed and wave potential reconstruction, see Section 3.3. We show that the wave speed can be uniquely determined with vanished wave potential using stable, non-iterative method. We also show that both wave speed and potential can be reconstructed using linearization with at least Hölder stability. However, the nonlinear IBVP are limited to vanished wave potential, the numerical experiment of linearized IBVP are limited to constant background speed and vanish background potential due to the accuracy requirement of second order temporal derivative, and we do not have algorithm to reconstruct wave speed and wave potential together from boundary measurement. In future, we will consider the nonlinear IBVP of wave speed reconstruction with nonvanished wave potential. We will also consider wave model with more parameters, such as wave equation with absorption effect.

BIBLIOGRAPHY

[1] V. Agoshkov. *Boundary Value Problems for Transport Equations*. Birkhauser Boston Inc., USA, 1998.

[2] I. B. Aïcha. Stability estimate for a hyperbolic inverse problem with time-dependent coefficient. *Inverse Problems*, 31(12):125010, 2015.

[3] A. Allers and F. Santosa. Stability and resolution analysis of a linearized problem in electrical impedance tomography. *Inverse problems*, 7(4):515, 1991.

[4] M. Anderson, A. Katsuda, Y. Kurylev, M. Lassas, and M. Taylor. Boundary regularity for the Ricci equation, geometric convergence, and Gel'fand's inverse boundary problem. *Invent. Math.*, 158(2):261–321, 2004.

[5] S. R. Arridge and J. C. Schotland. Optical tomography: forward and inverse problems. *Inverse problems*, 25(12):123010, 2009.

[6] G. Bal, F. J. Chung, and J. C. Schotland. Ultrasound modulated bioluminescence tomography and controllability of the radiative transport equation. *SIAM Journal on Mathematical Analysis*, 48(2):1332–1347, 2016.

[7] G. Bal and J. C. Schotland. Inverse scattering and acousto-optic imaging. *Physical review letters*, 104(4):043902, 2010.

[8] G. Bal and J. C. Schotland. Ultrasound-modulated bioluminescence tomography. *Physical Review E*, 89(3):031201, 2014.

[9] G. Bal and A. Tamasan. Inverse source problems in transport equations. *SIAM journal on mathematical analysis*, 39(1):57–76, 2007.

[10] G. Bao and H. Zhang. Sensitivity analysis of an inverse problem for the wave equation with caustics. *Journal of the American Mathematical Society*, 27(4):953–981, 2014.

[11] M. Belishev. On an approach to multidimensional inverse problems for the wave equation. In *Soviet Math. Dokl*, volume 36, pages 481–484, 1988.

[12] M. Belishev and V. Y. Gotlib. Dynamical variant of the bc-method: theory and numerical testing. *Journal of Inverse and Ill-Posed Problems*, 7(3):221–240, 1999.

[13] M. I. Belishev. Recent progress in the boundary control method. *Inverse Problems*, 23(5):R1–R67, 2007.

[14] M. I. Belishev. Recent progress in the boundary control method. *Inverse problems*, 23(5):R1, 2007.

[15] M. I. Belishev, I. B. Ivanov, I. V. Kubyshkin, and V. S. Semenov. Numerical testing in determination of sound speed from a part of boundary by the bc-method. *Journal of Inverse and Ill-posed Problems*, 24(2):159–180, 2016.

[16] M. I. Belishev and Y. V. Kuryiev. To the reconstruction of a Riemannian manifold via its spectral data (bc–method). *Communications in partial differential equations*, 17(5-6):767–804, 1992.

[17] M. Bellassoued and I. B. Aïcha. Stable determination outside a cloaking region of two time-dependent coefficients in an hyperbolic equation from Dirichlet to Neumann map. *Journal of Mathematical Analysis and Applications*, 449(1):46–76, 2017.

[18] M. Bellassoued and D. D. S. Ferreira. Stability estimates for the anisotropic wave equation from the Dirichlet-to-Neumann map. *Inverse Problems and Imaging*, 5(4):745–773, 2011.

[19] G. Beylkin and R. Burridge. Linearized inverse scattering problems in acoustics and elasticity. *Wave motion*, 12(1):15–52, 1990.

[20] K. Bingham, Y. Kurylev, M. Lassas, and S. Siltanen. Iterative time-reversal control for inverse problems. *Inverse Problems & Imaging*, 2(1):63, 2008.

[21] A. Blagoveshchenskii. The inverse problem in the theory of seismic wave propagation. In *Spectral Theory and Wave Processes*, pages 55–67. Springer, 1967.

[22] E. Blåsten, F. Zouari, M. Louati, and M. S. Ghidaoui. Blockage detection in networks: The area reconstruction method. *arXiv preprint arXiv:1909.05497*, 2019.

[23] A. Bogomolny. Fundamental solutions method for elliptic boundary value problems. *SIAM Journal on Numerical Analysis*, 22(4):644–669, 1985.

[24] R. Bosi, Y. Kurylev, and M. Lassas. Reconstruction and stability in Gel'fand's inverse interior spectral problem. *arXiv preprint arXiv:1702.07937*, 2017.

[25] R. Bosi, Y. Kurylev, and M. Lassas. Reconstruction and stability in Gel'fand's inverse interior spectral problem, 2019.

[26] D. Burago, S. Ivanov, M. Lassas, and J. Lu. Stability of the Gel'fand inverse boundary problem via the unique continuation, 2021.

[27] A. J. Chaudhari, F. Darvas, J. R. Bading, R. A. Moats, P. S. Conti, D. J. Smith, S. R. Cherry, and R. M. Leahy. Hyperspectral and multispectral bioluminescence optical tomography for small animal imaging. *Physics in Medicine & Biology*, 50(23):5421, 2005.

[28] F. Chung, T. Yang, and Y. Yang. Ultrasound modulated bioluminescence tomography with a single optical measurement. *Inverse problems*, 37(1):015004, 2020.

[29] C. H. Contag and M. H. Bachmann. Advances in in vivo bioluminescence imaging of gene expression. *Annual review of biomedical engineering*, 4(1):235–260, 2002.

[30] M. V. De Hoop, P. Kepley, and L. Oksanen. An exact redatuming procedure for the inverse boundary value problem for the wave equation. *SIAM Journal on Applied Mathematics*, 78(1):171–192, 2018.

[31] M. V. de Hoop, P. Kepley, and L. Oksanen. Recovery of a smooth metric via wave field and coordinate transformation reconstruction. *SIAM Journal on Applied Mathematics*, 78(4):1931–1953, 2018.

[32] R. DeVore and G. Petrova. The averaging lemma. *Journal of the American Mathematical Society*, 14(2):279–296, 2001.

[33] H. Dong and Z. Li. On the w 2 p estimate for oblique derivative problem in lipschitz domains. *International Mathematics Research Notices*, 2022(5):3602–3635, 2022.

[34] T. Durduran, R. Choe, W. B. Baker, and A. G. Yodh. Diffuse optics for tissue monitoring and tomography. *Reports on progress in physics*, 73(7):076701, 2010.

[35] A. El Badia and T. Ha-Duong. An inverse source problem in potential analysis. *Inverse Problems*, 16(3):651, 2000.

[36] G. Eskin. A new approach to hyperbolic inverse problems. *Inverse problems*, 22(3):815, 2006.

[37] G. Eskin. Inverse hyperbolic problems with time-dependent coefficients. *Communications in Partial Differential Equations*, 32(11):1737–1758, 2007.

[38] G. Eskin. Inverse problems for the schrödinger equations with time-dependent electromagnetic potentials and the aharonov–bohm effect. *Journal of Mathematical Physics*, 49(2):022105, 2008.

[39] G. Eskin. Inverse problems for general second order hyperbolic equations with time-dependent coefficients. *Bulletin of Mathematical Sciences*, 7(2):247–307, 2017.

[40] L. C. Evans. Partial differential equations. *Graduate studies in mathematics*, 19(4):7, 1998.

[41] L. C. Evans. *Partial differential equations*. American Mathematical Society, Providence, R.I., 2010.

[42] G. Fairweather and A. Karageorghis. The method of fundamental solutions for elliptic boundary value problems. *Advances in Computational Mathematics*, 9(1):69–95, 1998.

[43] A. Feizmohammadi and Y. Kian. Recovery of non-smooth coefficients appearing in anisotropic wave equations. *arXiv preprint arXiv:1903.08118*, 2019.

[44] B. J. Forbes, E. R. Pike, and D. B. Sharp. The acoustical klein–gordon equation: The wave-mechanical step and barrier potential functions. *The Journal of the Acoustical Society of America*, 114(3):1291–1302, 2003.

[45] S. Günter, Q. Yu, J. Krüger, and K. Lackner. Modelling of heat transport in magnetised plasmas using non-aligned coordinates. *Journal of Computational Physics*, 209(1):354–370, 2005.

[46] G. Hu and Y. Kian. Determination of singular time-dependent coefficients for wave equations from full and partial data. *arXiv preprint arXiv:1706.07212*, 2017.

[47] M. Ikehata, G. Makrakis, and G. Nakamura. Inverse boundary value problem for ocean acoustics. *Mathematical methods in the applied sciences*, 24(1):1–8, 2001.

[48] V. A. Il'in. Tikhonov's work on methods of solving ill-posed problems. *Russian Mathematical Surveys*, 22(2):142, 1967.

[49] V. Isakov and Z. Sun. Stability estimates for hyperbolic inverse problems with local boundary data. *Inverse problems*, 8(2):193, 1992.

[50] F. F. Jöbsis. Noninvasive, infrared monitoring of cerebral and myocardial oxygen sufficiency and circulatory parameters. *Science*, 198(4323):1264–1267, 1977.

[51] A. Kachalov, Y. Kurylev, and M. Lassas. *Inverse boundary spectral problems*. Chapman and Hall/CRC, 2001.

[52] J. Kaipio and E. Somersalo. *Statistical and computational inverse problems*, volume 160. Springer Science & Business Media, 2006.

[53] A. C. Kak and M. Slaney. *Principles of computerized tomographic imaging*. SIAM, 2001.

[54] Y. Kian. Recovery of time-dependent damping coefficients and potentials appearing in wave equations from partial data. *SIAM Journal on Mathematical Analysis*, 48(6):4021–4046, 2016.

[55] Y. Kian and L. Oksanen. Recovery of time-dependent coefficient on Riemannian manifold for hyperbolic equations. *International Mathematics Research Notices*, 2019(16):5087–5126, 2017.

[56] A. Kirsch. *An introduction to the mathematical theory of inverse problems*, volume 120. Springer Science & Business Media, 2011.

[57] J. Korpela, M. Lassas, and L. Oksanen. Discrete regularization and convergence of the inverse problem for 1+1 dimensional wave equation. *Inverse Problems & Imaging*, 13(3):575–596, 2019.

[58] V. D. Kupradze. On the approximate solution of problems in mathematical physics. *Russian Mathematical Surveys*, 22(2):58–108, 1967.

[59] Y. V. Kurylev and M. Lassas. Hyperbolic inverse problem with data on a part of the boundary. In *UAB-GIT International Conference on Differential Equations and Mathematical Physics*, pages 259–272. American Mathematical Society, 2000.

[60] P. Lailly and J. Bednar. The seismic inverse problem as a sequence of before stack migrations. In *Conference on inverse scattering: theory and application*, pages 206–220. Philadelphia, Pa, 1983.

[61] I. Lasiecka and R. Triggiani. Regularity theory of hyperbolic equations with non-homogeneous neumann boundary conditions. ii. general boundary data. *Journal of Differential Equations*, 94(1):112–164, 1991.

[62] M. Lassas and L. Oksanen. Inverse problem for the Riemannian wave equation with Dirichlet data and neumann data on disjoint sets. *Duke Mathematical Journal*, 163(6):1071–1103, 2014.

[63] M. M. Lavrent_ev, V. G. Romanov, and S. P. Shishatski_. *Ill-posed problems of mathematical physics and analysis*, volume 64. American Mathematical Soc., 1986.

[64] W. Li, Y. Yang, and Y. Zhong. Inverse transport problem in fluorescence ultrasound modulated optical tomography with angularly averaged measurements. *arXiv preprint arXiv:1902.09638*, 2019.

[65] G. M. Lieberman. Mixed boundary value problems for elliptic and parabolic differential equations of second order. *Journal of Mathematical Analysis and Applications*, 113(2):422–440, 1986.

[66] S. Liu and L. Oksanen. A lipschitz stable reconstruction formula for the inverse problem for the wave equation. *Transactions of the American Mathematical Society*, 368(1):319–335, 2016.

[67] R. Mathon and R. L. Johnston. The approximate solution of elliptic boundary-value problems by fundamental solutions. *SIAM Journal on Numerical Analysis*, 14(4):638–650, 1977.

[68] T. P. Matthews and M. A. Anastasio. Joint reconstruction of the initial pressure and speed of sound distributions from combined photoacoustic and ultrasound tomography measurements. *Inverse problems*, 33(12):124002, 2017.

[69] L. Mezzanotte, M. van't Root, H. Karatas, E. A. Goun, and C. W. Löwik. In vivo molecular bioluminescence imaging: new tools and applications. *Trends in biotechnology*, 35(7):640–652, 2017.

[70] C. Montalto. Stable determination of a simple metric, a covector field and a potential from the hyperbolic Dirichlet-to-Neumann map. *Communications in Partial Differential Equations*, 39(1):120–145, 2014.

[71] A. I. Nachman. Reconstructions from boundary measurements. *Annals of Mathematics*, 128(3):531–576, 1988.

[72] S. Nagayasu, G. Uhlmann, and J.-N. Wang. Increasing stability in an inverse problem for the acoustic equation. *Inverse Problems*, 29(2):025012, 2013.

[73] F. Natterer and F. Wubbeling. A propagation-backpropagation method for ultrasound tomography. *Inverse problems*, 11(6):1225, 1995.

[74] L. Oksanen. Solving an inverse obstacle problem for the wave equation by using the boundary control method. *Inverse Problems*, 29(3):035004, 2013.

[75] L. Oksanen, T. Yang, and Y. Yang. Linearized boundary control method for an acoustic inverse boundary value problem. *Inverse Problems*, 38(11):114001, 2022.

[76] L. Pestov, V. Bolgova, and O. Kazarina. Numerical recovering of a density by the bc-method. *Inverse Problems & Imaging*, 4(4):703, 2010.

[77] B. Ptashnik. Ill-posed boundary-value problems for partial differential equations, 1984.

[78] A. G. Ramm et al. Property c and an inverse problem for a hyperbolic equation. *Journal of Mathematical Analysis and Applications*, 156(1):209–219, 1991.

[79] N. V. Ruiter, M. Zapf, T. Hopp, R. Dapp, E. Kretzek, M. Birk, B. Kohout, and H. Gemmeke. 3d ultrasound computer tomography of the breast: A new era? *European Journal of Radiology*, 81:S133–S134, 2012.

[80] S. Sakadžić and L. V. Wang. High-resolution ultrasound-modulated optical tomography in biological tissues. *Optics letters*, 29(23):2770–2772, 2004.

[81] R. Salazar. Determination of time-dependent coefficients for a hyperbolic inverse problem. *Inverse Problems*, 29(9):095015, 2013.

[82] P. Shivakumar and K. H. Chew. A sufficient condition for nonvanishing of determinants. *Proceedings of the American mathematical society*, pages 63–66, 1974.

[83] P. Stefanov and G. Uhlmann. Stability estimates for the hyperbolic Dirichlet to Neumann map in anisotropic media. *journal of functional analysis*, 154(2):330–358, 1998.

[84] P. Stefanov and G. Uhlmann. Stable determination of generic simple metrics from the hyperbolic Dirichlet-to-Neumann map. *International Mathematics Research Notices*, 2005(17):1047–1061, 2005.

[85] P. Stefanov and G. Uhlmann. An inverse source problem in optical molecular imaging. *Analysis & PDE*, 1(1):115–126, 2008.

[86] P. Stefanov and Y. Yang. The inverse problem for the Dirichlet-to-Neumann map on Lorentzian manifolds. *Analysis & PDE*, 11(6):1381–1414, 2018.

[87] P. D. Stefanov. Uniqueness of the multi-dimensional inverse scattering problem for time dependent potentials. *Mathematische Zeitschrift*, 201(4):541–559, 1989.

[88] Z. Sun. On continuous dependence for an inverse initial boundary value problem for the wave equation. *Journal of Mathematical Analysis and Applications*, 150(1):188–204, 1990.

[89] J. Sylvester and G. Uhlmann. A global uniqueness theorem for an inverse boundary value problem. *Annals of mathematics*, pages 153–169, 1987.

[90] D. Tataru. Unique continuation for solutions to PDE's; between Hormander's theorem and Holmgren's theorem. *Communications in Partial Differential Equations*, 20(5-6):855–884, 1995.

[91] D. Tataru. Unique continuation for solutions to PDE's; between Hörmander's theorem and Holmgren's theorem. *Comm. Partial Differential Equations*, 20(5-6):855–884, 1995.

[92] D. Tataru. On the regularity of boundary traces for the wave equation. *Annali della Scuola Normale Superiore di Pisa-Classe di Scienze*, 26(1):185–206, 1998.

[93] A. N. Tikhonov. On the solution of ill-posed problems and the method of regularization. In *Doklady akademii nauk*, volume 151, pages 501–504. Russian Academy of Sciences, 1963.

[94] G. Wang, E. Hoffman, G. McLennan, L. Wang, M. Suter, J. Meinel, et al. Development of the first bioluminescent ct scanner. *Radiology*, 229(566):0033–8419, 2003.

[95] G. Wang, Y. Li, and M. Jiang. Uniqueness theorems in bioluminescence tomography. *Medical physics*, 31(8):2289–2299, 2004.

[96] T. Yang and Y. Yang. A stable non-iterative reconstruction algorithm for the acoustic inverse boundary value problem. *Inverse Problems & Imaging*, 2021.

[97] T. Yang and Y. Yang. The diffusive ultrasound modulated bioluminescence tomography with partial data and uncertain optical parameters. *arXiv preprint arXiv:2404.03124*, 2024.

[98] Y. Yang and J. Zhai. Unique determination of a transversely isotropic perturbation in a linearized inverse boundary value problem for elasticity. *Inverse Problems and Imaging*, 13(6):1309–1325, 2019.

[99] G. Yao and L. V. Wang. Theoretical and experimental studies of ultrasound-modulated optical tomography in biological tissue. *Applied Optics*, 39(4):659–664, 2000.

[100] A. Yodh and B. Chance. Spectroscopy and imaging with diffusing light. *Physics today*, 48(3):34–40, 1995.

[101] H. F. Zhang, K. Maslov, M.-L. Li, G. Stoica, and L. V. Wang. In vivo volumetric imaging of subcutaneous microvasculature by photoacoustic microscopy. *Optics Express*, 14(20):9317–9323, 2006.

APPENDIX A

APPENDIX FOR CHAPTER 2

A.1 Diffusion Approximation

In strong scattering medium, such as biological objects, the propagation of light is diffusive and can be approximately described by diffusion equation. The standard way to accomplish the approximation from RTE to diffusion equation is to expand functions in terms of spherical harmonics and truncate the series.

In order to derive the diffusion approximation, we need following assumptions on the optical coefficients:

1. $k(x,\theta,\vartheta) = k(x,-\vartheta,-\theta) \geq 0$ for any $x \in X$, $\theta, \vartheta \in \mathbb{S}^{n-1}$,
2. $\int_{\mathbb{S}^{n-1}} k(x,\theta,\vartheta)\,\mathrm{d}\theta = \int_{\mathbb{S}^{n-1}} k(x,\theta,\vartheta)\,\mathrm{d}\vartheta = \sigma_s(x) \geq 0$ for any $x \in X$, $\theta, \vartheta \in \mathbb{S}^{n-1}$,
3. $\sigma(x) \geq \sigma_s(x)$ for any $x \in X$,
4. $S(x,\theta)$ is either independent of direction θ, or compact supported on X for any $\theta \in \mathbb{S}^{n-1}$.

We introduce the diffusion approximation under spherical harmonics up to the first order. The space spanned by the spherical harmonics up to the first order in $\mathbb{S}^{n-1}$ is

$$\mathcal{H}_1 = \mathrm{span}\{1, \theta_1, \theta_2, \ldots, \theta_n\} \subset L^2(\mathbb{S}^{n-1}), \tag{A.1}$$

where θ_i denote the i-th entry of $\theta \in \mathbb{S}^{n-1}$.

Lemma A.1 ([52, Lemma 6.10])**.** *The orthogonal projection*

$$\mathcal{P} : L^2(\mathbb{S}^{n-1}) \to \mathcal{H}_1$$

is given as

$$\mathcal{P}f(\theta) = \fint_{\mathbb{S}^{n-1}} f(\vartheta)\,\mathrm{d}\vartheta + n \fint_{\mathbb{S}^{n-1}} \theta \cdot \vartheta f(\vartheta)\,\mathrm{d}\vartheta,$$

where $\fint$ denote the average integral.

Let $\mathcal{B}$ denote the integro-differential operator on the right hand side of (2.1), i.e. the RTE can be written as

$$\mathcal{B}u(x,\theta) = S(x,\theta).$$

The diffusion approximation is given by

$$\mathcal{P}\mathcal{B}\mathcal{P}u(x,\theta) = \mathcal{P}S(x,\theta).$$

Denote

$$\mathcal{P}u(x,\theta) = \fint_{\mathbb{S}^{n-1}} u(x,\vartheta)\,\mathrm{d}\vartheta + n \fint_{\mathbb{S}^{n-1}} \theta\cdot\vartheta u(x,\vartheta)\,\mathrm{d}\vartheta =: \phi(x) + n\theta\cdot J(x), \tag{A.2}$$

$$\mathcal{P}S(x,\theta) = \fint_{\mathbb{S}^{n-1}} S(x,\vartheta)\,\mathrm{d}\vartheta + n \fint_{\mathbb{S}^{n-1}} \theta\cdot\vartheta S(x,\vartheta)\,\mathrm{d}\vartheta =: S_0(x) + n\theta\cdot S_1(x), \tag{A.3}$$

Lemma A.2. *The explicit form is given by*

$$\mathcal{P}\mathcal{B}\mathcal{P}u(x,\theta) = (\sigma(x)-\sigma_s(x))\phi(x) + \nabla\cdot J(x) + n\theta\cdot\left(\frac{1}{n}\nabla\phi(x) + (\sigma(x)I - B(x))J(x)\right), \tag{A.4}$$

where I is $n\times n$ identity matrix, $B(x)$ is a $n\times n$ matrix with entries

$$B_{ij}(x) = \frac{n}{\mathrm{Vol}(\mathbb{S}^{n-1})}\int_{\mathbb{S}^{n-1}}\int_{\mathbb{S}^{n-1}} \theta_i\vartheta_j k(x,\theta,\vartheta)\,\mathrm{d}\theta\,\mathrm{d}\vartheta.$$

Proof. We first introduce following identities from the symmetricity

$$\begin{aligned}
&\fint_{\mathbb{S}^{n-1}} \theta_i\,\mathrm{d}\theta = 0,\\
&\fint_{\mathbb{S}^{n-1}} \theta_i\theta_j\,\mathrm{d}\theta = \frac{\delta_{ij}}{n},\\
&\fint_{\mathbb{S}^{n-1}} \theta_i\theta_j\theta_k\,\mathrm{d}\theta = 0,
\end{aligned}$$

where $1\le i,j,k\le n$, δ_{ij} is the Kronecker delta.

For any fixed x, it is clear that $\theta\cdot\nabla\phi(x), \sigma(x)(\phi(x)+n\theta\cdot J(x))\in\mathcal{H}_1$, we have

$$\mathcal{P}[\theta\cdot\nabla\phi(x)] = \theta\cdot\nabla\phi(x), \qquad \mathcal{P}[\sigma(x)(\phi(x)+n\theta\cdot J(x))] = \sigma(x)(\phi(x)+n\theta\cdot J(x)). \tag{A.5}$$

Since

$$\theta\cdot\nabla(\theta\cdot J(x)) = \theta^\top A(x)\theta$$

where $A(x)$ denote the Jacobian of $J(x)$, we have

$$\fint_{\mathbb{S}^{n-1}} \vartheta \cdot \nabla(\vartheta \cdot J(x))\,\mathrm{d}\vartheta = \fint_{\mathbb{S}^{n-1}} \sum_{i,j=1}^{n} A_{ij}(x)\vartheta_i\vartheta_j\,\mathrm{d}\vartheta = \frac{1}{n}\mathrm{tr}A(x) = \frac{1}{n}\nabla \cdot J(x),$$

$$\fint_{\mathbb{S}^{n-1}} (\theta \cdot \vartheta)(\vartheta \cdot \nabla(\vartheta \cdot J(x)))\,\mathrm{d}\vartheta = \fint_{\mathbb{S}^{n-1}} \sum_{i,j,k=1}^{n} A_{ij}(x)\vartheta_i\vartheta_j\vartheta_k\theta_k\,\mathrm{d}\vartheta = 0,$$

thus

$$\mathcal{P}[\theta \cdot \nabla(\phi(x) + n\theta \cdot J(x))] = \theta \cdot \nabla\phi(x) + \nabla \cdot J(x). \tag{A.6}$$

Consider the integral operator in $\mathcal{B}$. Since

$$\int_{\mathbb{S}^{n-1}} k(x,\theta,\vartheta)\,\mathrm{d}\theta = \int_{\mathbb{S}^{n-1}} k(x,\theta,\vartheta)\,\mathrm{d}\vartheta = \sigma_s(x),$$

we conclude

$$\begin{aligned}
\fint_{\mathbb{S}^{n-1}} \int_{\mathbb{S}^{n-1}} k(x,\theta,\vartheta)\phi(x)\,\mathrm{d}\vartheta\,\mathrm{d}\theta &= \sigma_s(x)\phi(x)\\
\fint_{\mathbb{S}^{n-1}} \int_{\mathbb{S}^{n-1}} k(x,\theta,\vartheta)\vartheta \cdot J(x)\,\mathrm{d}\vartheta\,\mathrm{d}\theta &= \sigma_s(x) \fint_{\mathbb{S}^{n-1}} \vartheta \cdot J(x)\,\mathrm{d}\vartheta = 0\\
\fint_{\mathbb{S}^{n-1}} \int_{\mathbb{S}^{n-1}} \theta \cdot \vartheta k(x,\vartheta,\vartheta')\phi(x)\,\mathrm{d}\vartheta'\,\mathrm{d}\vartheta &= \sigma_s(x)\phi(x) \fint_{\mathbb{S}^{n-1}} \theta \cdot \vartheta\,\mathrm{d}\vartheta = 0\\
\fint_{\mathbb{S}^{n-1}} \int_{\mathbb{S}^{n-1}} \theta \cdot \vartheta k(x,\vartheta,\vartheta')\vartheta' \cdot J(x)\,\mathrm{d}\vartheta'\,\mathrm{d}\vartheta &= \theta^\top \left[\fint_{\mathbb{S}^{n-1}} \int_{\mathbb{S}^{n-1}} k(x,\vartheta,\vartheta')\vartheta\vartheta'^\top\,\mathrm{d}\vartheta'\,\mathrm{d}\vartheta\right] J(x)\\
&= \frac{1}{n}\theta^\top B(x)J(x)
\end{aligned}$$

thus

$$\mathcal{P}\left[\int_{\mathbb{S}^{n-1}} k(x,\theta,\vartheta)(\phi(x) + n\vartheta \cdot J(x))\,\mathrm{d}\vartheta\right] = \sigma_s(x)\phi(x) + n\theta \cdot B(x)J(x) \tag{A.7}$$

Combining (A.5) (A.6) (A.7) gives (A.4). □

Lemma A.3. *$B(x)$ is positive definite with eigenvalues in $[0, \sigma_s(x)]$ for each $x \in X$.*

Proof. Since $k(x,\theta,\vartheta) = k(x,-\vartheta,-\theta) \geq 0$, we have $B_{ij}(x) = B_{ji}(x)$, i.e. $B(x)$ is symmetric. For

arbitrary vector $\omega \in \mathbb{S}^{n-1}$,

$$\begin{aligned}
\omega^\top B(x)\omega =& \frac{n}{\mathrm{Vol}(\mathbb{S}^{n-1})} \int_{\mathbb{S}^{n-1}} \int_{\mathbb{S}^{n-1}} (\omega\cdot\theta) k(x,\theta,\vartheta)(\omega\cdot\vartheta)\,\mathrm{d}\theta\,\mathrm{d}\vartheta \\
=& \frac{n}{\mathrm{Vol}(\mathbb{S}^{n-1})} \iint_{(\omega\cdot\theta)(\omega\cdot\vartheta)\geq 0} (\omega\cdot\theta) k(x,\theta,\vartheta)(\omega\cdot\vartheta)\,\mathrm{d}\theta\,\mathrm{d}\vartheta \\
&+ \frac{n}{\mathrm{Vol}(\mathbb{S}^{n-1})} \iint_{(\omega\cdot\theta)(\omega\cdot\vartheta)<0} (\omega\cdot\theta) k(x,\theta,\vartheta)(\omega\cdot\vartheta)\,\mathrm{d}\theta\,\mathrm{d}\vartheta \\
=& \frac{n}{\mathrm{Vol}(\mathbb{S}^{n-1})} \iint_{(\omega\cdot\theta)(\omega\cdot\vartheta)\geq 0} (\omega\cdot\theta) k(x,\theta,\vartheta)(\omega\cdot\vartheta)\,\mathrm{d}\theta\,\mathrm{d}\vartheta \\
&+ \frac{n}{\mathrm{Vol}(\mathbb{S}^{n-1})} \iint_{(\omega\cdot\theta)(\omega\cdot\vartheta)<0} (\omega\cdot\theta) k(x,\theta,\vartheta)(\omega\cdot-\vartheta)\,\mathrm{d}\theta\,\mathrm{d}(-\vartheta) \\
=& \frac{n}{\mathrm{Vol}(\mathbb{S}^{n-1})} \iint_{(\omega\cdot\theta)(\omega\cdot\vartheta)\geq 0} (\omega\cdot\theta)\left[k(x,\theta,\vartheta)+k(x,\theta,-\vartheta)\right](\omega\cdot\vartheta)\,\mathrm{d}\theta\,\mathrm{d}\vartheta \\
\geq& 0,
\end{aligned}$$

$$\begin{aligned}
&\omega^\top B(x)\omega \\
=& \frac{n}{\mathrm{Vol}(\mathbb{S}^{n-1})} \iint_{\mathbb{S}^{n-1}\times\mathbb{S}^{n-1}} \left[(\omega\cdot\theta)\sqrt{k(x,\theta,\vartheta)}\right]\left[(\omega\cdot\vartheta)\sqrt{k(x,\theta,\vartheta)}\right]\mathrm{d}\theta\,\mathrm{d}\vartheta \\
\leq& \frac{n}{\mathrm{Vol}(\mathbb{S}^{n-1})} \sqrt{\iint_{\mathbb{S}^{n-1}\times\mathbb{S}^{n-1}} (\omega\cdot\theta)^2 k(x,\theta,\vartheta)\,\mathrm{d}\theta\,\mathrm{d}\vartheta \iint_{\mathbb{S}^{n-1}\times\mathbb{S}^{n-1}} (\omega\cdot\vartheta)^2 k(x,\theta,\vartheta)\,\mathrm{d}\theta\,\mathrm{d}\vartheta} \\
\leq& \frac{n\sigma_s(x)}{\mathrm{Vol}(\mathbb{S}^{n-1})} \sqrt{\int_{\mathbb{S}^{n-1}} (\omega\cdot\theta)^2\,\mathrm{d}\theta \int_{\mathbb{S}^{n-1}} (\omega\cdot\vartheta)^2\,\mathrm{d}\vartheta} \\
=& \frac{n\sigma_s(x)}{\mathrm{Vol}(\mathbb{S}^{n-1})} \int_{\mathbb{S}^{n-1}} \theta_1^2\,\mathrm{d}\theta \\
=& \sigma_s(x).
\end{aligned}$$

we conclude $B(x)$ is positive definite with eigenvalues in $[0, \sigma_s(x)]$. □

Proposition A.4. *The diffusion approximation of* (2.1) *is given by*

$$-\nabla\cdot D(x)\nabla\phi(x) + \sigma_a(x)\phi(x) = q(x),$$

where

$$D(x) = \frac{1}{n}(\sigma(x)I - B(x))^{-1}, \qquad \sigma_a(x) = \sigma(x) - \sigma_s(x), \qquad q(x) = S_0(x) - n\nabla\cdot D(x)S_1(x).$$

Proof. According to (A.4)

$$\mathcal{P}\mathcal{B}\mathcal{P}u(x,\theta) = \mathcal{P}S(x,\theta),$$

gives

$$(\sigma(x) - \sigma_s(x))\phi(x) + \nabla \cdot J(x) + n\theta \cdot \left(\frac{1}{n}\nabla\phi(x) + (\sigma(x)I - B(x))J(x)\right) = S_0(x) + n\theta \cdot S_1(x),$$

thus

$$\begin{aligned} S_0(x) &= (\sigma(x) - \sigma_s(x))\phi(x) + \nabla \cdot J(x) = \sigma_a(x)\phi(x) + \nabla \cdot J(x), \\ S_1(x) &= \frac{1}{n}\nabla\phi(x) + (\sigma(x)I - B(x))J(x) = \frac{1}{n}(\nabla\phi(x) + D^{-1}(x)J(x)), \end{aligned}$$

which gives

$$S_0(x) = \sigma_a(x)\phi(x) + \nabla \cdot J(x) = \sigma_a(x)\phi(x) + \nabla \cdot D(x)(nS_1(x) - \nabla\phi(x)),$$

or equivalently

$$-\nabla \cdot D(x)\nabla\phi(x) + \sigma_a(x)\phi(x) = q(x).$$

□

Remark A.5. *When $\sigma(x) > \sigma_s(x)$ or the eigenvalues of $B(x)$ are strictly smaller than $\sigma_s(x)$ for any $x \in X$, $D(x)$ is well defined.*

Proposition A.6. *$D(x)$ is isotropic if $k(x,\theta,\vartheta)$ is invariant under rotation*

Proof. When $k(x,\theta,\vartheta)$ is invariant under rotation,

$$B_{ij} = \frac{n}{\mathrm{Vol}(\mathbb{S}^{n-1})}\int_{\mathbb{S}^{n-1}}\int_{\mathbb{S}^{n-1}} \theta_i\vartheta_j k(x,\theta\cdot\vartheta)\,\mathrm{d}\theta\,\mathrm{d}\vartheta.$$

From the symmetricity, $B_{ij} = 0$ if $i \neq j$, and the diagonal terms are identical:

$$\begin{aligned} B_{ii}(x) =& \frac{1}{n}\mathrm{tr}B(x) = \frac{1}{\mathrm{Vol}(\mathbb{S}^{n-1})}\int_{\mathbb{S}^{n-1}}\int_{\mathbb{S}^{n-1}} \theta\cdot\vartheta k(x,\theta\cdot\vartheta)\,\mathrm{d}\theta\,\mathrm{d}\vartheta \\ =& \int_{\mathbb{S}^{n-1}} \theta\cdot\vartheta k(x,\theta\cdot\vartheta)\,\mathrm{d}\theta = \int_{-1}^{1} tk(x,t)\mathrm{Vol}(\mathbb{S}^{n-2})(1-t^2)^{\frac{n-3}{2}}\,\mathrm{d}t =: b(x). \end{aligned}$$

Thus $B(x) = b(x)I$ if $k(x,\theta,\vartheta)$ is invariant under rotation, which implies $D(x)$ is isotropic. □

Proposition A.7. *The diffusion approximation of* (2.2) *is given by*

$$\phi(x) + \gamma \nu \cdot D(x) \nabla \phi(x) = 0,$$

where

$$\gamma = \frac{\sqrt{\pi}(n-1)\Gamma\left(\frac{n-1}{2}\right)}{2\Gamma\left(\frac{n}{2}\right)}.$$

Proof. The photon flux intensity at $x \in \partial X$ into the body is

$$\Phi_-(x) = -\int_{\theta \cdot \nu < 0} u(x, \theta) \theta \cdot \nu \, \mathrm{d}\theta = 0.$$

With the diffusion approximation, it is

$$-\int_{\theta \cdot \nu < 0} (\phi(x) + n\theta \cdot J(x)) \theta \cdot \nu \, \mathrm{d}\theta = 0.$$

Since

$$-\int_{\theta \cdot \nu < 0} \theta \cdot \nu \, \mathrm{d}\theta = \frac{1}{2} \int_{\mathbb{S}^{n-1}} |\theta_1| \, \mathrm{d}\theta = \frac{1}{2} \int_{-1}^{1} |t| \mathrm{Vol}(\mathbb{S}^{n-2}) (1-t^2)^{\frac{n-3}{2}} \, \mathrm{d}t = \frac{\mathrm{Vol}(\mathbb{S}^{n-2})}{n-1},$$

$$\int_{\theta \cdot \nu < 0} \theta \cdot J(x) \theta \cdot \nu \, \mathrm{d}\theta = \nu^\top \left[\int_{\theta \cdot \nu < 0} \theta\theta^\top \, \mathrm{d}\theta \right] J(x) = \frac{1}{2} \nu^\top \left[\int_{\mathbb{S}^{n-1}} \theta\theta^\top \, \mathrm{d}\theta \right] J(x) = \frac{\mathrm{Vol}(\mathbb{S}^{n-1})}{2n} \nu \cdot J(x),$$

we conclude

$$\phi(x) = \frac{(n-1)\mathrm{Vol}(\mathbb{S}^{n-1})}{2\mathrm{Vol}(\mathbb{S}^{n-2})} \nu \cdot J(x) = \frac{(n-1)\mathrm{Vol}(\mathbb{S}^{n-1})}{2\mathrm{Vol}(\mathbb{S}^{n-2})} \nu \cdot D(x)(nS_1(x) - \nabla \phi(x)).$$

Since $S(x, \theta)$ is either independent of direction θ, or compact supported on X for any $\theta \in \mathbb{S}^{n-1}$, $S_1(x) = 0$, thus

$$\phi(x) + \frac{(n-1)\mathrm{Vol}(\mathbb{S}^{n-1})}{2\mathrm{Vol}(\mathbb{S}^{n-2})} \nu \cdot D(x) \nabla \phi(x) = \phi(x) + \gamma \nu \cdot D(x) \nabla \phi(x) = 0.$$

□

Thus the diffusion approximation of RTE is given by the diffusion equation with Robin boundary condition.

APPENDIX B

APPENDIX FOR CHAPTER 3

B.1 Adjoint of ND Map

Lemma B.1. *Suppose $\Lambda_{\rho,q}$ is the ND map of following wave equation*

$$\begin{cases} \Box_{\rho,q} u(t,x) = 0 & \text{in } [0,2T]\times\Omega, \\ u(0,x) = \partial_t u(0,x) = 0 & \text{on } \Omega, \\ \partial_\nu u(t,x) = f & \text{on } [0,2T]\times\partial\Omega, \end{cases} \tag{B.1}$$

we have $\Lambda^*_{\rho,q} = R\Lambda_{\rho,q}R$.

Proof. Let v denote the solution of the following adjoint wave equation

$$\begin{cases} \Box_{\rho,q} v(t,x) = 0 & \text{in } [0,2T]\times\Omega, \\ v(2T,x) = \partial_t v(2T,x) = 0 & \text{on } \Omega, \\ \partial_\nu v(t,x) = g & \text{on } [0,2T]\times\partial\Omega, \end{cases} \tag{B.2}$$

with g in $L^2((0,2T)\times\partial\Omega)$, where $L^* = -\nabla\cdot A\nabla - b\cdot\nabla + c$ is the adjoint operator of L. Let Λ^* denote the ND map of the adjoint equation.

The weak formulation gives

$$\int_\Omega \int_0^{2T} [\rho(x)\partial_t^2 u^f(t,x) - \Delta u^f(t,x) + q(x)u^f(t,x)]v(t,x)\,\mathrm{d}t\,\mathrm{d}x = 0.$$

Define

$$I_1 := \int_\Omega \int_0^{2T} \rho(x) u^f_{tt}(t,x)v(t,x)\,\mathrm{d}t\,\mathrm{d}x = \int_\Omega \int_0^{2T} \rho(x)u^f(t,x)v_{tt}(t,x)\,\mathrm{d}t\,\mathrm{d}x,$$

$$\begin{aligned} I_2 &:= \int_\Omega \int_0^{2T} [-\Delta u^f(t,x) + q(x)u^f(t,x)]v(t,x)\,\mathrm{d}t\,\mathrm{d}x \\ &= \int_\Omega \int_0^{2T} [-\Delta v(t,x) + q(x)v(t,x)]u^f(t,x)\,\mathrm{d}t\,\mathrm{d}x \\ &\quad + (\Lambda_{\rho,q} f, g)_{L^2((0,2T)\times\partial\Omega)} - (f, \Lambda^*_{\rho,q} g)_{L^2((0,2T)\times\partial\Omega)} \end{aligned}$$

thus

$$I_1 + I_2 = (\Lambda_{\rho,q} f, g)_{L^2((0,2T)\times\partial\Omega)} - (f, \Lambda^*_{\rho,q} g)_{L^2((0,2T)\times\partial\Omega)} = 0,$$

which implies $\Lambda^*_{\rho,q}$ is the adjoint operator of $\Lambda_{\rho,q}$ in $L^2((0,2T)\times\partial\Omega)$. Notice that the solution of equation

$$\begin{cases} \Box_{\rho,q} u(t,x) = 0 & \text{in } [0,2T]\times\Omega, \\ u(0,x) = \partial_t u(0,x) = 0 & \text{on } \Omega, \\ \partial_\nu u(t,x) = Rg & \text{on } [0,2T]\times\partial\Omega, \end{cases} \tag{B.3}$$

is the time reversed adjoint solution of (B.2), which means the adjoint operator can be represent as

$$\Lambda^*_{\rho,q} = R\Lambda_{\rho,q} R$$

□

B.2 Frechét Differentiability of ND map Λ_q

In this section, we collect a few results that are used in the main text. First, we provide the rigorous justification for the formal linearization process in the introduction to derive (3.63) (3.64) (3.65). Recall that $c_0 \in C^\infty(\overline{\Omega})$.

For $f \in L^2((0,2T)\times\partial\Omega)$, the solution $u = u^f$ of the boundary value problem (3.1) satisfies $u \in C([0,2T]; H^{5/6-\varepsilon}(\Omega))$ for any $\varepsilon > 0$ with the norm estimate [61]

$$\|u\|_{C([0,2T];H^{5/6-\varepsilon}(\Omega))} \leq C\|f\|_{L^2((0,2T)\times\partial\Omega)} \tag{B.4}$$

where $\|u^f\|_{C([0,2T];H^{5/6-\varepsilon}(\Omega))} := \operatorname{ess\,sup}_{0\leq t\leq 2T}\|u(t)\|_{H^{5/6-\varepsilon}(\Omega)}$. As a result, the ND map $\Lambda_q : L^2((0,2T)\times\partial\Omega) \to L^2((0,2T)\times\partial\Omega)$ is a bounded linear operator.

Denote by $\mathcal{L}(L^2((0,2T)\times\partial\Omega), L^2((0,2T)\times\partial\Omega))$ the Banach space of bounded linear operators over $L^2((0,2T)\times\partial\Omega)$. The IBVP aims to invert the following nonlinear map

$$\mathcal{F}: \quad q \in L^\infty(\Omega) \mapsto \Lambda_q \in \mathcal{L}(L^2((0,2T)\times\partial\Omega), L^2((0,2T)\times\partial\Omega))$$

Suppose $q = q_0 + \dot{q}$ with $q_0 \in C^\infty(\overline{\Omega})$. Define a linear operator (which will turn out to be the Frechét differentiation of $\mathcal{F}$):

$$d\mathcal{F}: \quad \dot{q} \in L^\infty(\Omega) \mapsto \dot{\Lambda}_{\dot{q}} \in \mathcal{L}(L^2((0,2T)\times\partial\Omega), L^2((0,2T)\times\partial\Omega)).$$

where $\dot{\Lambda}_{\dot{q}}$ is the operator defined in (3.65).

Proposition B.2. *The nonlinear map $\mathcal{F}$ is Frechét differentiable at a fixed $q_0 \in C^\infty(\overline{\Omega})$, and the Frechét derivative along $\dot{q} \in L^\infty(\Omega)$ is $\dot{\Lambda}_{\dot{q}}$.*

Proof. It suffices to show that as $\|\dot{q}\|_{L^\infty(\Omega)} \to 0$, we have

$$\|\mathcal{F}(q) - \mathcal{F}(q_0) - d\mathcal{F}(\dot{q})\|_{\mathcal{L}(L^2((0,2T)\times\partial\Omega),L^2((0,2T)\times\partial\Omega))} = O(\|\dot{q}\|^2_{L^\infty(\Omega)})$$

(or equivalently, $\|\Lambda_q - \Lambda_{q_0} - \dot{\Lambda}_{\dot{q}}\|_{\mathcal{L}(L^2((0,2T)\times\partial\Omega),L^2((0,2T)\times\partial\Omega))} = O(\|\dot{q}\|^2_{L^\infty(\Omega)})$) to justify that $d\mathcal{F}$ is indeed the Frechét differentiation of $\mathcal{F}$. To this end, we will prove for any $f \in L^2((0,2T)\times\partial\Omega)$ that

$$\|\Lambda_q f - \Lambda_{q_0} f - \dot{\Lambda}_{\dot{q}} f\|_{L^2((0,2T)\times\partial\Omega)} \leq C\|\dot{q}\|^2_{L^\infty}\|f\|_{L^2((0,2T)\times\partial\Omega)} \tag{B.5}$$

for some constant $C > 0$ that is independent of f. For ease of notation, we will denote all the constants independent of f by C.

We continue to denote the solutions of (3.1) and (3.63) by u and u_0, respectively. Write $u = u_0 + \delta u$. Then δu satisfies $\delta u|_{[0,2T]\times\partial\Omega} = \Lambda_q f - \Lambda_{q_0} f$ and

$$\begin{cases} \Box_{c_0,q_0}\delta u(t,x) &= -u\dot{q}, & \text{in } (0,2T)\times\Omega \\ \partial_\nu \delta u &= 0, & \text{on } (0,2T)\times\partial\Omega \\ \delta u(0,x) = \partial_t \delta u(0,x) &= 0 & x \in \Omega. \end{cases} \tag{B.6}$$

Using the regularity estimate for the wave equation [40] and the trace theorem, we obtain

$$\|\delta u\|_{H^1((0,2T)\times\Omega)} \leq C\|u\dot{q}\|_{L^2((0,2T)\times\Omega)} \leq C\|u\|_{L^2((0,2T)\times\Omega)}\|\dot{q}\|_{L^\infty(\Omega)}. \tag{B.7}$$

Next, set $w := \delta u - \dot{u}$, then $w|_{[0,2T]\times\partial\Omega} = \Lambda_q f - \Lambda_{q_0} f - \dot{\Lambda}_{\dot{q}} f$, and w satisfies

$$\begin{cases} \Box_{c_0,q_0} w(t,x) &= -\dot{q}\delta u, & \text{in } (0,2T)\times\Omega \\ \partial_\nu w &= 0, & \text{on } (0,2T)\times\partial\Omega \\ w(0,x) = \partial_t w(0,x) &= 0 & x \in \Omega. \end{cases} \tag{B.8}$$

Applying the regularity estimate for the wave equation again yields

$$\begin{aligned}\|\Lambda_q f - \Lambda_{q_0} f - \Lambda_{\dot{q}} f\|_{L^2((0,2T)\times\partial\Omega)} &\leq \|w\|_{H^1((0,2T)\times\Omega)} \leq C\|\dot{q}\delta u\|_{L^2((0,2T)\times\Omega)} \\ &\leq \|\dot{q}\|_{L^\infty(\Omega)}\|\delta u\|_{L^2((0,2T)\times\Omega)}. \end{aligned} \tag{B.9}$$

Combining the estimates (B.4) (B.7) (B.9) yields the desired estimate (B.5). □

B.3 Frechét Differentiability of ND map Λ_ρ

According to [61, Theorem A], if $f(0) = \partial_t f(0) = \cdots = \partial_t^{k-1} f(0) = 0$, we have

$$\|u\|_{C([0,2T],H^{k+\frac{3}{5}-\varepsilon}(\Omega))} \leq C\|f\|_{H^k((0,2T)\times\partial\Omega)},$$

where $k \geq 0$, ε is an arbitrary positive real number. Thus we have

$$\|u\|_{H^3((0,2T)\times\Omega)} \leq C\|f\|_{H^{\frac{5}{2}}}, \tag{B.10}$$

then the linearized ND map should be in Banach space

$$\mathcal{L}(H^{\frac{5}{2}}((0,2T)\times\partial\Omega), H^{\frac{1}{2}}((0,2T)\times\partial\Omega))$$

The IBVP aims to invert the following nonlinear map

$$\mathcal{F} : \rho \in C^\infty(\overline{\Omega}) \mapsto \Lambda_\rho \in \mathcal{L}(H^{\frac{3}{2}}((0,2T)\times\partial\Omega), H^{\frac{1}{2}}((0,2T)\times\partial\Omega))$$

Assuming that $\rho = \rho_0 + \dot{\rho}$ with $\rho_0 \in C^\infty(\overline{\Omega})$, define the following linear operator

$$\mathrm{d}\mathcal{F} : \dot{\rho} \in C^\infty(\overline{\Omega}) \mapsto \dot{\Lambda}_{\dot{\rho}} \in \mathcal{L}(H^{\frac{3}{2}}((0,2T)\times\partial\Omega), H^{\frac{1}{2}}((0,2T)\times\partial\Omega))$$

where $\dot{\Lambda}_{\dot{\rho}}$ is the linearized ND map defined in (3.65).

Proposition B.3. *The nonlinear map $\mathcal{F}$ is Frechét differentiable at $\rho_0 \in C^\infty(\overline{\Omega})$, and the Frechét derivative along the direction $\dot{\rho} \in C^\infty(\overline{\Omega})$ is $\dot{\Lambda}_{\dot{\rho}}$.*

Proof. In order to show that $\mathcal{F}$ is Frechét differentiable, we need to show

$$\|\mathcal{F}(\rho) - \mathcal{F}(\rho_0) - \mathrm{d}\mathcal{F}(\dot{\rho})\|_{\mathcal{L}(H^{\frac{5}{2}}((0,2T)\times\partial\Omega), H^{\frac{1}{2}}((0,2T)\times\partial\Omega))} = O\left(\|\dot{\rho}\|^2_{W^{1,\infty}(\overline{\Omega})}\right)$$

as $\|\dot{\rho}\|_{W^{1,\infty}(\overline{\Omega})} \to 0$, which is equivalent to

$$\|\Lambda_\rho f - \Lambda_{\rho_0} f - \dot{\Lambda}_{\dot{\rho}} f\|_{H^{\frac{1}{2}}((0,2T)\times\partial\Omega)} = O\left(\|\dot{\rho}\|^2_{W^{1,\infty}(\overline{\Omega})} \|f\|_{H^{\frac{5}{2}}((0,2T)\times\partial\Omega)}\right) \tag{B.11}$$

for any $f \in H^{\frac{5}{2}}((0,2T)\times\partial\Omega)$ as $\|\dot{\rho}\|_{W^{1,\infty}(\overline{\Omega})} \to 0$.

Write $u = u_0 + \delta u$, where u and u_0 are the solutions of (3.1) and (3.63), respectively. Then δu satisfy equation

$$\begin{cases} \rho_0 \delta u_{tt} - \Delta \delta u + q\delta u = -\dot{\rho} u_{tt} & \text{in } (0,2T)\times\Omega \\ \partial_\nu \delta u = 0 & \text{on } (0,2T)\times\partial\Omega \\ \delta u(0,x) = \delta u_t(0,x) = 0 & x \in \Omega \end{cases} \tag{B.12}$$

Using the regularity estimate for wave euation and the trace theorem, we have

$$\|\delta u\|_{H^2((0,2T)\times\Omega)} \le C\|\dot{\rho} u_{tt}\|_{H^1((0,2T)\times\Omega)} \le C\|u\|_{H^3((0,2T)\times\Omega)} \|\dot{\rho}\|_{W^{1,\infty}(\Omega)} \tag{B.13}$$

Denote $w \coloneqq \delta u - \dot{u}$, then $w|_{[0,2T]\times\partial\Omega} = \Lambda_\rho f - \Lambda_{\rho_0} f - \dot{\Lambda}_{\dot{\rho}} f$ and satisfies

$$\begin{cases} \rho_0 w_{tt} - \Delta w + qw = -\dot{\rho}\delta u_{tt} & \text{in } (0,2T)\times\Omega \\ \partial_\nu w = 0 & \text{on } (0,2T)\times\partial\Omega \\ w(0,x) = w_t(0,x) = 0 & x \in \Omega \end{cases} \tag{B.14}$$

Applying similar estimate yields

$$\|w\|_{H^{\frac{1}{2}}((0,2T)\times\partial\Omega)} \le \|w\|_{H^1((0,2T)\times\Omega)} \le C\|\dot{\rho}\delta u_{tt}\|_{L^2((0,2T)\times\Omega)} \le C\|\delta u\|_{H^2((0,2T)\times\Omega)} \|\dot{\rho}\|_{L^\infty(\Omega)} \tag{B.15}$$

Combining (B.10) (B.13) (B.15) gives (B.11).

□